Electronic Theses and Dissertations   Theses, Dissertations, and Major Papers

12-20-2018

Prediction of Exhaust Skin Temperature Integrating 1D Model with Vehicle Level CFD Model

Sudharsan Annur Balasubramanian
University of Windsor

Follow this and additional works at: https://scholar.uwindsor.ca/etd

Prediction of Exhaust Skin Temperature Integrating 1D Model with Vehicle Level CFD Model

By

Sudharsan Annur Balasubramanian

A Dissertation

Submitted to the Faculty of Graduate Studies

through the Department of Mechanical, Automotive & Materials Engineering

in Partial Fulfillment of the Requirements for

the Degree of Doctor of Philosophy

at the University of Windsor

Windsor, Ontario, Canada

2018

**Prediction of Exhaust Skin Temperature Integrating 1D Model
with Vehicle Level CFD Model**

by

Sudharsan Annur Balasubramanian

APPROVED BY:

_____

R. Kiran, External Examiner
Fiat Chrysler Automobiles

_____

M. Malik
Fiat Chrysler Automobiles

_____

K. Srinivasan
Fiat Chrysler Automobiles

_____

N. Kar
Department of Electrical and Computer Engineering

_____

G. Reader
Department of Mechanical, Automotive and Materials Engineering

_____

V. Stoilov
Department of Mechanical, Automotive and Materials Engineering

_____

R. Balachandar, Co-Advisor
Department of Mechanical, Automotive and Materials Engineering

_____

R. Barron, Co-Advisor
Department of Mechanical, Automotive and Materials Engineering

19 October 2018

DECLARATION OF ORIGINALITY

I hereby certify that I am the sole author of this thesis and that no part of this thesis has been published or submitted for publication.

I certify that, to the best of my knowledge, my thesis does not infringe upon anyone's copyright nor violate any proprietary rights and that any ideas, techniques, quotations, or any other material from the work of other people included in my thesis, published or otherwise, are fully acknowledged in accordance with the standard referencing practices. Furthermore, to the extent that I have included copyrighted material that surpasses the bounds of fair dealing within the meaning of the Canada Copyright Act, I certify that I have obtained a written permission from the copyright owner(s) to include such material(s) in my thesis and have included copies of such copyright clearances to my appendix.

I declare that this is a true copy of my thesis, including any final revisions, as approved by my thesis committee and the Graduate Studies office, and that this thesis has not been submitted for a higher degree to any other University or Institution.

ABSTRACT

Studies involving flow and heat transfer in automotive exhaust systems are regularly employed in the design and optimization phases. Both internal as well as external heat transfer are key to provide a better understanding of the underbody heat transfer, cold start warm-up and thermal aging of the catalytic converter for gasoline engines and adequate thermal protection for the underbody components. The internal flow in a typical automobile exhaust system can be simplified using a 1D model employing correctional factors to encompass the three-dimensional effects. However, the external flow and heat transfer underbody of a vehicle is highly complex as it involves the overall front-end design of the car as well as the packaging of components underhood and underbody. This would require the use of a full scale 3D model of a vehicle.

The proposed research involves the prediction of exhaust skin (outer surface) temperature combining a 1D model with a full vehicle 3D model as well as investigating heat transfer characteristics of the exhaust system. The 1D model is developed using a commercial code, GT-Power and the 3D vehicle level model is simulated using STAR-CCM+. The 1D and the 3Dmodel will provide a real time closed loop control system based on the combustion requirements and exhaust system readings for internal flow and external flow.

In the first stage, the gas side internal heat transfer is simulated using the 1D model by adding available heat transfer correlations considering entrance effects, engine induced pulsation, geometrical effects and surface conditions. Initially, the model is simulated for steady state wide open throttle (WOT) cases and validated with results available from

bench test. In the second stage, the use of the model is extended further in transient heat transfer studies.

In the third stage, the 3D vehicle level model is simulated using the commercial code STAR-CCM+ at various wind speeds based on a set of cluster points representing a transient drive cycle. A Reynold Averaged Navier-Stokes (RANS) based k-ε turbulence model is used for modeling flow and turbulence. Thermal models for free convection and thermal radiation, are used to account for external heat transfer. The initial thermal boundary condition of the exhaust for the simulation is obtained from the preliminary 1D simulation data. The predicted external heat transfer coefficients from the 3D model are then used as a boundary condition for the 1D model for heat transfer as a third phase of the study. The iterative of the process of using the 3D model as boundary condition for the 1D model and vice versa until convergence will ensure a more accurate prediction of the exhaust skin temperature. Further a parametric study involving the influence of external emissivity on exhaust system heat transfer was carried out. The results indicate that the effect of the external emissivity is significant on the skin temperature and external heat transfer. The variation in emissivity is seen to contribute to more than 50% in the overall heat transfer. A temperature difference of up to 200°C was seen on the heat shields of the exhaust at high loads. Similar results were seen for the other components underbody close to the exhaust system. This would potentially be higher at idling after a drive cycle where free convection and radiation are seen to be more dominant, indicating a strong influence of external radiation as a key parameter in the heat transfer from an exhaust. Further the study revealed that the variation in emissivity does not influence the convective heat transfer by more than 4%.

DEDICATION

"Where there is FAITH, there is LOVE; Where there is LOVE; there is PEACE; Where

there is PEACE; there is GOD; Where there is GOD; there is BLISS."

- Sri Sathya Sai Baba

To my parents and my beloved wife.

ACKNOWLEDGEMENT

TABLE OF CONTENTS

LIST OF TABLES

LIST OF FIGURES

NOMENCLATURE

A	Flow area (cross-sectional)
A_s	Heat transfer surface area
A_{eff}	Effective area for flow
C_f	Friction coefficient
$C_{f,rough}$	Friction coefficient of rough pipe
C_p	Pressure loss coefficient
C_P	Specific heat at constant pressure
c	Speed of sound
$C_{\varepsilon_1}, C_{\varepsilon_2}, C_{\varepsilon_3}$	Model coefficient
C_t	Model coefficient
$C_{p,f}$	Fluid-specific heat capacity
C_V	Specific heat at constant volume
D	Equivalent diameter
d	Pipe diameter
dx	Length of mass element in the flow direction (discretization length)
dp	Pressure differential acting across dx
e	Total internal energy (internal energy plus kinetic energy) per unit mass
E	Total energy
f_2	Damping function
f_c	Curvature correction
f_b	Body force vector representing the combined body forces

G_k	Turbulent production
G_b	Buoyancy production
H	Total enthalpy
h	Heat transfer coefficient
$h_{g,rough}$	Heat transfer coefficient of rough pipe
$h_{external}$	Heat transfer coefficient for external convection.
h_{user}	The "External Convection Coefficient" as input by the user
k	Thermal conductivity
l_ε	Length scale function
$\dot{m}$	Boundary mass flux into volume
m	Mass of the volume
Nu	Nusselt number
p	Pressure
Pr	Prandtl number
$\bar{p}$	Mean pressure
P_k, P_ε	Production terms
q	Heat flux
q''	Heat flux vector
q_s''	Local surface heat flux
Re	Reynolds number
S_k, S_ε	User-specified source terms
S_u	Energy source terms, such as radiation sources
T	Temperature

t	Time
Δt	Timestep
T_{fluid}	Fluid temperature
T_g	Temperature of gas
T_w	Temperature of wall
T_s	Surface temperature
T_{ref}	Reference temperature of the fluid moving over the surface
T^+	Dimensionless temperature
T_c	Temperature of the near-wall cell
u	Velocity at the boundary
u_τ	Velocity scale that is based on the wall shear stress
U_{eff}	Effective velocity outside boundary layer
V	Volume
$\bar{v}$	Mean velocity
v_g	Reference frame velocity relative to the laboratory frame
Δx	Minimum discretization element length
y^+	Wall normal distance

Greek Symbols

ε	Emissivity
ε_0	Ambient turbulence value in source terms counteracting turbulence decay
Υ_M	Compressibility modification
μ	Dynamic viscosity
ρ	Density

σ	Stefan-Boltzmann constant
$\sigma_k, \sigma_\varepsilon$	Model coefficients

Tensors and Vectors

I	Identity tensor
T	Viscous stress tensor
S	Mean strain rate tensor
v	Velocity vector

CHAPTER 1

Introduction

1.1 Introduction:

In an internal combustion (IC) engine, exhaust gases or flue gases are emitted as a result of the combustion of fuels such as gasoline, diesel, natural gas or bio-diesel blends. The exhaust system guides the exhaust or flue gases away from the combustion chamber of the IC engine. The overall system transports the burnt gas from the engine and released it into the atmosphere. Figure 1.1 shows a vehicle underbody with the exhaust system and some of its components. An exhaust system usually includes one or more exhaust pipes depending on the number of components and size of the engine. The components in a typical exhaust system consist of the following:

- Exhaust manifold – Collects the exhaust gases from multiple cylinders into one pipe.
- Catalytic converter – To reduce that air pollution by eliminating harmful gases and other unburnt hydrocarbon in the exhaust.
- Resonator/Muffler – An acoustic soundproofing device used to reduce the noise level in the exhaust by cancelling out pressure waves created by the engine.
- Exhaust pipes – These are pipes that connect the above-mentioned components and are used for funnelling them towards the tailpipe. They create and effectively sealed pathway for the exhaust gases. A regular pipe or a flexible pipe is used depending on the thermal expansion requirements of the system.
- Tailpipe – Final length of the exhaust pipe that vents to the atmosphere.
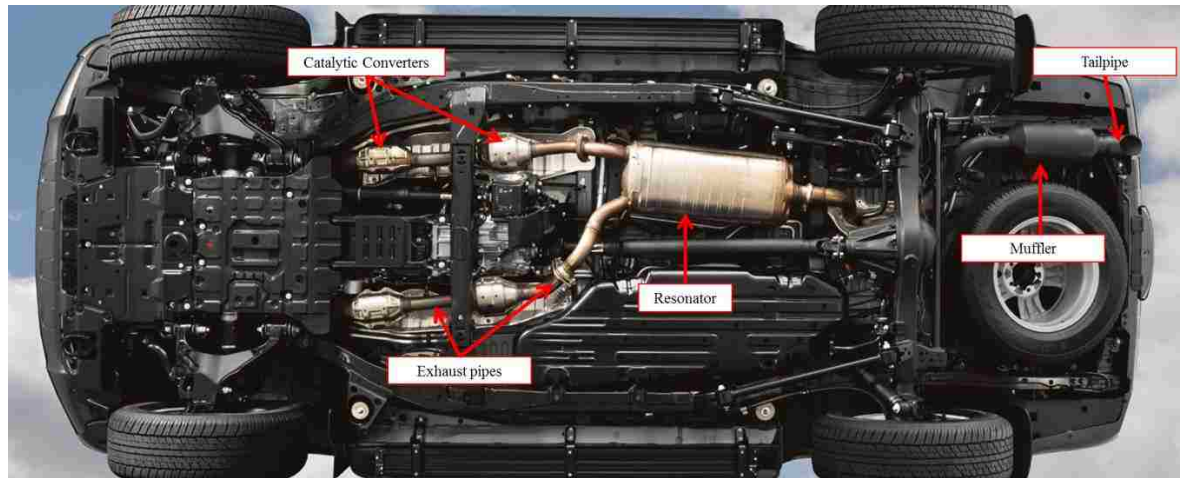
Figure 1.1 Underbody of a vehicle showing some components of the exhaust system

(https://www.team-toyota.com/blogs/1862/uncategorized/2014-toyota-land-cruiser-near-baton-rouge)

Automotive exhaust system has attracted a lot of attention in recent years due to stringent emission, noise vibration and harshness (NVH) and fuel reduction requirements. Hardware components and technologies such as active catalytic converters, flexible exhaust gas recirculation (EGR), sequential turbocharging (twin turbo), and selective catalytic reduction (SCR) have emerged in order to keep up with these norms. The thermal management of an exhaust system is highly important in a vehicle studies involving flow and heat transfer. They are regularly employed in the design and optimization phases to provide a better understanding of the underbody heat transfer, cold start warm-up and thermal aging of the catalytic converter (CAT) for gasoline engines and ADPF for diesel engines. Several parameters affect these components and technologies. One such key parameter is the exhaust skin (surface) temperature.

Accurately predicting the skin temperature of an exhaust system will help in the estimation of the maximum operating temperature of the system. Further, it helps in effectively routing the exhaust system, design and development of heat shields to protect the underbody

components in terms of thermal protection. So far, physical testing allows only in the verification of exhaust routing and thermal protection rather than the development of heat shields (Srinivasan et al., 2005). Physical tests are time intensive and require extensive instrumentation, as well as a number of tests are required to completely understand the system. Furthermore, the costs associated with testing in the product development are very high due to the number of prototypes required.

Over the past few years, automotive industries are resorting to Computational Fluid Dynamics (CFD) simulation techniques, which are very efficient during the design phases in a vehicle development and counter the setbacks from physical tests. Some key applications of CFD in the automotive development are not limited to and include engine cooling, optimizing power-train and exhaust system components, aerodynamics and thermal management.

1.2 Research Objective:

University of Windsor Automotive Research and Development Center (ARDC)/Fiat Chrysler Automobiles (FCA) Canada are interested in developing an efficient process and best practices methodology to predict the exhaust skin temperature. This would then be used in the vehicle development stage. Given the high level of importance in predicting the skin temperature for thermal protection during the design phase, challenges in understanding key aspects of heat transfer and thermal simulations have been identified. The complexities, as well as high costs involved in conducting physical tests have been a motivation for this work to pursue an alternative in using a niche CFD methodology for predicting the skin temperature.

The goal of this dissertation is the development of a CFD methodology for investigating the heat transfer characteristics and accurately predicting the exhaust skin temperature. The region, consisting of manifold and CAT are relatively underexposed to the outside environment than the other components where high skin temperatures are expected. Other components in the exhaust system such as resonator and muffler have higher surface area and are exposed to the flow underbody. Hence, the skin temperatures are expected to be relatively lower. Both internal as well as external flows are key to predicting the exhaust skin temperature. The internal flow in the exhaust is complex and three-dimensional due to the bends and flow restriction devices. However, this could be simplified to a one-dimensional (1D) model. Whereas, the external flow for the full vehicle cannot be simplified similar to the internal flow and requires a vehicle level 3D CFD model. However, the 3D modeling of heat transfer on the external side of exhaust system involves complexities in-terms of geometry, meshing, physics, moving parts etc. Use of complex mesh and reference frame techniques are required, such as Moving Reference Frame (MRF) for emulating the rotation of radiator fan. Transient momentum and energy equations are to be solved in case of a drive cycle which involves high level of computations as key flow and thermal variables have to be solved for every crank angle to obtain a high degree of accuracy. An optimized process for numerical simulations will significantly help in achieving the goal of exhaust temperature predictions.

The aim of this research is to:

- Develop and simulate a 1D model consisting of the engine coupled with the exhaust system of interest for internal flow and heat transfer which would provide a real time closed loop control system based on the combustion requirements and exhaust

4

system readings of mass flow rate, velocity, pressure and temperature of exhaust gas for internal flow.

- Perform 1D simulation for steady state Wide Open Throttle (WOT) cases and compare with available physical test data from bench test.

- Extend the model to transient heat transfer studies by simulating a complex drive cycle.

- Build and simulate a 3D vehicle level CFD model to account for external heat transfer effects that include coupled radiation, convection and to obtain flow and heat map of the exhaust system.

- Investigate effects of underhood heat rejection on the external heat transfer coefficients which will serve as a boundary condition in the 1D model.

- Couple 1D and 3D model for efficient and accurate prediction of skin temperature.

- Expedite computational solution and reduce the cost in terms of CPU time

- Investigate contribution of radiation to external heat transfer.

- Provide efficient process and computational methodology for similar problems which would serve as a best practice and benchmark for ongoing FCA vehicle development programs.

1.3 Organization of Dissertation:

The dissertation for the current work is divided into six chapters. Chapter 2 contains a brief summary of literatures/research that indicates several aspects pertaining to heat transfer and skin temperature prediction in an exhaust system. In Chapter 3 we discuss the numerical methodology and solvers used to solve for Navier-Stokes equations, modelling turbulence etc. Chapter 4 summarizes steady state WOT and transient drive cycle

simulation of a 3.6L V6 engine and dual exhaust configuration is carried out using the 1D code GT-SUITE. The results are compared with available test data and discussed in the same chapter.

In Chapter 5 a 3D vehicle level CFD simulation of vehicle housing the above mentioned engine and exhaust system is simulated using STAR-CCM+, for same transient driving cycle. The heat transfer variables are then mapped as external boundary conditions for 1D simulation for predicting the skin temperature. A summary of the above mentioned 3D simulations and coupling with 1D code is also provided. A parametric study involving effect exhaust pipe thickness as well as external radiation has also been carried out, results of which are presented in the same chapter. Chapter 6 concludes the dissertation by summarizing the research and possible recommendations for future works.

CHAPTER 2

Literature Review

2.1 Introduction:

This chapter, reviews several aspects of research pertaining to exhaust system heat transfer and skin temperature prediction. This will serve as a good initial starting point for the current investigation into exhaust skin temperature prediction and heat transfer characteristics. The objective of this chapter is to provide a brief description of the technical and fundamental details pertaining to flow and heat transfer studies in automotive exhaust system.

2.2 Literature Review:

The key to predicting the exhaust skin temperature requires a good understanding of the internal as well external fluid flow and heat transfer characteristics of the exhaust system. Experimental studies were performed by Malchow et al. (1979) in the straight section of an exhaust port of a four stroke spark ignition engine. Their objective was to construct an experimental set up to determine the heat flux from the exhaust gas to the wall for the straight portion of the exhaust port. Experiments were performed to investigate the time-averaged heat transfer based on the effects of location in the exhaust and engine variables.

7

The data was correlated in the form of Nusselt-Reynolds number relationship for local and spatially averaged steady state heat transfer. The results revealed that the conventional steady state heat transfer relationships for developing flows underpredicts the heat transfer rates observed in the experiments. They found that, the deviation was mainly due to high frequency periodic flow and geometrical effects. Further, they developed an empirical correlation based on Nusselt-Reynolds relationship for the heat transfer rates based on the experiments. The constants in the correlating equation were found to be different for each of the four axial locations of measurement. The spatial averaged correlating equation is given as equation 2.1:

$$Nu = 0.0483 \, Re^{0.8} * Pr^{1/3} \tag{2.1}$$

An augmentation factor was defined based on the ratio between the experienced Nusselt number and the ideal Nusselt number accounting for the effects due to engine induced pulsation.

Temperature measurements were carried out by Wendland (1993) in the exhaust manifold, takedown pipes and post converter components. Wendland (1993) used both single and double walled pipes for the takedown portion of the exhaust along with several designs for the manifold. The measured Nusselt numbers were found to be always higher than that calculated for ideal flow with fully developed boundary layers similar to Malchow et al.

(1979). Wendland (1993) termed the ratio of a measured Nusselt number to the one from ideal flow correlation as Convective Augmentation Factor (CAF). Further, he found that the CAF is relatively constant across the range of engine loads and speeds tested. The Nusselt number correlation used by Wendland (1993) was based on the Sider-Tate (1936) relationship as given in equation 2.2:

$$Nu = 0.027Re^{0.8} * Pr^{1/3} \qquad (2.2)$$

The CAF values averaged over a component interior Reynolds number range of 4000-20000 were 2.3, 3.0, and 1.6 for the manifold, takedown, and tailpipe respectively. It was also found that the percentage of the total external heat transfer from thermal radiation varied from 12%-18% for the tailpipe at low load to high load and 20-30% for the manifold. For the transient test cases Wendland (1993) applied steady state correlations to transient test. Instantaneous CAF values were calculated for the takedown and tailpipe and the equilibrium values were almost the same as in steady state testing. Wendland (1993) further suggested that the equilibrium CAF values could be used in modelling the performance of warmed up components.

Condie and McEligot (1995) examined the effects of pulsating flow, heat transfer parameters on a heated takedown pipe for a commercial V-6 engine. The engine was operated as an air compressor for engine speeds between 750 to 3250 rpm. The non-

dimensional frequencies for the pulsating flow were in the range of 0.045 to 0.97, higher than typical quasi-steady conditions. The secondary objective of their work was to provide a documented data for heat transfer for correlating the predictions from one-dimensional model or a CFD model. Similar to previous experiments their results demonstrated heat transfer rates higher than the ones calculated using ideal flow correlations. As pointed out by Wendland (1993) and other researchers before, the authors termed this ratio as convective enhancement factor. The further confirmed that the use of steady flow correlations can under predict the heat losses in the exhaust system. The values for CAF ranged between 2.7 to 8 varying with pulsation frequency and axial position. A previous work before this from the authors involved experimental study with real exhaust systems but with steady and non-pulsating flow. The results implied enhanced heat transfer rates were also observed in the absence of pulsations.

Alkidas et al. (2004) examined the steady state and transient internal heat transfer in the exhaust system of a diesel powered light-duty vehicle. The study dealt with two types of transient test and an estimation of external heat transfer as well. Transient heat transfer tests were evaluated using a simple fuel-step transient cycle under constant engine speed and New European Driving Cycle (NEDC). The vehicle used for the measurements was an Opel Corsa with a 1.3 L experimental diesel engine. For the measurements of exhaust gas stream temperatures, radiation shielded thermocouples were located at the flow centerline

along different axial locations through every exhaust component. Similar type of thermocouples was used for the measurement of skin temperatures at 38 axial locations along the exhaust. The purpose of the steady state tests was to encompass the load range of the NEDC by producing a broad range of Reynolds numbers. This included six variable engine speed, three different fuelling rates per stroke at high and low fan speed, for two different engine speeds. All the tests were run using the chassis dynamometer holding the engine speed constant and vehicle engine compartment hood open. The result showed that increase in gas stream temperatures with engine speed for each fuelling. Reduction in temperatures ranges were seen after the catalyst. An interesting observation was a near constant heat flux between the takedown inlet and the tailpipe exit. They related the increasing heat flux with engine speed to the engine speed and the associated exhaust gas flow rate on the convective heat transfer coefficient. In contrast the influence of fuelling rate on the surface heat flux was directly related to the exhaust gas temperatures. They obtained the following correlation for Nusselt vs Reynolds number, with the latter ranging from 7000 to 32000.

For take down pipe: $Nu = 0.209\,\mathrm{Re}^{0.60}$ (2.3)

For tailpipe: $Nu = 0.453\,\mathrm{Re}^{0.51}$ (2.4)

The correlation again proved that the convection coefficient in the takedown portion of the exhaust is significantly higher than the one the tailpipe, which lined with Wendland's (1993) findings. Further, the comparison of CAF values from their experiments with Wendland (1993) and Shayler et al. (1999) showed that the values were significantly lower than the formers and in close agreement with the latter. They indicated that, the CAF values were independent of the Reynolds number same as Shayler et al. (1999), contradicting Wendland's (1993) claim of Reynolds number dependency. The work also laid more emphasis on the part role of external heat transfer characteristics. The authors mentioned the difficulties in accurately estimating the external heat transfer characteristics due to free and forced convection flows underhood and underbody of a vehicle, radiative interactions between the exhaust and other components underhood and underbody and the uncertainties in the radiative properties of the exhaust surface. The authors study on the external heat transfer was limited to a vertical takedown pipe. Further it was a crude estimation of the external heat flux based on an assumption that the contributions from radiation, free and forced convection heat transfer are independent. Based on their calculations for six different cases, free convection heat transfer contributed to nearly half of the total heat flux, while forced convection and radiation heat transfer contributed to the other half equally. The transient tests further revealed the significance of thermal energy storage implying that

the quasi-steady assumption commonly used in the analysis of transient processes, may result in significant errors.

Apart from the key experimental work, studies involving numerical modelling and simulation to predict the exhaust temperature and heat transfer characteristics of an exhaust system were also carried out. Some of these include experimental work complementing the numerical studies to provide good validation.

Zhang et al. (1992) developed a computer modelling algorithm based on the finite volume method in order to predict the temperature distribution along an automotive exhaust system. They developed heat transfer equations to include forced convection inside the exhaust component and natural convection and radiation on the outside. The algorithm solved for both exhaust gas and skin temperature. A parametric study was conducted to relate the effect of changes in the pipes diameter, thickness and material to the changes in temperature. Further the effect of an air gap width between the inner and outer pipe to the pipe skin temperature were indicated. Though the heat transfer in the exhaust is multi-dimensional the authors simplified it to one dimensional flow in the modelling. Modelling was done for both single wall and air gap type exhaust pipe. For heat transfer between the exhaust gas and the pipe wall forced conduction was taken in to account. Natural convection and radiation was accounted for heat transfer between the external surface of

the pipe and the ambient. They neglected radial conduction as the thickness of the pipe is very thin. For the internal heat transfer the heat transfer coefficient was calculated from what seemed as a correlation similar to Sider-Tate correlation for Nusselt Number. They verified the code with a series of tests to validate the analytical solution. Results from a straight section of a single wall pipe indicated minimal variation of skin temperature with respect to the diameter of pipes used in the auto industries. However this might not be the case for applications outside the auto industry.

Chen (1993) developed a numerical model for the transient heat transfer phenomena occurring in automotive exhaust system. The model considered heat convection along with the gas flow, convection between the gas and the pipe wall, conduction in the pipe wall, and radiation and convection to ambient. In the model the exhaust gas flow was considered as one-dimensional. The secondary objective of his study was the effectiveness of thermal energy conservational concepts on converter light-off during FTP cold start procedure. Chen (1993) re-iterated on the use of the Nusselt number correlation along with an augmentation factor representing correlation for pulsation and effects of joints and bends. However, most of the study was focused towards the light-off periods for CAT.

Liu et al. (1995) developed a computer simulation model to predict the transient thermal responses of automotive exhaust system. Heat transport due to, convective heat transfer

between exhaust gas and pipe wall, conduction within pipes along axial direction, and radiation to ambient were considered in the model. The results from the model were compared to measurements for temperature under transient and steady driving cycles. For the measurements four FTP test cycles were performed with a 2.5L 4-cylinder engine. These tests were conducted using both single wall and double walled pipes with air gap. Measurements were taken at two locations; inlet of the exhaust pipe and outlet of the exhaust pipe just before the CAT. The measured inlet gas temperature, volume flow rate, air/fuel ratio and various initial conditions were then used as for initializing the computer model. The results indicate over prediction of the gas temperature between 20-50ºC in the single walled pipe, especially at the peaks pertaining to the test curve. Further the CAF values used in this study were same as Wendland (1993). The model was predominantly used to study the converter light-off period for transient drive cycles. Although the study provides a brief outlook into the modelling of heat transfer in exhaust system, it doesn't give detailed study of the complete exhaust system.

Konstantinidis et al. (1997) developed a transient computer model covering different exhaust piping configurations. The objective was to propose a novel solution procedure which could result in significant savings in-terms of processing time, as well as integration of the model in a CAE package for exhaust system design optimization. The model was validated with the help of full-scale measurements on vehicles. The study brings out the

importance of modelling the component interior heat transfer accurately. The idea behind was to account for gas phase energy balance in the exhaust system which would reduce the computing time as well. Experimental assessment for internal heat transfer coefficients were made from a small number of steady state measurements on a 2 litre car along with NEDC measurements.

These results were presented as Nusselt-Reynolds correlations similar to previous work and compared with Gnielinksi (1976) and Wendland (1993) obtaining a correlation based on their work. They further studied the effect of added mass such as welds and flanges on heat transfer. The conclusion was that the loss in temperature response due to the concentrated mass is not important, but would be significantly enhanced if the flange were positioned at the inlet section of the pipe. In a hotter pipe section the flange would accumulate higher thermal energy at a faster rate and reject heat to ambient more intensely, affecting the exhaust gas temperature response. Further there were no detailed studies involving thermal radiation.

Shayler et al. (1999) developed computational model to support studies of exhaust and aftertreatment system design for steady and transient engine operating conditions. Independent correlations were developed based on their results. Comparing steady and transient cases, they identified heat transfer coefficients deviated from the corresponding

steady state values. One of the reasons for this behavior was said to be the transient effects that tend to increase the Nusselt number, particularly at low Reynolds number. Based on a table containing Nusselt-Reynolds correlation for gas side heat transfer from previous studies, the authors rethought about the use of steady flow correlations applied to transient conditions without any modifications.

Their comparison of results with previous data showed deviations more significant upstream of the first elements in the exhaust system which provides damping of flow pulsations. They developed Nusselt number correlation for transient study by modifying the steady flow correlation. However, they concluded that this cannot be applied directly to the more general patterns of transient exhaust flow conditions pertaining to drive cycles. They made a further modification to the above mentioned correlation for use in drive cycles. However, these studies were geared towards CAT.

Grose and Austin (2001) developed a software tool that allowed the one dimensional and three dimensional fluid flow simulation packages to interact in a heterogeneous environment. The objective of the methodology was to enable the details of internal flow to be retained whilst conserving the overall mass flow in the network, thereby eliminating uncertainties in the boundary values used in three-dimensional model. This model was predominantly used for power-train studies and described the ideology for the coupling

between two commercial codes. Further the results from the study were from a simple network without an actual power-train or exhaust model. The transient studies for the model were for a very short duration and not a complete drive cycle. Hence it is unknown as to the actual performance of the coupling of the codes for heat transfer studies.

Depcik and Assanis (2002) surveyed available correlations proposed in previous literatures for the gas side heat transfer in the intake and exhaust system of a spark ignition IC engine. They noticed that correlations from the literature were often of the form $Nu = aRe^b$ and differed only by empirically fitted constants. Their objective was to develop a universal correlation. The authors used a scaling approach using microscales of turbulence to fix the exponential factors on the Reynolds number, there by reducing the number of adjustable correlation to just one. They later used various data, available from the literature to determine the other adjustable coefficient using a least square curve fit.

The final correlation derived by the authors is given as:

$$Nu = 0.07Re^{3/4} \qquad (2.5)$$

Zhang et al. (2005) used CFD to calculate skin temperature of CAT in the exhaust system. They supplemented the numerical calculation, with experimental results. The simulations involved 3D compressible turbulent fluid flow with natural and forced convection, heat conduction and radiation. They further employed the developed method to investigate the

effect of different materials and thickness, different cell structures of substrate and different kinds of cone insulations on skin temperature. However, these were targeted more towards CAT.

2.3 Remarks:

The brief study of literature reveal the use of a Nusselt-Reynolds correlation based on turbulent pipe flow correlations. Out of these, the Sider-Tate correlation used along with the augmentation factor calculated by Wendland (1993) seems to be the most commonly used either with CAF and the correlation or just the CAF values by itself combined with other flow correlation. Based on this the same correlation proposed by Wendland (1993) along with the CAF is used for the current study. This correlation would be denoted as Wendland Heat transfer Correlation (WHT) in subsequent chapters.

Along with this the universal correlation developed by Depcik and Assanis (2002) is used along with the CAF values proposed by Wendland (1993). This correlation would be denoted as Universal Heat transfer Correlation (UHT) in subsequent chapters.

Further, most of the studies in the literature are geared either towards the CAT studies or steady state simulations in nature with a very few stressing on the transient heat transfer. Though very few studies seem to have touched on the necessity of considering free convection and radiation for heat transfer, none of the studies provide detailed insight into

the factors affecting radiation and convection. Further, the use of both a 1D model and 3D

model for the skin temperature prediction seem to be sparse. This provides motivation for

the current study to develop a methodology for predicting skin temperature integrating both

1D and 3D models.

CHAPTER 3

Numerical Methodology

3.1 Introduction (GT-Power):

In the study, for the problem associated with internal flow and heat transfer, the computational analysis is done using GT-Power, a licensed product and a tool with in GT-SUITE from Gamma Technologies is used. GT-SUITE is a comprehensive code for the design and analysis of engine thermal management systems used during both design and development phases by majority of automobile manufacturers including FCA. GT-SUITE is based on one-dimensional fluid dynamics, representing flow and heat transfer in piping and in other components of a system (GT-SUITE: Flow Theory Manual, 2013) by resolving the Navier-Stokes equations in 1D. It further includes built-in vehicle/engine simulation for calculation of thermal loads under any driving cycle. This enables the users to account for the trade-off between a model accuracy and necessary computational run-time when performing a simulation.

3.2 General Flow Solution

The flow in an automobile exhaust system is similar to that of a pipe flow. Some of the components that were used in GT-Power to model exhaust system include pipes, flow-splits, orifices etc. This section describes the method of flow solution used in pipes and flowsplits. The flow model in GT-SUITE solves for Navier-Stokes equations, namely continuity, momentum and energy equation in one-dimension. This means that all the quantities are averages across the direction of the flow. Initially to solve this discretization interms of space and time are required. As for space, the whole system is discretized into

many volumes where, every pipe is divided into one or more volumes and each flow split is represented by a single volume. These volumes are connected by means of boundaries. The scalar variables (pressure, density, temperature, internal energy, enthalpy etc.) are assumed to be uniform over each volume. The vector variables (velocity, mass flux etc.) are calculated for each boundary. This type of discretization is referred to as "staggered grid" as shown in Figure 3.1.
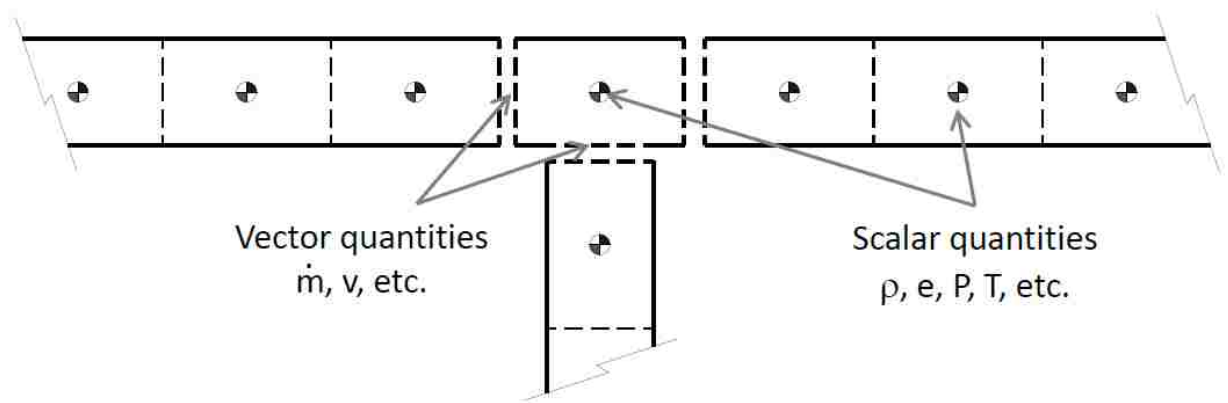
Figure 3.1. Schematic representation of staggered grid approach in GT-SUITE (GT-SUITE: Flow Theory Manual, 2013)

As for the temporal discretization there are two time integration methods, explicit and implicit integrators. These two time integration methods affect the solution variables and limits on the time step. The primary solution variables in explicit method are mass flow, density and internal energy. The primary solution variables in the implicit method are mass flow, pressure and total enthalpy.

3.2.1 Governing Equations

The governing equations that are solved by GT-SUITE are shown below. The left side of the equation represents the derivatives of primary solution variables. The right side

22

represents the secondary variables, calculation of which will be described in the next section.

Continuity equation,

$$\frac{dm}{dt} = \sum_{boundaries} \dot{m} \tag{3.1}$$

Energy equation, (Explicit Solver)

$$\frac{d(me)}{dt} = -p\frac{dV}{dt} + \sum_{boundaries} (\dot{m}\,H) - hA_s(T_{fluid} - T_{wall}) \tag{3.2}$$

Enthalpy equation, (Implicit Solver)

$$\frac{d(\rho HV)}{dt} = \sum_{boundaries} (\dot{m}\,H) + V\frac{dp}{dt} - hA_s(T_{fluid} - T_{wall}) \tag{3.3}$$

Momentum equation,

$$\frac{d\dot{m}}{dt} = \frac{dpA + \sum_{boundaries}(\dot{m}u) - 4C_f\frac{\rho u|u|}{2}\frac{dxA}{D} - C_p\left(\frac{1}{2}\rho u|u|\right)A}{dx} \tag{3.4}$$

where:

$\dot{m}$ = Boundary mass flux into volume, $\dot{m} = \rho Au$

m = Mass of the volume

V = Volume

p = Pressure

ρ = Density

A = Flow area (cross-sectional)

A_s = Heat transfer surface area

e = Total internal energy (internal energy plus kinetic energy) per unit mass

H = total enthalpy, $H = e + p/\rho$

h = heat transfer coefficient

T_{fluid} = Fluid temperature

T_{wall} = Wall temperature

u = Velocity of the fluid

C_f = Skin friction coefficient

C_p = Pressure loss coefficient

D = Equivalent diameter

dx = Length of mass element in the flow direction (discretization length)

dp = Pressure differential acting across dx

3.2.2 Explicit Method

In the explicit method, the right hand side of the equations is calculated using values from the previous time step. This yields the derivative of the primary variables and allows the value at the new time to be calculated by integration of that derivative over the time step. The explicit solver uses only the values of the subvolume in question and not its neighbouring subvolumes. To ensure numerical stability, the time step must be restricted to satisfy the Courant condition. More details on time stepping are shown in a following

section. The small time steps required by this method make the explicit method is undesirable for simulations that are relatively long (on the order of minutes in real time), but is well suited for highly unsteady flow where a high degree of resolution is already required to capture the extremes of the flow behaviour. This method will produce more accurate predictions of pressure pulsation that occurs in engine air flows and fuel injection systems and is required when prediction of pressure wave dynamics is important (GT-SUITE: Flow Theory Manual, 2013). At each time step, the pressure and temperature are calculated in the following way:

- Continuity and energy equations yield the mass and energy in the volume.
- With the volume and mass known, the density is calculated yielding density and energy
- The equations of state for each species define density and energy as a function of pressure and temperature. The solver iterates on pressure and temperature until they satisfy the density and energy already calculated for this time step. The transfer of mass between species is also accounted for during this iteration.

The relation between the time step and the discretization length is determined by the Courant number, when the explicit solver is used. (The discretization length is the length of a subvolume in a pipe.) The solver remains stable by choosing its timesteps such that the Courant condition (given below) is met:

CFL Condition

$$\frac{\Delta t}{\Delta x}(|u| + c) \leq 0.8 * M \qquad (3.5)$$

where:

Δt = Timestep

Δx = Minimum discretization element length

c = Speed of sound

M = Timestep multiplier specified by the user

The timestep in flowsplits use a similar methodology as pipes and is given as

$$\Delta t \propto \frac{V}{A_{eff}c} \qquad\qquad (3.6)$$

This indicates that the timestep must be small enough such that only a fraction of mass could be emptied in a given timestep if the fluid was leaving the flowsplit travelling at the speed of sound.

To determine A_{eff} the solver will check each port of the flowsplit. The area for flow at each port is defined as the smaller of the area based on the flowsplit expansion diameter at that port and the diameter of the connection to the flowsplit at that port. The port with the largest area for flow determines the value of A_{eff}, and ultimately controls the time step requested by the flowsplit (GT-SUITE: Flow Theory Manual, 2013).

3.2.3 Implicit Method

The primary solution variables in the implicit method are mass flow, pressure, and total enthalpy. In the implicit method, non-linear systems of algebraic equations are iteratively solved for the values of all subvolumes at the new time simultaneously. Since the implicit solution is iterative, it is important to verify that the solution for each step has numerically

converged. This approach is used for fluid systems where high frequency pressure fluctuations are not of interest (i.e. cooling systems) and typical simulation durations are higher, so that large time steps may be taken. For this type of system the implicit solution is considered more efficient (the ability to take relatively large steps with a stable solution outweighs the CPU cost of an iterative solution for each step). While it has a significant advantage in terms of speed, the implicit solver is used only in simulations that satisfy both of the following criteria:

- There are minimal wave dynamics in the system, or accurate prediction of wave dynamics is unimportant, and
- The maximum Mach number in the system is less than 0.3

The time step used by the implicit method is not dynamically determined by GT-SUITE, as in the explicit method, but is imposed by the user (GT-SUITE: Flow Theory Manual, 2013). For the present study both the explicit and implicit methods are used in steady state and transient simulations respectively.

3.3 Heat Transfer

This section describes the theory used for modelling heat in pipes and flowsplits. The heat transfer from fluids inside of pipes and flowsplit to the inner surface of the walls is calculated using a heat transfer coefficient (GT-SUITE: Flow Theory Manual, 2013). This is done by calculating the heat transfer coefficient at every timestep from the fluid velocity, the thermo-physical properties and the wall surface roughness. The heat transfer coefficient of smooth pipes is calculated using the Colburn analogy (GT-SUITE: Flow Theory Manual, 2013).

$$h_g = \frac{1}{2} C_f \rho U_{eff} C_p Pr^{(-\frac{2}{3})}$$ (3.7)

where:

C_f = Friction coefficient of smooth pipe

U_{eff} = Effective velocity outside boundary layer

C_p = Specific heat

Pr = Prandtl number

The Colburn analogy is used for turbulent, laminar and transitional flow. A Nusselt number of 3.66 is used for Reynolds number less than 2000; the heat transfer coefficient is defined by:

$$h_g = \frac{Nu \cdot k}{d}$$ (3.8)

where:

Nu = Nusselt number

k = Thermal conductivity (W/m-K)

d = pipe diameter (m)

The surface roughness in a pipe can strongly influence the heat transfer coefficient. The heat transfer coefficient in this case is initially calculated using (3.8) and then increased using equation (3.9)

Correction for Surface Roughness:

$$h_{g,rough} = h_g \left(\frac{C_{f,rough}}{C_f} \right)^n \quad \quad (3.9)$$

$$n = 0.68 * Pr^{0.215} \quad \quad (3.10)$$

where:

$h_{g,rough}$ = Heat transfer coefficient of rough pipe

$C_{f,rough}$ = Friction coefficient of rough pipe

3.4 Wall Thermal Solution:

The wall temperatures in the pipes and flowsplits are calculated using a "WallTempSolver" object in GT-Power. The calculated wall temperatures are solved using the internal heat transfer, the external heat transfer, the thermal capacitance of the walls, and the initial wall temperature entered by the user. The external heat transfer (from outside of the pipe walls to the environment) is calculated from the data entered in the 'WallTempSolver' reference object describing forced convection, free convection, and/or radiation. The wall temperature is solved either in a steady state or transient simulation. When a steady state simulation is used, the code reaches the final steady-state wall temperatures as quickly as possible so that a fully-warmed system may be simulated in only a few cycles. A transient simulation is used to study the warm-up characteristics of the system considering the effect of structural heat capacity.

The wall temperature solver uses equations resulting from discretized energy conservation using the finite volume method as shown below:

Conservation of Energy:

$$\int \frac{\partial (\rho C_V T)}{\partial t} dV = \int (-\nabla . q) dV \tag{3.11}$$

where:

C_V = Specific heat

q = Heat flux

After integration we have:

$$\rho C_V \frac{\Delta T}{\Delta t} = \sum_{faces} -qA \tag{3.12}$$

Each of the wall layers for a pipe subvolume is used as a control volume for the energy equation. Heat transfer across the radial faces of the volumes are calculated using a resistance to conductive heat transfer as well as radiation between the surfaces on either side of an air gap, and conductive heat transfer at the axial boundaries (GT-SUITE: Flow Theory manual, 2013).

The heat transfer from the gas to pipe is calculated at every timestep using the equations shown below.

Heat flux due to conduction is given as:

$$q_{conduction} = -k\nabla T \tag{3.13}$$

where:

T = Surface Temperature

Heat flux due to convection is given as:

$$q_{convection} = h(T_g - T_w)$$ (3.14)

where:

h = heat transfer coefficient

T_g, T_w = Temperature of gas and wall, respectively

External convection coefficient:

$$h_{external} = max\left(Nu.\frac{k}{D}, h_{user}\right)$$ (3.15)

where:

$h_{external}$ = Heat transfer coefficient for external convection

h_{user} = The "External Convection Coefficient" as input by the user into the WallTempSolver object

Nu = 0.5 + 0.10 (Rayleigh Number) ^ (1/3)

Heat flux due to radiation is given as:

$$q_{radiation} = -\varepsilon\sigma(T_1^4 - T_2^4)$$ (3.16)

where:

ε = Emissivity

σ = Stefan-Boltzmann constant

3.5 Introduction to STAR-CCM+:

The third stage of the study is concerned with the simulation of external flow and heat transfer for a vehicle level 3D model. This is performed using Siemens' STAR-CCM+ which intern uses finite volume method (FVM) to solve the governing equations of fluid flow. The general transport equation and other simulation set up methodology are briefly explained in the forthcoming sections.

3.6 General Transport Equation:

Equation (3.17) gives the conservative differential form of the transport equation governing the three-dimensional flow and heat transfer for Newtonian fluids (Versteeg and Malasekara, 2010),

$$\frac{\partial(\rho\phi)}{\partial t} + div(\rho\phi\mathbf{u}) = div(\Gamma\ grad\ \phi) + S_\phi \qquad (3.17)$$

The integral form of the transport equation (3.17) is obtained by integrating the generic transport equation (3.17) over a control volume V and applying Gauss divergence theorem,

$$\frac{d}{dt}\int_V \rho\phi dV + \int_A \rho v\phi\ .\ da = \int_A \Gamma\nabla\phi\ da + \int_V S_\phi dV \qquad (3.18)$$

ϕ represents the scalar property being transported. The four terms from left to right in equation (3.18) indicate transient term or local acceleration, convective flux, diffusive flux and the source term. The transient term signifies the rate of change of the property ϕ in the control volume. The convective flux indicates the net rate of decrease of the fluid property across the control volume boundary due to convection. Diffusive flux signifies the increase

of the fluid property inside the control volume due to diffusion. The source term indicates the generation/destruction of the fluid property inside the control volume. By setting term ϕ, equal to 1, u, v, w and E and selecting appropriate values for the diffusion coefficient Γ and the source term, Navier-Stokes equations are obtained. A semi-discrete form of the transport equation (3.18) can be written as (STAR-CCM+ Manual, 2016):

Semi-discrete transport equation:

$$\frac{d}{dt}(\rho\phi V)_0 + \sum_f [\rho\phi(\mathrm{v}\cdot\mathrm{a})]_f = \sum_f (\Gamma\nabla\phi\cdot\mathrm{a})_f + (S_\phi V)_0 \qquad (3.19)$$

where the subscripts f and 0 denotes a quantity at face and cell 0 respectively. The approximations used to solve these terms as functions of cell variables are discussed in the following subsections.

In STAR-CCM+, the transient term is mainly used for transient calculations. The current work involves steady state simulations for the full vehicle model. Hence this term is neglected.

3.6.1 Convective Flux:

At a face, the discretized convective term can be written as:

$$(\phi\rho\,\mathrm{v}\cdot\mathrm{a})_f = (\dot{m}\phi)_f = \dot{m}_f\phi_f \qquad (3.20)$$

where $\dot{m}_f$ and ϕ_f are mass flow rate and scalar value at the face respectively. The manner in which the fluid property face value ϕ_f is computed from the cell values has an extensive effect on the stability and accuracy of the numerical scheme. Several numerical schemes

are available to evaluate this, namely, first order upwind, second order upwind, central differencing etc.

The first order schemes are based on the transport properties of the flow: due to convection, ϕ is transported only downstream. In order for the approximations from first order schemes to be good, the streamlines have to be aligned with the gridlines. Deviation from this induces a numerical diffusion. The first order schemes are unconditionally bounded, which helps the solver with stability and achieve robust convergence. For the current study a first order scheme is used for the initial solution and later on switched to a second order scheme for a more accurate final, converged solution. Details regarding these schemes are provided in the STAR-CCM+ Manual.

3.7 Segregated Models:

The segregated flow solver solves the integral conservation equations for mass, momentum equations in turn or sequentially, one for each dimension. Since the governing equations are non-linear and coupled, the solution loop is carried out iteratively to obtain the convergence of numerical solution. The approach gets its name "segregated" from the fact that, the governing equations, when solved, are decoupled or segregated. It has separate solvers for pressure and velocity. Due to the uncoupled manner of solving the equations, the solution convergence is relatively slow. However, since the discretized equations have to be stored in the memory only one at a time, the algorithm is memory efficient.

The momentum equations are discretized in a similar way to the scalar transport equation as described in equation (3.20) by setting $\phi = u, v, w$ as shown below:

$$\frac{\partial}{\partial t}(\rho vV)_0 + \sum_f [\rho vv.\,a]_f = -\sum_f (p\,\text{I}.\,a)_f + \sum_f \text{T}.\,a \qquad (3.36)$$

The model is widely used in constant density flows. Although, it can be used for mildly compressible flows and low Rayleigh number natural convection. Given the large mesh size and flow conditions, it was appropriate to choose the segregated model for the current problem.

3.8 Turbulence Models:

Most of the fluid flows are characterized by fluctuating flow quantities. The fluctuations are mostly of high frequencies and small scales. In order to resolve these fluctuations in time and space high computational costs are incurred. Instead of solving for the exact governing equations of turbulent flows (Direct Numerical Simulation), it is less expensive to solve for averaged or filtered quantities and approximate the impact of the small fluctuating structures. Turbulence models provide different approaches for modeling these structures (STAR-CCM+ Manual, 2016).There are two approaches to reformulate the Navier-Stokes equations (Hoffmann & Chiang, 2000) namely:

- Reynolds-Averaged Navier-Stokes (RANS)
- Favre-Averaged Navier-Stokes (FANS)

As a general recognition, all existing turbulence models are said to be approximate representations of the physical phenomena of turbulence. The degree of approximation in

a given model usually depends on the nature of the flow to which it is applied (STAR-CCM+ Manual, 2016).

RANS turbulence models provide closure relations for the Reynolds-Averaged Navier-Stokes equations to solve for the transport of mean flow quantities. The instantaneous quantities are decomposed into a mean value and a fluctuating component. To obtain the Reynolds-Averaged Navier-Stokes equations, each solution variable ϕ in the instantaneous Navier-Stokes equations is decomposed into a mean, or averaged, value $\bar{\phi}$ and a fluctuating component ϕ' given in equation (3.37):

$$\phi = \bar{\phi} + \phi' \tag{3.37}$$

where ϕ represents velocity components, pressure, energy, or species concentration. The averaging process may be thought of as time averaging for steady-state situations and ensemble averaging for repeatable transient situations. Inserting the decomposed solution variables into the Navier-Stokes equations results in equations for the mean quantities. The mean mass and momentum transport equation can be written as:

$$\frac{\partial p}{\partial t} + \nabla \cdot \left[\rho (\bar{\mathbf{v}} - \mathbf{v}_g) \right] = 0 \tag{3.38}$$

$$\frac{\partial}{\partial t} (\rho \bar{\mathbf{v}}) + \nabla \cdot \left[\rho (\bar{\mathbf{v}} - \mathbf{v}_g) \right]$$
$$= -\nabla \cdot \bar{p}\, \mathbf{I} + \nabla \cdot (\mathbf{T} - \rho \overline{\mathbf{v}'\mathbf{v}'}) + f_b \tag{3.39}$$

where:

- $\bar{\mathbf{v}}$ and $\bar{p}$ are the mean velocity and pressure respectively

- $\mathbf{v}_g$ is the reference frame velocity relative to the laboratory frame

- $\mathbf{I}$ is the identity tensor

- **T** is the stress tensor

- $\boldsymbol{f}_b$ is the resultant of the body forces

These equations are essentially identical to the original equations, except that an additional term now appears in the momentum transport equation. This additional term is a tensor quantity, known as the Reynolds stress tensor. The challenge is thus to model the Reynolds stress tensor T_t in terms of the mean flow quantities, and hence provide closure of the governing equations. Two basic approaches are used in STAR-CCM+:

- Eddy viscosity models

- Reynolds stress transport models

Eddy viscosity models are based on the analogy between the molecular gradient-diffusion process and turbulent motion. The concept of a turbulent eddy viscosity μ_t makes it possible to model the Reynolds stress tensor as a function of mean flow quantities. The most common model is known as the Boussinesq approximation:

$$\mathbf{T}_t = 2\mu_t\mathbf{S} - \frac{2}{3}(\mu_t\nabla\cdot\bar{\mathbf{v}})\mathrm{I} \tag{3.41}$$

where **S** is the mean strain rate tensor.

While simpler models rely on the concept of mixing length to model the turbulent viscosity in terms of mean flow quantities, the eddy viscosity models solve additional transport equations for scalar quantities that enable the turbulent viscosity μ_t to be derived (STAR-CCM+ Manual, 2016). For the current research, one of the important requirements of the computational model is, to account for the fluid flow over the exhaust system and account for various mode of heat transfer to obtain good results for the heat transfer coefficient. On

the other hand, cost of the simulation and industrial applicability must also be considered. For accurately modelling the fluid flow for the current work a Realizable k-ε model with a two-layer approach (RKE2L) is used. More details pertaining to this model is provided in the upcoming section.

3.8.1 Realizable k-ε Model:

As explained in the previous subsection the Realizable k-ε (RKE) model is an improved version of the standard k-ε model. The model was first proposed by Shih et al. (1994). It consists of a new model dissipation rate equation and a new realizable eddy viscosity formulation. Also, a critical coefficient of the model, $C\mu$, is expressed as a function of mean flow and turbulence properties, rather than assumed to be constant as in the standard model. This procedure lets the model satisfy certain mathematical constraints on the normal stresses consistent with the physics of turbulence (realizability). The concept of a variable $C\mu$ is also consistent with experimental observations in boundary layers. This model is substantially better than the standard k-ε model for many applications, and can generally be relied upon to give answers that are at least as accurate as RSM.

The transport equations for the kinetic energy k and the turbulent dissipation rate ε are:

$$\frac{\partial}{\partial t}(\rho k) + \nabla \cdot \left[\rho k (\bar{\mathbf{v}} - \mathbf{v}_g)\right] = \nabla \cdot \left[\left(\mu + \frac{\mu_t}{\sigma_k}\right)\nabla k\right] + P_k - \rho\left((\varepsilon - \varepsilon_0)\right) + S_k \quad (3.42)$$

$$\frac{\partial}{\partial t}(\rho \varepsilon) + \nabla \cdot \left[\rho \varepsilon (\bar{\mathbf{v}} - \mathbf{v}_g)\right]$$

$$= \nabla \cdot \left[\left(\mu + \frac{\mu_t}{\sigma_\varepsilon}\right)\nabla \varepsilon\right] + \frac{1}{T_\varepsilon}C_{\varepsilon 1}P_\varepsilon - C_{\varepsilon 2}f_2\rho\left(\frac{\varepsilon}{T_\varepsilon} - \frac{\varepsilon_0}{T_0}\right) + S_\varepsilon$$

$$(3.43)$$

where:

- $\bar{\mathbf{v}}$ and $\mathbf{v}_g$ are the mean velocity and the reference frame velocity relative to the laboratory frame, respectively

- μ is the dynamic viscosity

- $\sigma_k, \sigma_\varepsilon, C_{\varepsilon 1}, C_{\varepsilon 2}$ are model coefficients

- P_k and P_ε are production terms

- f_2 is a damping function

- S_k and S_ε are the user-specified source terms

- ε_0 is the ambient turbulence value in the source terms that counteracts turbulence decay

The formulation of the production terms P_k and P_ε depends on the k-ε model variant. For the RKE2L these are defined as:

$$P_k = G_k + G_b + Y_M \tag{3.44}$$

$$P_\varepsilon = f_c Sk + C_{\varepsilon 3} G_b \tag{3.45}$$

where:

- f_c is the curvature correction

- C_{ε_3} is a model coefficient

- G_k is turbulent production

- G_b is buoyancy production

- Y_M is compressibility modification

The terms G_k, G_b and Y_M are represented as:

$$G_k = f_c(\mu_t S^2| - \frac{2}{3}\rho k \nabla \cdot \bar{\mathbf{v}} - \frac{2}{3}\mu_t(\nabla \cdot \bar{\mathbf{v}})^2) \tag{3.46}$$

$$G_b = \beta \frac{\mu_t}{Pr_t}(\nabla \bar{T} \cdot \mathbf{g}) \tag{3.47}$$

$$Y_M = \frac{C_{M^{k\varepsilon}}}{c^2} \tag{3.48}$$

where:

- β is coefficient of thermal expansion

- Pr_t is the turbulent Prandtl number

- $\bar{T}$ is the mean temperature

- g is the gravitational vector

- C_M is a model coefficient

The possibility to impose an ambient source term counteracting the turbulence decay, also leads to the definition of a specific time-scale T_0 that is defined as:

$$T_0 = max\left(\frac{k_0}{\varepsilon_0}, C_t\sqrt{\frac{v}{\varepsilon_0}}\right) \tag{3.49}$$

where C_t is a model coefficient.

Relation for turbulent viscosity in the RKE2L model is given as:

$$\mu = \rho C_\mu \frac{k^2}{\varepsilon} \tag{3.50}$$

The term C_μ is no longer the model coefficient which was used in the standard k-ε model. Instead it is evaluated as:

$$C_\mu = \frac{1}{A_0 + A_s U^{(*)} \frac{k}{\varepsilon}} \tag{3.51}$$

The term $U^{(*)}$ is further evaluated as:

$$U^{(*)} = \sqrt{\mathbf{S}:\mathbf{S} + \mathbf{W}:\mathbf{W}} \tag{3.52}$$

where $\mathbf{S}$ and $\mathbf{W}$ are the strain rate and rotation rate tensor respectively.

Further, the coefficients in equation (3.50) are:

$$A_s = \sqrt{6}\cos\phi \tag{3.53}$$

$$\phi = \frac{1}{3}\mathrm{acos}\,\sqrt{6}W \tag{3.54}$$

$$W = \frac{S_{ij}S_{jk}S_{ki}}{\sqrt{S_{ij}S_{ij}}^3} \tag{3.55}$$

$$A_0 = 4 \tag{3.56}$$

In the two layer approach for the turbulence model, the computation is divided into two layers. In the layer next to the wall, the turbulent dissipation rate ε and the turbulent viscosity μ_t are specified as functions of wall distance. The values of ε specified in the near-wall layer are blended smoothly with the values computed from solving the transport equation far from the wall. The equation for the turbulent kinetic energy is solved in the entire flow. The results from explicit specification of ε and μ_t is no less empirical than the damping function approach, are often as good or better. In STAR-CCM+, the two-layer

41

formulations work with either low-Reynolds number type meshes $y+ \sim 1$ or wall-function type meshes $y+ > 30$ (STAR-CCM+ Manual, 2016).

For the two layer model the dissipation rate near the wall is simply prescribed as:

$$\varepsilon = \frac{k^{3/2}}{l_\varepsilon} \tag{3.57}$$

where l_ε is a length scale function that is calculated depending on the model variant.

The wall proximity indicator that is used to combine the two layer formulation with the full two-equation model is given in equation (3.58)

$$\lambda = \frac{1}{2}\left[1 + tanh\left(\frac{Re_d - Re_y^*}{A}\right)\right] \tag{3.58}$$

where:

- Re_d is the wall-distance Reynolds number

- Re_y^* defines the limit of applicability of the two-layer formulation and is a model coefficient

- A determines the width of the wall-proxmity indicator and is defined such that the value of λ is within 1% of its far-field value for a given variation of $\Delta\, Re_y$,

$$A = \frac{|\Delta\, Re_y|}{atanh\, 0.98} \tag{3.59}$$

where $\Delta\, Re_y$ is a model coefficient.

The turbulent viscosity from the k-ε model $\mu_t|_{k-\varepsilon}$ is then blended with the two-layer value as follows:

$$\mu_t = \lambda \mu_t|_{k-\varepsilon} + (1 - \lambda)\mu \left(\frac{\mu_t}{\mu}\right)_{2layer} \tag{3.60}$$

where $\left(\frac{\mu_t}{\mu}\right)_{2layer}$ is calculated depending on the model variant.

3.9 Segregated Energy Model:

Three types of segregated energy models are available with STAR-CCM+; segregated iso-thermal, segregated fluid enthalpy and segregated fluid temperature. The Segregated Fluid Isothermal model keeps the temperature in the continuum constant. This model is recommended where the temperature changes are negligible. The segregated fluid enthalpy model solves the total energy equation with chemical thermal enthalpy as the solved variable. Temperature is then computed from enthalpy according to the equation of state. The segregated fluid enthalpy model is recommended for problems involving combustion. The segregated fluid temperature model solves the total energy equation with temperature as the solved variable. Enthalpy is then computed from temperature according to the equation of state. This model is the common choice for most heat transfer problems. The current problem involves the computation of heat transfer coefficients using the predicted temperatures from the 1D model. Hence this model is used.

The energy equation in fluids is given as:

$$\frac{\partial}{\partial t}\int_V \rho E dV + \oint_A \rho H \mathbf{v}.\,d\mathbf{a} = -\oint_A \mathbf{q}''.\,d\mathbf{a}$$

$$+ \oint_A \mathbf{T}.\mathbf{v}da + \int_V f_b.\mathbf{v}dV + \int_V S_u dV \tag{3.61}$$

where:

- E is the total energy

- $\mathbf{q}''$ is the heat flux vector

- S_u contributes energy source terms, such as radiation sources, interphase energy sources or energy sources due to chemical reactions. User-defined volumetric sources also enter through this term.

Total energy is related to total enthalpy H by:

$$E = H - p/\rho \tag{3.62}$$

where

$$H = h + |\mathbf{v}|^2/2 \tag{3.63}$$

Similar to the finite volume discretization, the equation (3.61) contains four terms namely the unsteady term, convection term, diffusion term and viscous dissipation term respectively. The discrete form of the energy equation at a cell-centred control volume V_o is given as:

$$\frac{\partial}{\partial t}(\rho E V_0) + \sum_f \{[\rho H(\mathbf{v} - \mathbf{v_g}) + \mathbf{v_g}p + \dot{\mathbf{q}}'' - (\mathbf{T}.\mathbf{v})]\cdot \mathbf{a}\}_f$$

$$= (f.\mathbf{v} + s)V_0 \tag{3.64}$$

Since the current study doesn't involve transient analysis the unsteady term is omitted. The convection term $\sum_f\{\rho H(\mathbf{v} - \mathbf{v_g}) \cdot \mathbf{a}\}_f$ is evaluated as in section 3.6.1 and the diffusion term $\sum_f\{\dot{\mathbf{q}}'' \cdot \mathbf{a}\}_f$ is evaluated as in 3.6.3. The viscous work term $\sum_f\{(\mathbf{T} \cdot \mathbf{v}) \cdot \mathbf{a}\}_f$ is evaluated straightforward fashion using the stress tensor that is calculated in the segregated flow model formulation as in section 3.8.1. Detailed evaluation is available in the STAR-CCM+ manual, and is being omitted here to keep the dissertation succinct.

3.10 Modelling Heat Transfer:

Heat transfer is linked with fluid flow by means of convection, and coupled to thermodynamics through fluid properties such as density, thermal conductivity, fluid viscosity etc. This makes heat transfer a multi-physics problem from modelling perspective. The forthcoming sections briefly describe the individual modes of heat transfer for the current work from the 3D perspective. Heat transfer by means of conduction is modelled in 1D (see section 3.4) as a part of the internal flow, while external convection (natural and forced) and radiation is modelled in 3D.

3.10.1 Modelling Convection:

The mechanisms driving the convective heat transfer in fluids are: energy transfer due to random molecular motion (diffusion) and energy transfer due to the larger-scale bulk motion of the fluid (advection -the collective movement of groups of molecules). The convective heat transfer contribution from molecular motion dominates near the surface where the velocity tends to zero. At the interface between the solid and the fluid, the mode of heat transfer is solely by diffusion. This is due to the fact that at the interface, there is

no relative motion between the fluid and surface. The convective heat transfer at a surface is governed by Newton's law of cooling:

$$q_s'' = h(T_s - T_{ref}) \qquad (3.65)$$

where:

- T_s is the surface temperature
- T_{ref} is the reference or characteristic temperature of the fluid moving over the surface

The Newton's law of cooling expresses a linear relationship between the local surface heat flux and the difference between the local surface and fluid temperatures. This relationship is only an approximation; in reality the relationship could strongly be nonlinear. Since the flow conditions can vary from point to point on the surface, both q_s'' and h can vary as a function of space and time. There are two forms of convection namely:

- Free convection or natural convection
- Forced convection

Natural convection or free convection in a gravitational field occurs due to temperature differences which affect the density, and thus the relative buoyancy, of the fluid. The denser components fall, while lighter (less dense) components rise, leading to bulk fluid movement. In order to quantify natural convection, the dimensionless Rayleigh number is used and can be viewed as the ratio of buoyant and viscous forces times the ratio of momentum and thermal diffusivities.

In forced convection, fluid movement results from external sources (for example, a fan, pump, or the action of a propeller) or movement of the object in a fluid stream, and is typically used to increase the rate of heat transfer at a surface in cooling or heating applications. In cases of mixed convection, the rate of heat transfer due to natural convection and forced convection could be determined. The relative magnitudes of Rayleigh (Ra), Prandtl (Pr) and Reynolds (Re) numbers indicate dominant form of convection:

If $\frac{Ra}{PrRe^2} \gg 1$, natural convection dominates, forced convection is neglected.

If $\frac{Ra}{PrRe^2} \ll 1$, forced convection dominates, natural convection is neglected.

If $\frac{Ra}{PrRe^2} \simeq 1$, mixed convection occurs, neither forced or free convection dominate, so both are taken into account.

In eqn. (3.65), q_s'' , T_s, and T_{ref} are fundamental in nature, while the heat transfer coefficient is a constant of proportionality that relates the three fundamental parameters. While q_s'' and T_s are unambiguous, there is some latitude in the choice of the fluid temperature T_{ref}. Depending upon the choice of T_{ref}, the heat transfer coefficient is different in order to satisfy eqn. (3.65). Therefore, heat transfer coefficients cannot be defined without also defining a reference temperature; there is infinite number of heat transfer coefficient and reference temperature combinations that give the same surface heat flux. The standard wall functions (SWF) approach is the conceptual centerpiece for modeling convective heat transfer at the wall for turbulent flows in STAR-CCM+ (STAR-CCM+

Manual, 2016). Based on this, the expression for local surface heat flux is given as:

$$q_s'' = \frac{\rho_f(y_c)C_{p,f}(y_c)u_\tau}{T^+(y^+(y_c))}(T_s - T_c) \qquad (3.66)$$

In this equation:

- ρ_f is the fluid density

- $C_{p,f}$ is the fluid-specific heat capacity

- u_τ is a velocity scale that is based on the wall shear stress

- T^+ is the dimensionless temperature

- $y^+ = (u_\tau y_c)/v_f$ is Reynolds number

- y_c and T_c are the normal distance and temperature of the near-wall cell, respectively

Four different heat transfer coefficients are defined in STAR-CCM+:

- Specified y+ heat transfer coefficient

- Heat transfer coefficient

- Local heat transfer coefficient

- Virtual local heat transfer coefficient

These heat transfer coefficients are all grounded to varying degrees in the standard wall function treatment. The local heat transfer coefficient is the one that is used internally within the STAR-CCM+ solver. The other three heat transfer coefficients are computed during post-processing. In the case, of multi-phase flow, volume-fraction-weighted versions of these heat transfer coefficients and reference temperatures are defined for use

with co-simulation or coupling to other CAE codes (STAR-CCM+ Manual, 2016). Of these, the two that are used for the current work includes:

- Specified y+ heat transfer coefficient
- Heat transfer coefficient

This was chosen based on the current work and specific guidelines provided in the STAR-CCM+ manual.

For the specified $y+$ heat transfer coefficient STAR-CCM+ calculates the heat transfer coefficient as in local heat transfer coefficient, but at a user-specified $y+$ value instead of the value that is associated with the near-wall cell. This is given as:

$$h = \frac{\rho_f(y_c)C_{p,f}(y_c)u_\tau}{T^+(y_{user}^+)}$$

(3.67)

Using the surface heat flux as calculated in eqn. (3.66), eqn. (3.65) is solved for the reference temperature and is computed as:

$$T_{ref} = T_s - \frac{q_s''}{h}$$

(3.68)

The other heat transfer coefficient used in the current work, calculates the surface heat flux using eqn. (3.66), and then recasts eqn. (3.65) as:

$$h_3 = \frac{q_s''}{T_s - T_{ref,3}}$$

(3.69)

This heat transfer coefficient is calculated using a user-defined reference temperature (T_{ref}). The result from both the types of heat transfer coefficients is a pair of (h,T_{ref}) that could then be viewed or exported as boundary conditions for other codes.

3.10.2 Modelling Thermal Radiation:

Thermal radiation is the emission of electromagnetic waves from all matter that has a temperature greater than absolute zero, and represents a conversion of thermal energy into electromagnetic energy. It is generated by the thermal motion of charged particles in matter, which results in charge acceleration and dipole oscillation. This drives the electrodynamic generation of coupled electric and magnetic fields, which cause the emission of thermal radiation. For most heat transfer applications, thermal radiation can be treated as unpolarized (multiple reflections and scattering usually nullify polarization effects) and incoherent (waves or photons are usually out of phase). The length scale for transport is usually much larger than the wavelength of radiation, so the limiting description of geometric optics (that is, the wavelength approaches zero) can be applied and the waves are described as bundles of rays carrying energy in a small volume that is associated with the solid angle in the direction of the rays.

The maximum flux at which radiation can be emitted from a surface is given by the Stefan-Boltzmann law:

$$\dot{q_{bb}}'' = \sigma T_s^4 \tag{3.70}$$

In this expression, $\dot{q_{bb}}''$ is the local surface heat flux, T_s is the temperature of the surface and σ is the Stefan-Boltzmann constant given as $\sigma = 5.67 \times 10^{-8}$ W/m^2 K^4.

The heat flux is given by,

$$q_\varepsilon'' = \varepsilon q_{bb}'' = \varepsilon \sigma T_s^4 \tag{3.71}$$

where $0 \leq \varepsilon \leq 1$ is the surface emissivity.

Modelling the thermal radiation in STAR-CCM+ requires the selection of:

- Radiative transfer model
- Radiation spectrum model

The radiative transfer model defines the overall solution method for the governing Radiative Transfer Equation (RTE), including how the RTE is discretized with respect to space and solid angle. While the radiation spectrum model defines how the radiation wavelength spectrum is considered (and potentially discretized) within the context of the transfer model.

The radiative transfer model consists of two models:

- Surface-to-Surface (S2S) radiative heat transfer for modelling non-participating media radiation.
- Participating Media Radiation (the Discrete Ordinates Method, or DOM).

Similarly the radiation spectrum model consists of:

- Gray Thermal Radiation for modeling wavelength-independent radiation properties.
- Multiband Thermal Radiation for modeling wavelength-dependent radiation properties.

For the current work S2S is chosen for the radiative transfer model and Gray thermal radiation model is chosen as the spectrum model.

S2S (Surface-to-Surface) Radiation simulations concerns only the radiating and absorbing surfaces, not any intervening medium. The medium that fills the space between the surfaces is non-participating. That is, it does not absorb, emit, or scatter radiation. Under these circumstances, the radiation properties and the thermal boundary conditions that are imposed on each surface uniquely define the amount of radiation that a surface receives and emits. The surface properties are quantified in terms of emissivity, reflectivity, transmissivity, and radiation temperature. These properties are not dependent on direction; however, when using the Multiband Radiation model they can be dependent on radiation wavelength. The S2S Radiation model relies on:

- A spatial discretization of the boundary surfaces into patches.
- View factors that quantify, for each patch, the proportion of surface area that the other patches illuminate.

View factors are calculated from non-diffuse surfaces to other partially diffuse surfaces, but not the other way round. The net radiant flux on each surface is a function of the surface properties, the thermal boundary conditions that are imposed on that surface, and is calculated so that radiation is balanced. The radiation balance is enforced on the entire closed set of surfaces, by considering each surface and how it exchanges radiation with all other surfaces. Details regarding the calculation of view factors are specified in the STAR-CCM+ Manual.

For the gray thermal radiation model, radiation is said to be gray, when radiation properties are invariant with wavelength. The radiation properties are taken to be same over the entire thermal spectrum, and only a single radiative transfer solution is necessary for the full thermal spectrum. This means that the full thermal wavelength domain is considered as a whole, and all radiative properties are considered invariant within this single spectrum. More details pertaining to this is provided in the STAR-CCM+ Manual.

3.11 Conclusion:

A commercial code GT-SUITE is used as a part of the present study to model the engine and exhaust system in 1D for internal fluid flow and heat transfer in the exhaust system. The model is then used to simulate steady state WOT and transient drive cycle for investigating the heat transfer characteristics and predicting the skin temperature. In the second phase of the study a commercial code STAR-CCM+ is used to simulate the external flow over and heat transfer for a full scale vehicle in 3D. A RANS based Realizable k-ε model with a two layer approach is used to model the turbulence. Gravity and radiation models are used to model free convection and thermal radiation.

Chapter 4

1D GT-Power Model for Steady State and Transient Simulations

4.1 Introduction to Steady State Wide Open Throttle (WOT) and Transient Simulations:

Before launching a detailed investigation into the heat transfer characteristics and skin temperature prediction, the 1D model has to be validated with available test results. As a first stage of the work a set of steady state WOT simulations were carried out to validate the build of the 1D model. Based on the validation with test data, the model is then modified and tweaked for the simulation of a transient drive cycle. The results from the transient tests are then validated again with the aerothermal vehicle test data. In this chapter details pertaining to both the steady state and transient tests are described.

4.2 Steady State Simulation Setup:

In this section the 1D modelling and simulation set up for steady state WOT simulations are presented. Modelling an internal combustion engine as well as exhaust system from scratch is very time consuming due to the large information required regarding engine characteristics, intake and exhaust systems, cylinder geometry, valves, fuel injection system. Further information pertaining to heat loses as well as combustion has to be accounted for. In order to perform the required task in the current work, FCA has provided an initial model of engine and exhaust system resulting from previous analysis and studies performed by the company involved in both Canadian and American sides. This model provides a complete description of a 3.5L V6 engine from the intake, all the way to the tailpipe.
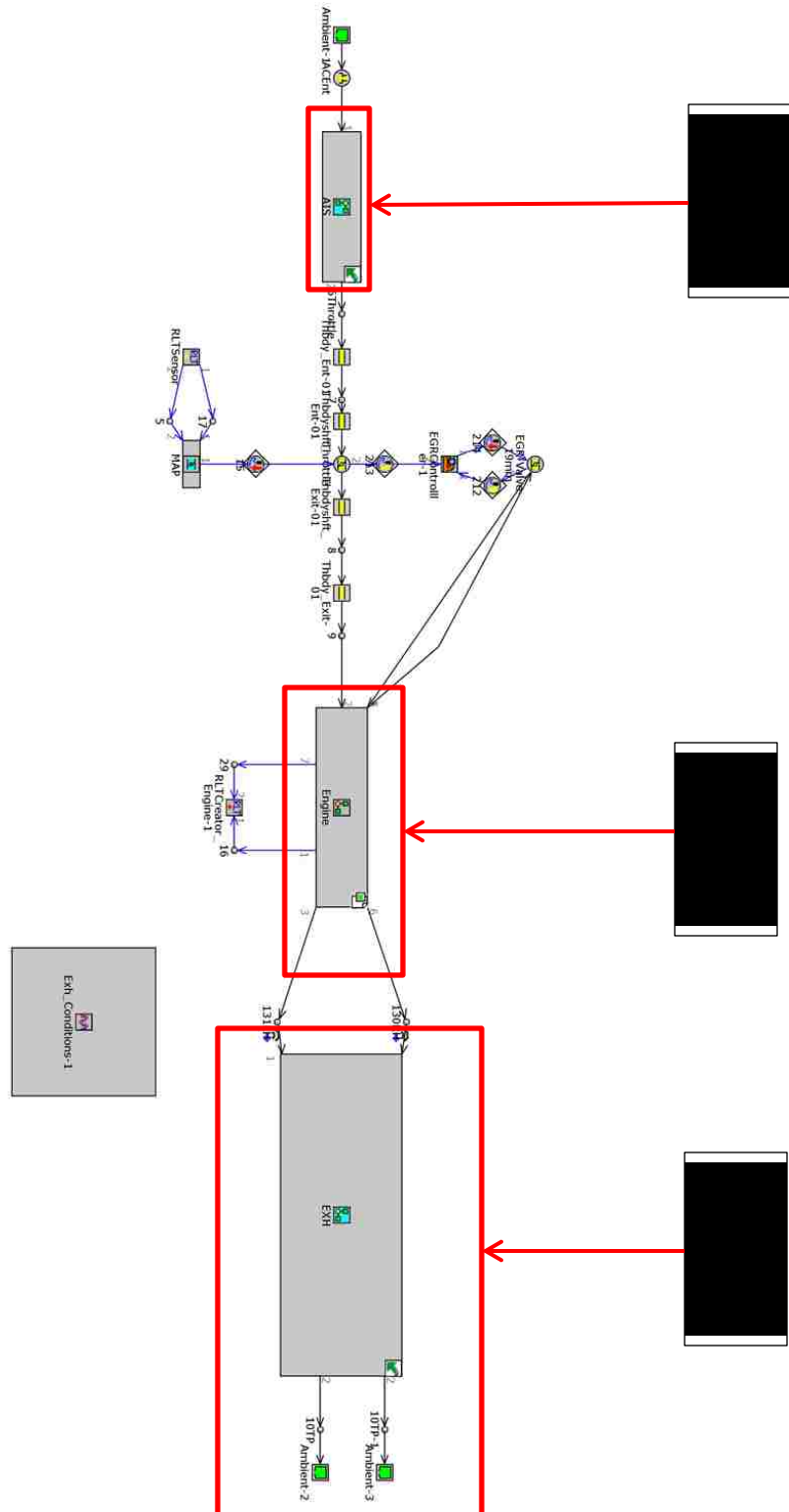
Figure 4.1 Engine and exhaust model used in the current study

Exhaust downpipe
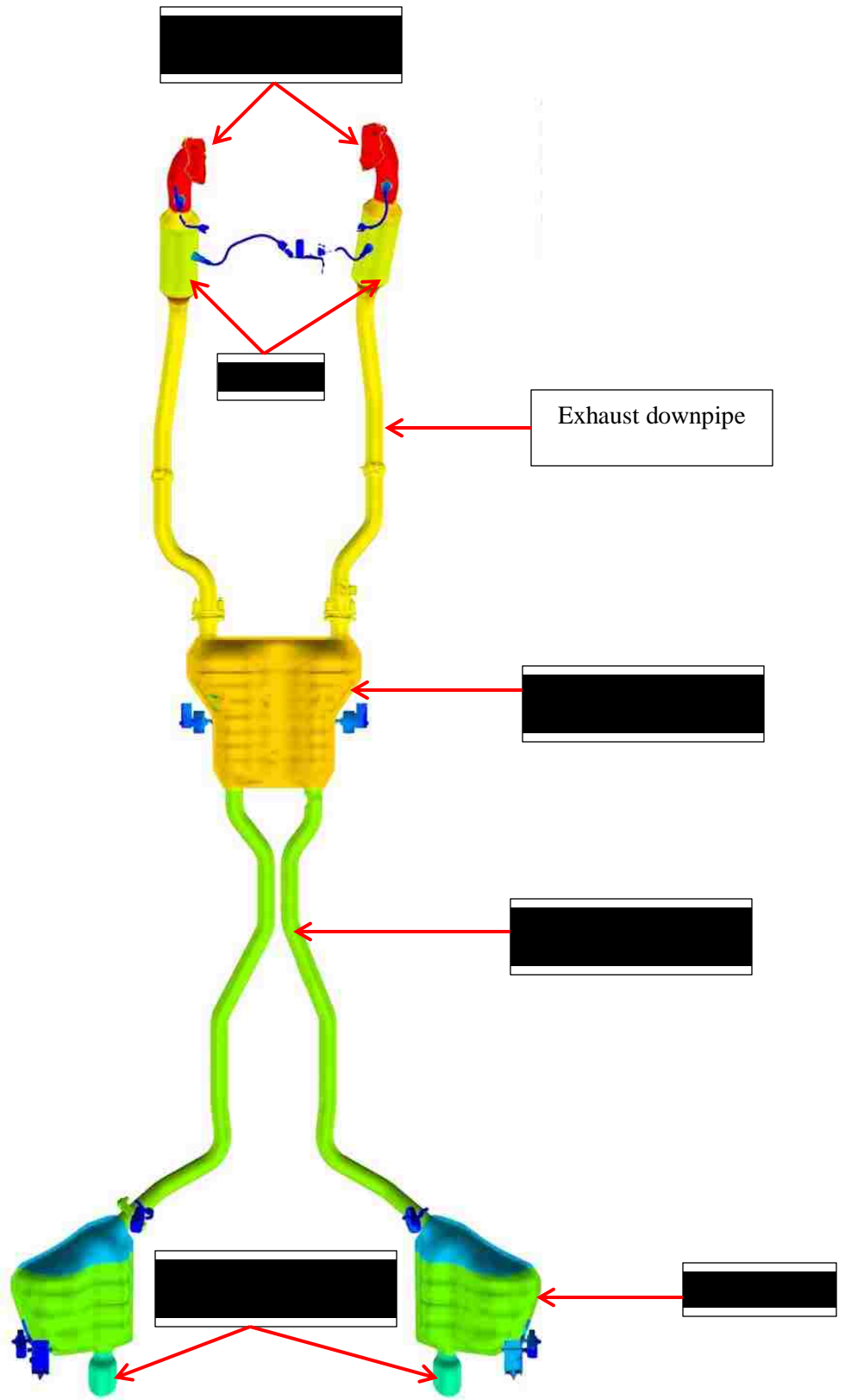
Figure 4.2 Exhaust system for current study
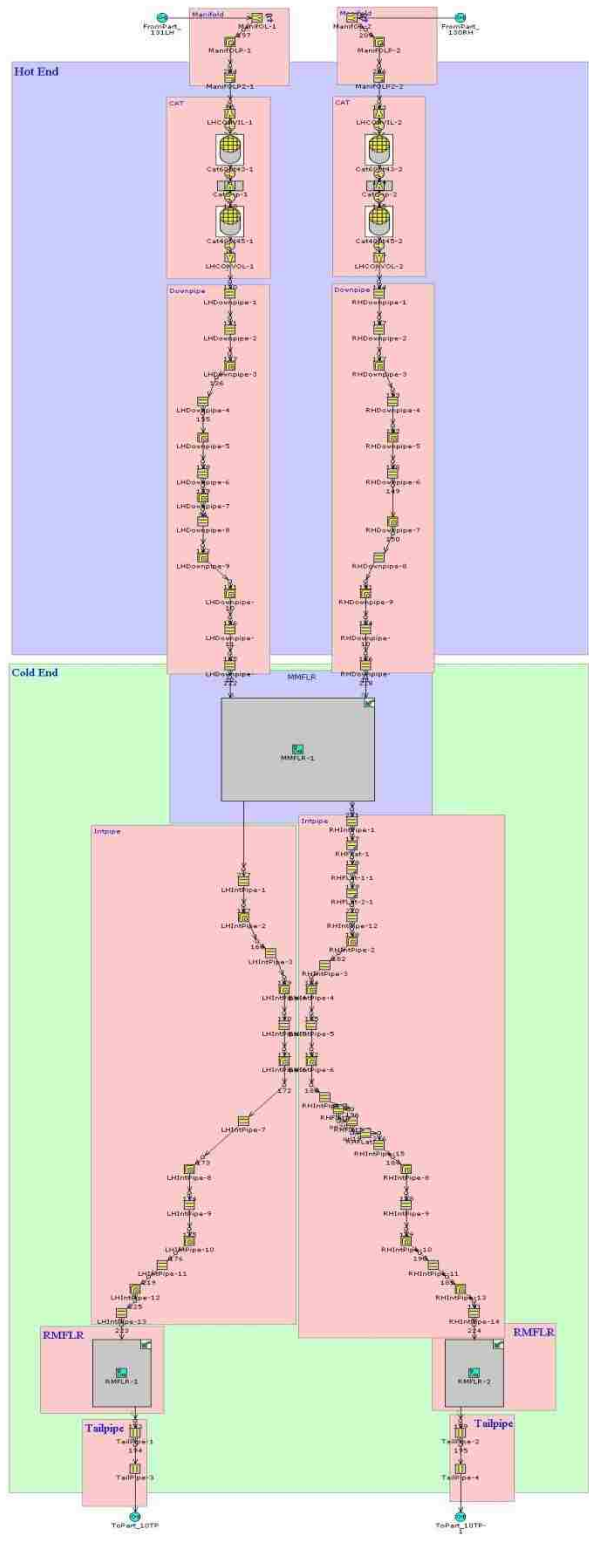
Figure 4.3 1D model of exhaust system for current study

The base model of the engine and the exhaust are shown in the Figures 4.1 and 4.3 respectively. The detailed set up for the engine model will not be described in detail as the focus is mainly on the exhaust system for skin temperature prediction.

Figure 4.2 shows the exhaust system for the current study. This type of configuration is known as a dual exhaust. The vehicle utilizing the engine and exhaust is equipped with a 4-wheel drive. Hence the engine is mounted in the North-South configuration. The manifold and the CAT are in the underhood region of the vehicle whereas; the components after the CAT are underbody of the vehicle. In the study, the exhaust pipes connecting the CAT and the resonator is called as the downpipe. The exhaust pipes connecting the resonator and the muffler is called the intermediate pipe. The region consisting of manifold, CAT and the exhaust downpipe is denoted as the hot-end. The region after the resonator is denoted as the cold-end. Figure 4.3 shows the exhaust system in 1D model. It can be seen that the components are divided into several subvolumes. Each subvolumes are then discretized further to solve the Navier-Stokes equations in one-dimension. Further the flow in the exhaust pipes is treated to flow in a pipe. Some of the details required for the computation include, the discretization length for the exhaust, the diameter of the exhaust pipes, heat input rate for the CAT, and material thermal properties etc. These data have been included in the model provided by FCA. Thermal masses such as flanges and bellrod are not included in the current model.

For the WOT simulations an explicit solution method is chosen. This option is used when capturing the wave dynamics in the system is important, since the complete engine is used. Further, this provides crank angle resolved results, since the simulations are run for steady state. Both the flow and the thermal solver are set for steady state. By setting the solvers to

steady state, the simulations run until the flow convergence is attained. However the number of cycles for the simulations is set to 30. 15 cases have been considered , and they cover different engine speeds ranging from 1200 RPM to 6800 RPM, all at WOT. These RPM ranges produce mass flow rates close to bench test data, used for validating the model. These have been presented in Table 4.1.

Engine speed (RPM) for simulation	Mass flow rate of exhaust gas for simulation (g/s)	Mass flow rate of exhaust gas from test data (g/s)
1200	39.07	22.3
1600	49.33	29.4
2000	72.92	35.6
2400	85.49	58.3
2800	98.59	75.0
3200	114.99	81.8
3600	132.28	92.9
4000	153.85	104.5
4400	169.56	121.1
4800	187.35	140.9
5200	206.14	157.6
5600	220.71	173.3
6000	234.49	193.1
6400	244.96	207.6
6800	252.83	215.4
		224.2

Table 4.1 Comparison of engine speed and corresponding mass flow rates of simulation with test data

Three different cases are simulated, shown in Table 4.2. Two cases utilize a user defined empirical correlation for estimating the gas side heat transfer. While the third utilizes the default correlation empirical correlation used by the software. The first case uses the universal heat transfer correlation (UHT) from the literature as mentioned in Chapter 2 to account for the gas side heat transfer. The second case uses the Sider-Tate correlation used by Wendland (1993) along with the CAF values of 2.3, 3 and 1.6 for the manifold takedown and tailpipe portion. The third case doesn't use any user defined empirical correlation and instead uses the default correlation (Chapter 3) for gas side heat transfer.

Case	Empirical Correlation	CAF values used
Case-1 Universal heat transfer (UHT) correlation	$Nu = 0.07Re^{3/4}$	2.3, 3 and 1.6 for manifold, takedown and tailpipe respectively
Case-2 Wendland heat transfer (WHT) correlation	$Nu = 0.027Re^{0.8} * Pr^{1/3}$	2.3, 3 and 1.6 for manifold, takedown and tailpipe respectively
Case-3 No user defined correlations	n/a	n/a

Table 4.2 Simulation cases used in the current study

By default the software controls the convergence of mass flow, pressure and temperate. Steady state is reached for all those quantities. The simulation is considered converged and automatically shut-off. In general when the fractional variation with respect to the previous

cycle is lower than a certain value, and when this condition is repeated for two or more cycles, convergence is reached.

4.2.1 Results and Discussion:

In this section, results pertaining to simulation of WOT cases will be discussed. The WOT cases are compared with flow bench test data consisting of the same exhaust system. The tests were performed by FCA before this study for various exhaust gas mass flow rates. The results from these tests were obtained from FCA and were used to compare the simulation results. However, the simulations were performed for different RPM ranges producing mass flow rates close to the test data. Figure 4.4 shows the plot of gas temperature at the manifold inlet using the mentioned empirical correlations along with the experiments for WOT. The simulation results show considerable variation from the experiment at low and high mass flow rates. There is a good match at the between low and high mass flow rates. Clearly there is very minimal difference between the gas temperature predicted for the cases with and without the correlation. This might be due to the fact that the effects of these correlations aren't induced until the flow reaches the downstream of the manifold. Further the match at the mid rpm ranges could be due to the fact that the effect of engine induced pulsation is lower compared to the low and high rpm ranges.

Figure 4.5 shows the gas temperature comparison before resonator. Here in too, the results with the empirical correlations provide a good match with the experiments. The case without any empirical correlation highly over predicts the gas temperatures. This is due to the fact that, the commercial code GT-Power uses Colburn analogy for calculating the internal heat transfer coefficients. Whereas, the empirical correlations used in the current

work are based on Sider-Tate correlation. The Sider-Tate correlation is an implicit function since, it analyses the system as a non-linear boundary value problem. The results from this correlation could be more accurate due to the nature of the problem.
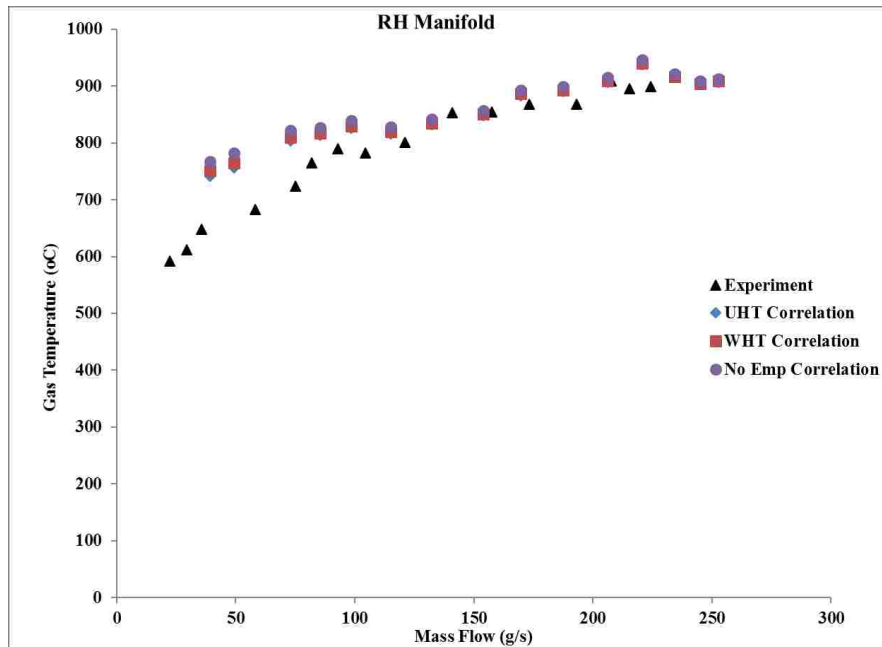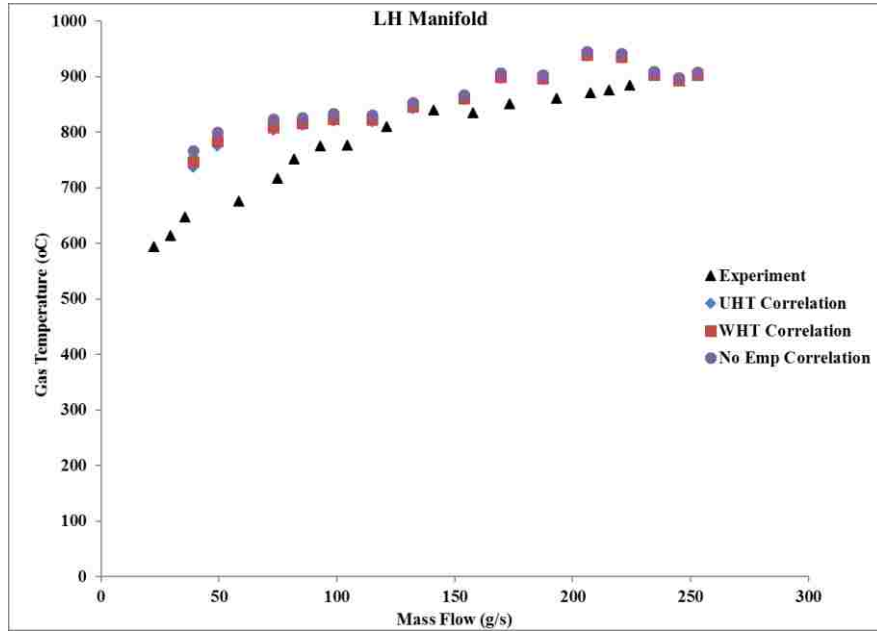
Figure 4.4 Gas temperatures at left and right manifold inlet

Figure 4.6 Show the results at the location after the resonator. The case with UHT correlation provides a very good match with the experiment. The WHT correlation provides a good match at the lower rpm ranges, but over predicts the gas temperatures between 10-15ºC.
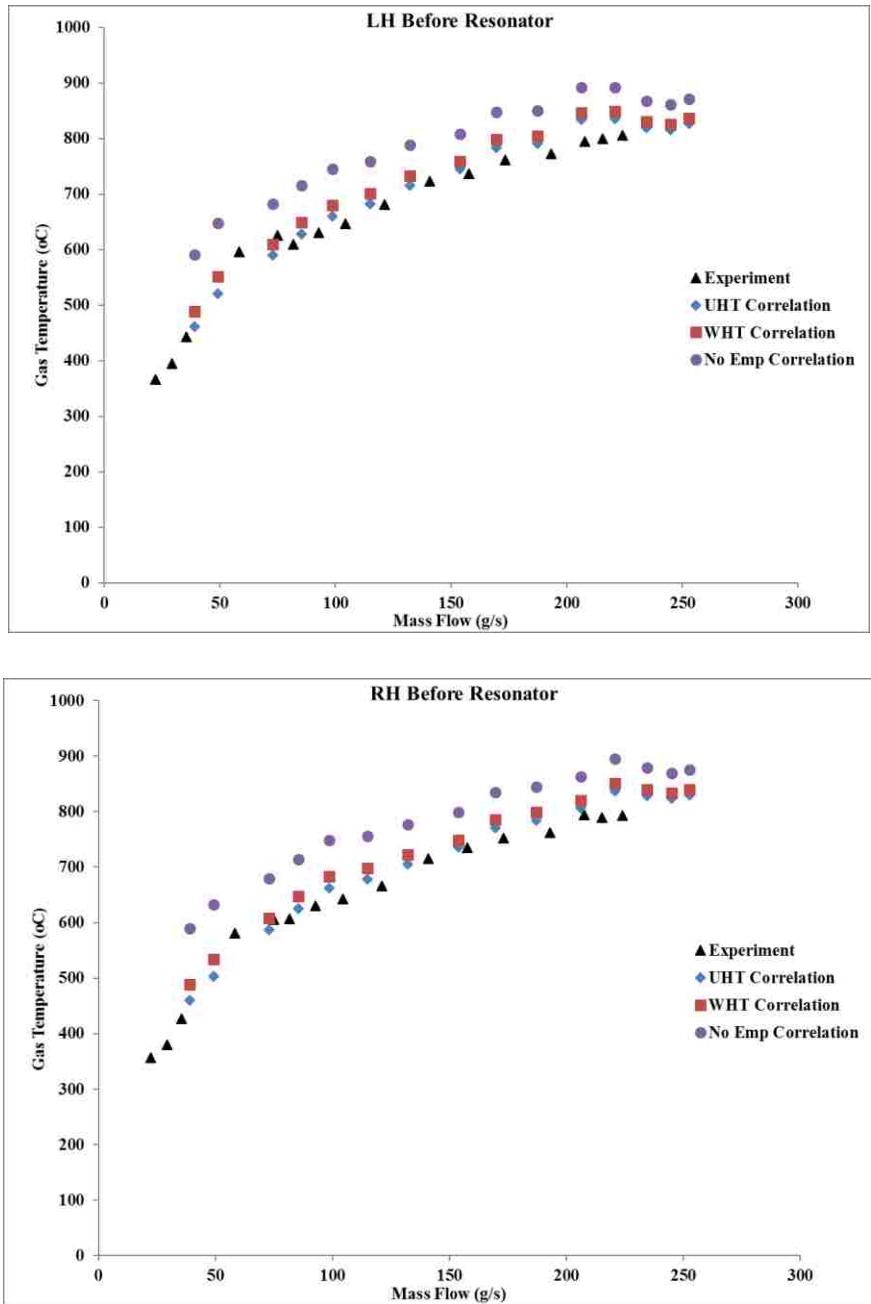
Figure 4.5 Gas temperatures at left and right before resonator

This might be primarily due to the effect of turbulence. Since the point of measurement is close to the exit of resonator, the highly turbulent nature of the flow has been captured by the universal heat transfer correlation.
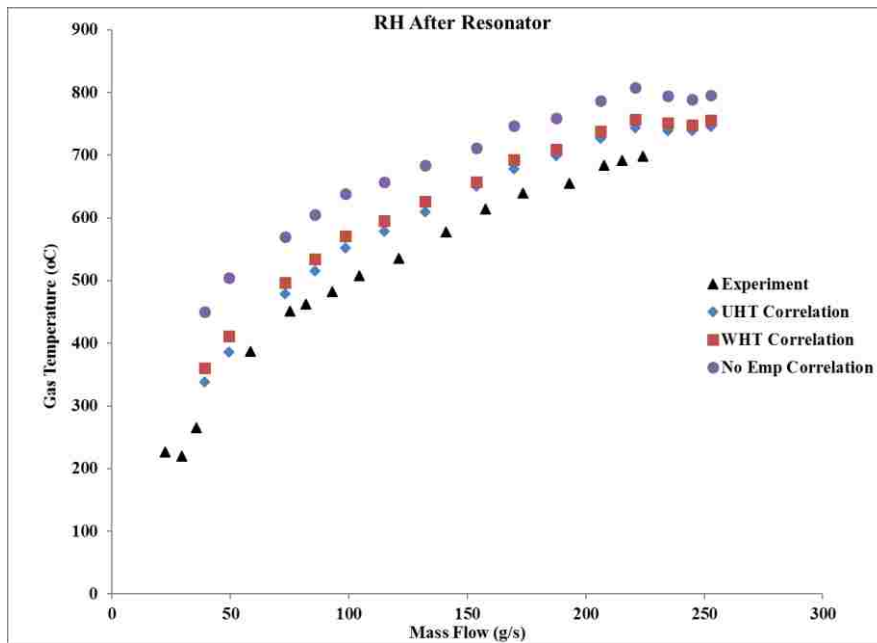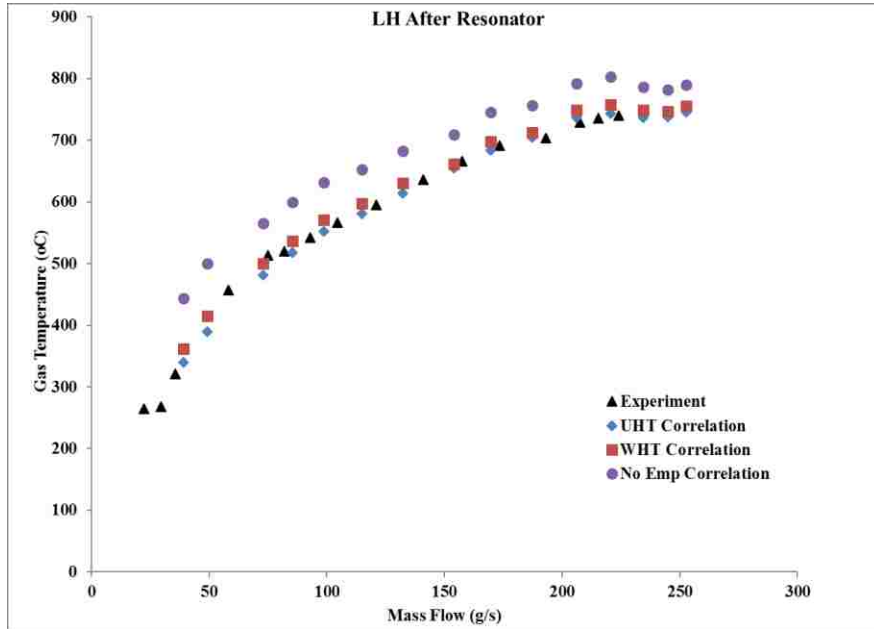
Figure 4.6 Gas temperatures at left and right after resonator

A similar trend of results could be seen for gas temperatures before and after the muffler as shown in the Figure 4.7 and 4.8.
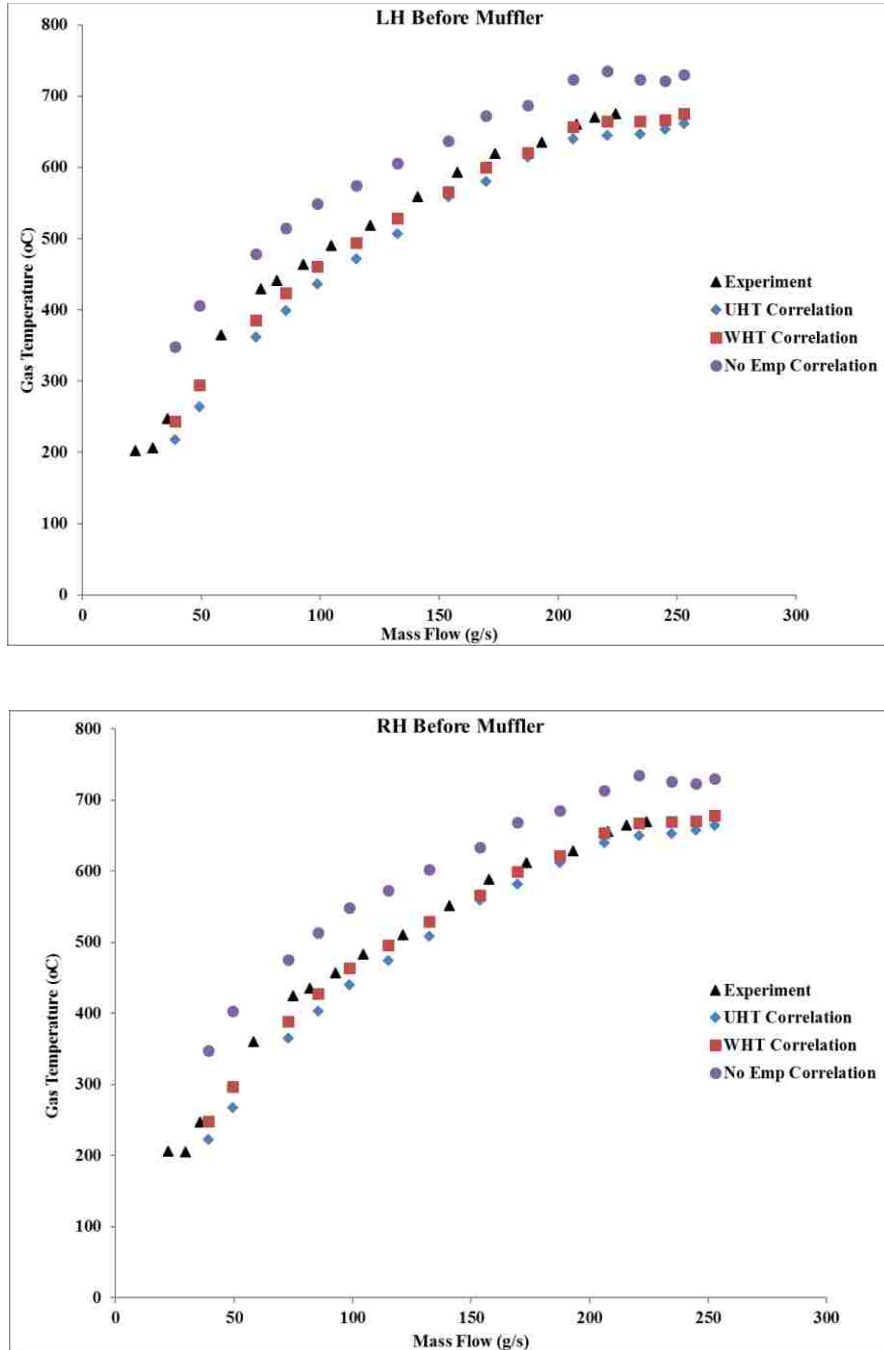
Figure 4.7 Gas temperatures at left and right before muffler
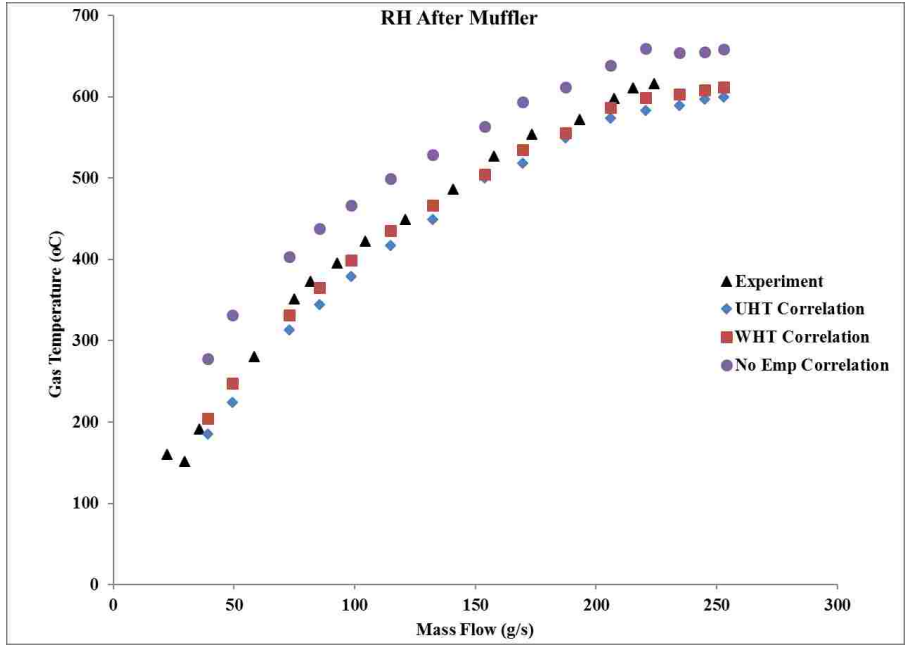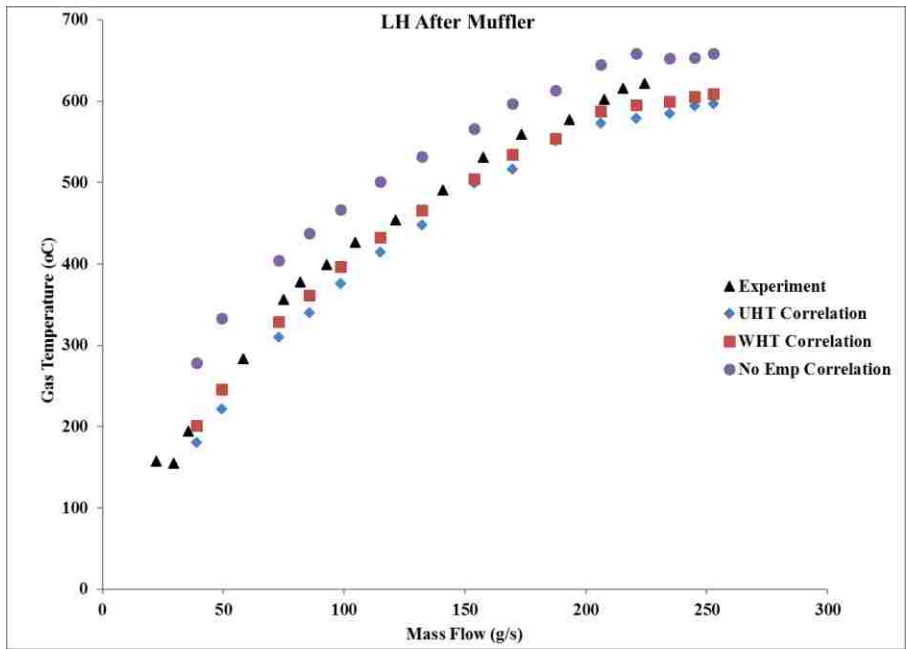
Figure 4.8 Gas temperatures at left and right after muffler

Previous information regarding the definition of CAF is sparse. A parametric study was carried out to evaluate the individual contribution of CAF along with and without WHT correlation. These CAF values are the same used in the WOT cases. Results indicate that

using only CAF values instead of using it along with the correlation over predicts the gas temperatures by 20-25°C up to the muffler. For the locations before and after the muffler it matches well with the experiments. This signifies that the CAF is as important as the empirical correlation. However, the optimum value of CAF for the current problem is yet to be identified, as this might vary due to lot of factors such as the boundary conditions pertaining to external heat transfer. Other geometrical factors such as the variation in diameter have to be studied for external skin temperature prediction.

4.3 Transient Simulation:

The following sections elaborate the simulation set-up and discussions pertaining to transient drive cycle simulations. The same engine and the exhaust model used in the steady state wide open throttle are used for the transient simulations. However there are some inclusions to account for the variable CA50 and 10 to 90 data, Manifold Absolute Pressure (MAP) values, variable valve timing data for intake and exhaust valves etc. These will be briefly explained in the following subsections.

4.3.1 Simulation Setup:

The transient drive cycle used for the current study is a Davis dam test cycle. The driving cycle is similar to the test standards provided in SAE J2807 standards with a small difference. The towing and trailer conditions are not accounted for in the current study. The drive cycle based on the actual vehicle driven in the test location is shown in Figure 4.9. The cycle consists of an approach segment where the speed is more or less constant. The grade portion is from 15 mins and 38 mins where the speed and the load varies significantly. In the cooldown portion the vehicle is in a complete standstill condition. In

order to simulate the entire transient drive cycle, further information pertaining to the actual vehicle in the chassis dyno tests were required as an input. Some of these include engine speed, fuel air ratio, MAP values, intake and exhaust cam centerline, variable valve timing data, spark timing, coolant temperature data etc. These were provided as input on the engine side for it to operate similar to the transient drive cell tests. A key difference of the current study from the previous ones is accounting for the heat transfer from the engine to the coolant as well as engine oil. There are no major additions of data for the exhaust side as the gas temperatures are dependent on the engine speed and the combustion parameters. For the preliminary simulations the external heat transfer coefficient is assumed based on the steady state test information. This data was obtained from FCA.
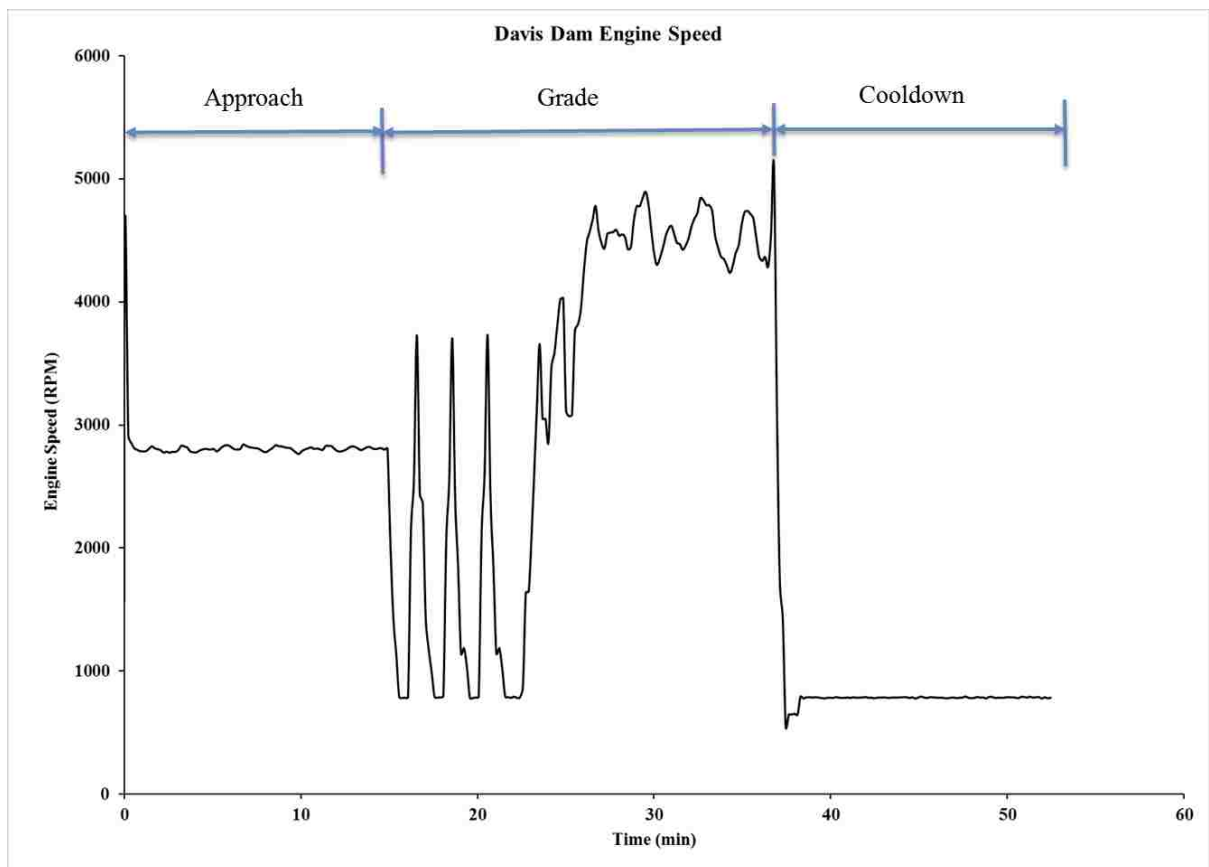
Figure 4.9 Engine speed representing Davis dam drive cycle

Due to the lack of drive cell data for all the locations on the exhaust, a select few were compared which are presented. The results discussed below are for the left side of the exhaust. The right side of the exhaust was compared and was of similar range as the left. For abbreviation of the dissertation, the results of the right side are not being presented here. The initial objective is to match the gas temperatures at the manifold, so that the exhaust system could be studied in detailed without having to refine the engine side of the model.

For the other external convection parameters such as the sink temperatures for convection and radiation were set to 310 K, identical to the drive cell test data. The values for the external emissivities were kept the same as the steady state simulations. With respect to the computational time, the transient simulation for one cycle was 8 days. This was due to the complexity of the model as the engine simulation is done for every crank angle degree for drive cycle. In order to reduce the computational time and increase the efficiency, the engine and exhaust were decoupled. Before the decoupling, quantities such as velocity, pressure, temperature and mass flow rate were exported when the engine and exhaust were coupled. These quantities were then used as inlet condition for the decoupled exhaust. Since the engine was decoupled from the exhaust, an implicit method was used for the transient simulation. This would allow the use of larger time-steps thereby reducing the simulation time.

Following this, the simulation time was reduced from 8 days to 3.5 hours for the entire transient drive cycle. In order to make sure that decoupling the exhaust didn't result in changes to flow and heat transfer downstream, the results from both the methods were compared.

The comparison showed negligible to no difference in any parameters from manifold, all the way to the tailpipe. Hence the decoupled model was then used for all the simulations. To validate the simulation results for transient simulations, experimental data from pre-conducted vehicle tests were obtained from FCA. The tests were conducted for a vehicle with the same engine and exhaust system as in the simulation model. These tests were run in a drive cell with a dyno for the Davis Dam drive cycle matching an actual field test scenario. Further the above-mentioned data was correlated by FCA before being used in further studies. The simulation results are compared with the drive cell test data for all the cases at each of the locations where the test data was available.

4.3.2 Results and Discussion:

In this section the results from the transient drive cycle are discussed. The results are based on the simulations using the decoupled exhaust model, since no significant difference was seen in any quantities from manifold to tailpipe. Figure 4.10 shows the manifold gas temperature. The result indicates good agreement with the test data. However, after the approach segment, the peaks corresponding to higher and lower RPM ranges are over predicted for the simulation. This is due to the fact that the thermal mass such as the flanges between the exhaust runners and the manifold haven't been accounted for. Similarly during the cooldown portion of the drive cycle, the temperature ranges seen in the simulation is well within 15°C. This could be considered as a good match for the entire drive cycle.
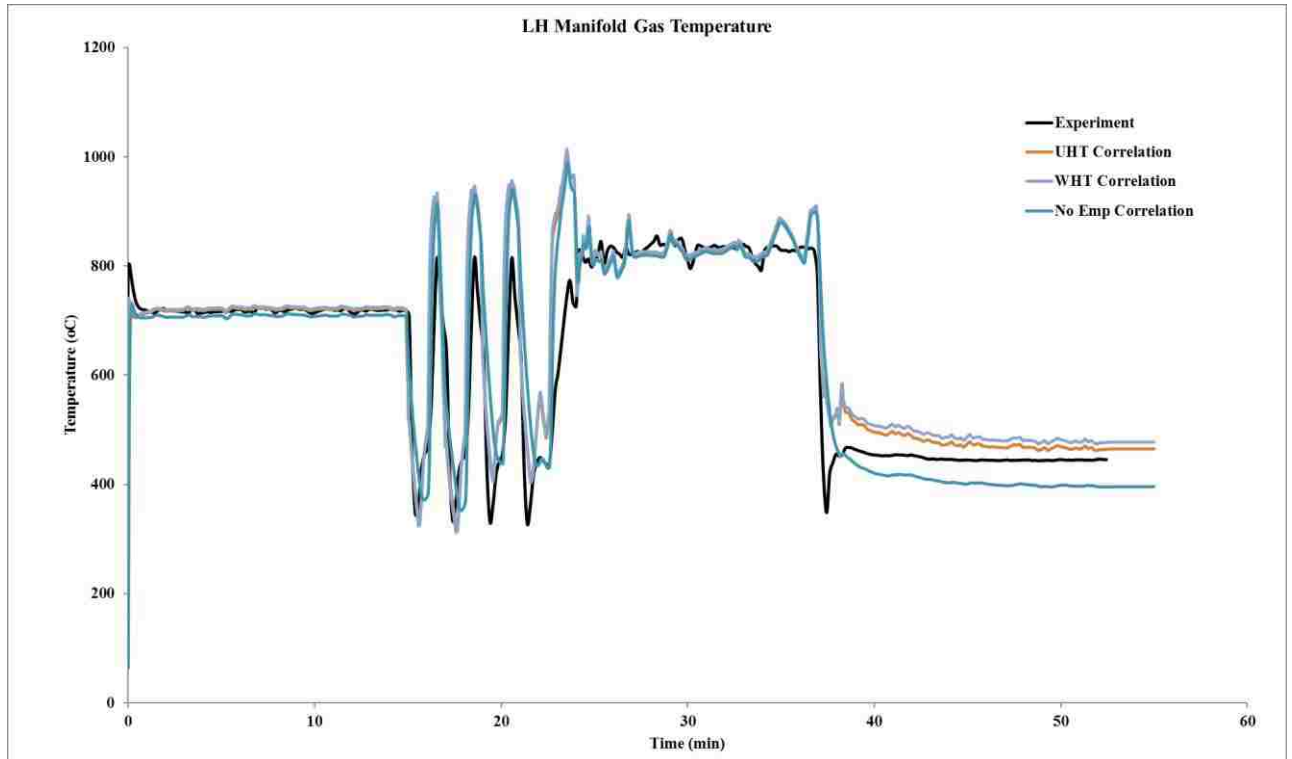
Figure 4.10 LH manifold gas temperature

The cases with empirical correlations and the one without any empirical correlation match with the test data. This is due to the fact that, the data is taken at the inlet to the exhaust manifold and there are no effects passed upstream of the exhaust affecting the manifold temperature. The addition of any empirical correlation does not take effect until the downstream of the manifold. Figure 4.11 shows the gas temperature at the left tailpipe. For the approach segment, both the WHT and UHT correlation under predicts the gas temperatures close to the test data. However there is severe under prediction for the grade portion of the drive cycle. This again could be due to the effect of the unaccounted thermal masses in the system after the resonator.
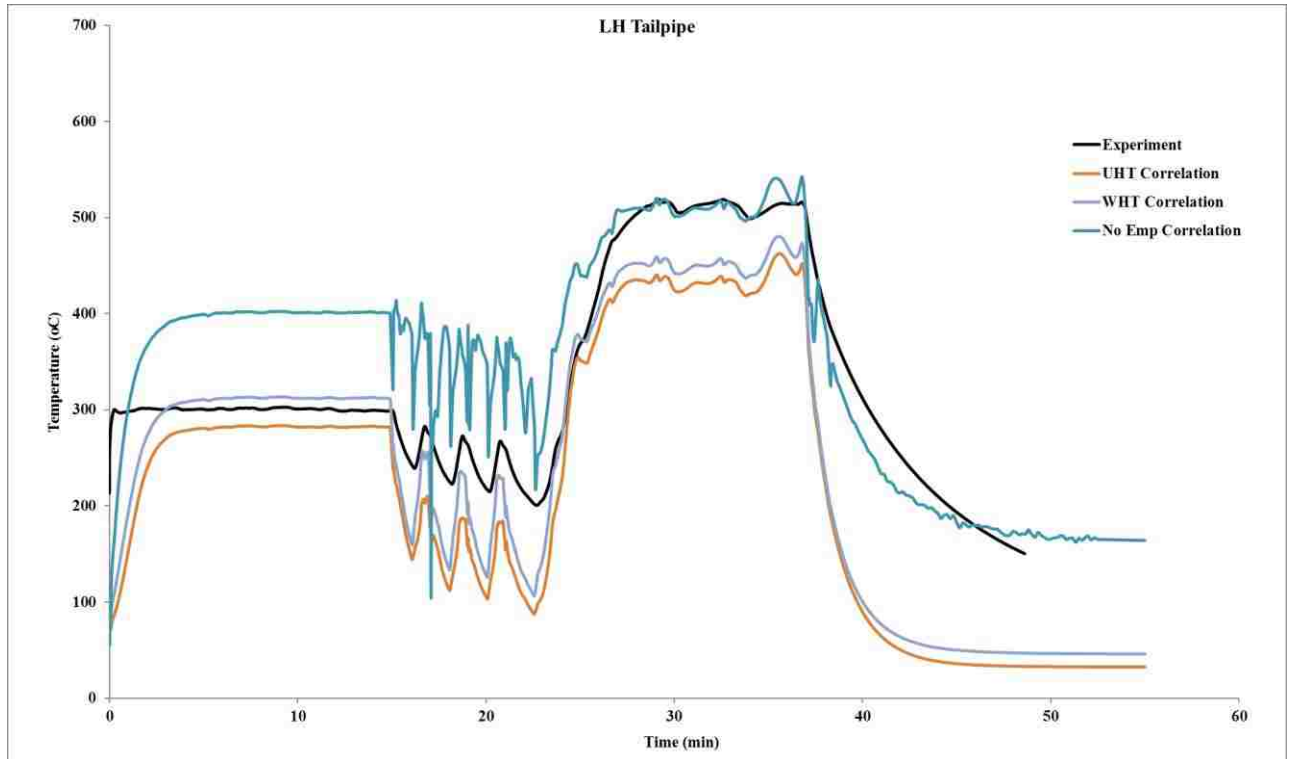
Figure 4.11 LH tailpipe gas temperature

Due to the lack of sufficient data it will be impossible to predict the start of the trend in the under prediction. In order to find an explanation for this behavior as well as study the gas side heat transfer in detail, the skin temperatures at the locations similar to the test data are compared. Figure 4.12 shows the manifold surface temperature. It can be seen clearly that the effect of internal flow correlations produce better gas side energy balance, thereby accurately predicting the exhaust skin temperature. Within this the UHT correlation is the most accurate for the approach as well as the grade and the cooldown. The WHT correlation under predicts in all the three segments of the drive cycle. The case without any empirical correlations highly over predicts the skin temperature in all the three segments of the drive cycle. This is due to the fact that the manifold gas temperatures were measured close to the inlet which neutralizes the effect of internal flow heat transfer correlations. However, the

72

manifold surface temperatures are measured partially downstream for both the test and simulations. The under prediction for the cooldown segment of the drive cycle could be due to the assumption of a constant heat transfer coefficient for the complete drive cycle.
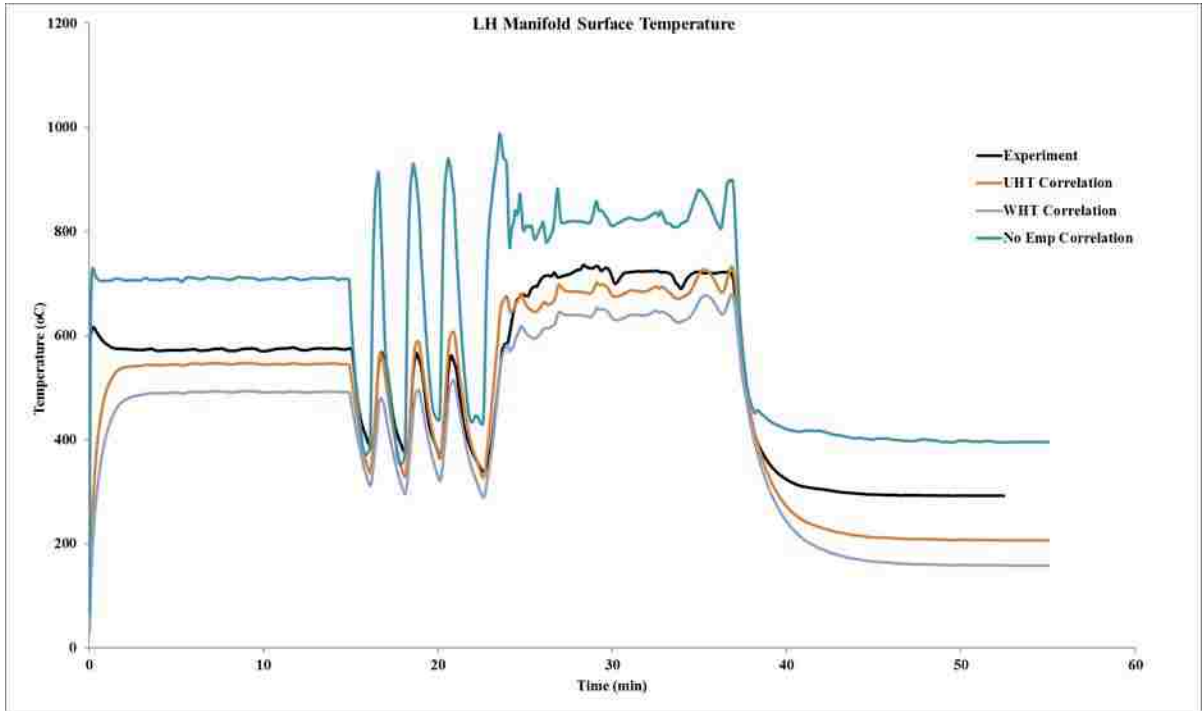
Figure 4.12 LH manifold surface temperature

As we proceed downstream of the exhaust Figure 4.13 shows the skin temperature before resonator. In the approach segment, both UHT and WHT correlation highly over predicts the skin temperature. The difference from the test data is about 70°C. The case without any empirical correlation highly under predicts the skin temperature in all the three segments. Though the difference in the approach is around 35°C, the difference in the grade portion is over 120°C. This again solidifies the argument for the need of internal flow heat transfer correlations.

For the cooldown segment all the three cases under predict the skin temperature. The behaviour indicating a sudden drop in the skin temperature indicates the lack of data for boundary conditions pertaining to the external heat transfer.

Similar behaviour is not seen for the manifold (Figure 4.12), since the manifold is present underhood of the vehicle. Further the effect due to the assumption of the heat transfer coefficient is minimum for the manifold due to the forced convection from the radiator fan. However a similar assumption for all the components underbody of the vehicle seems questionable.
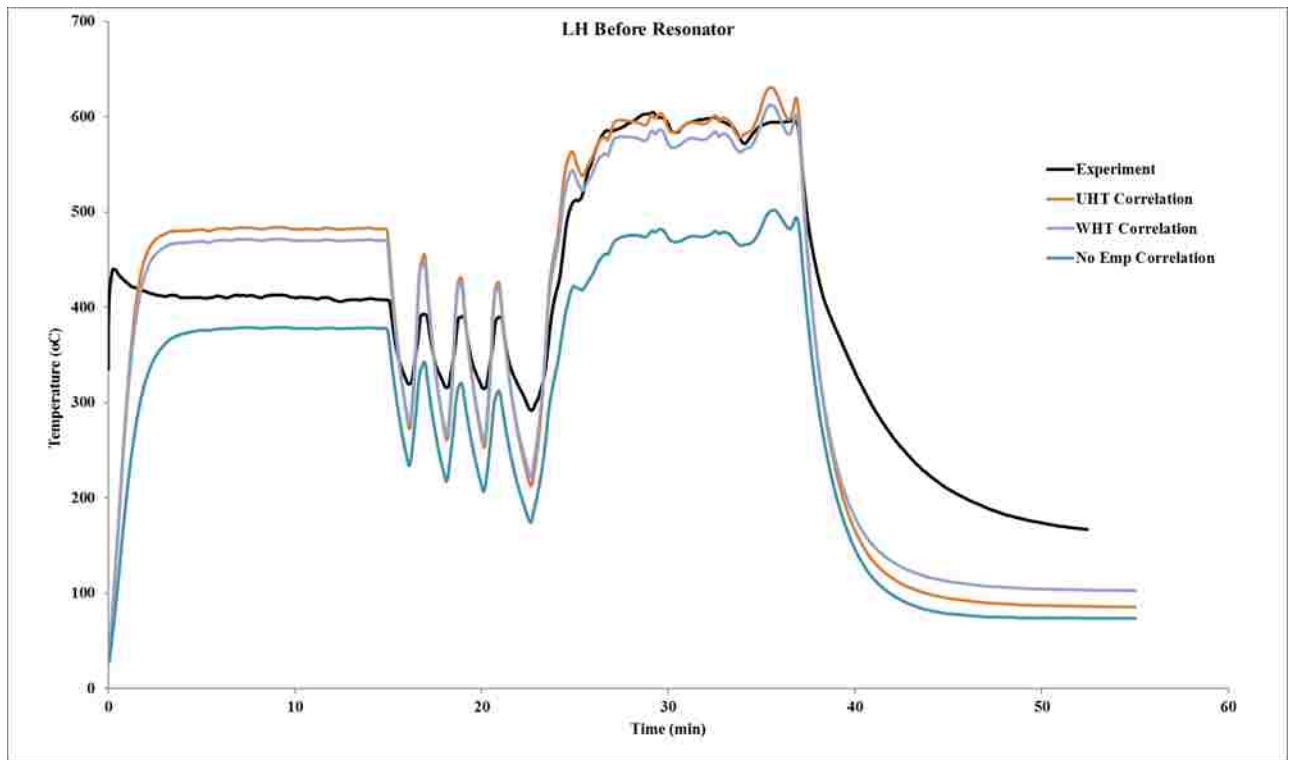
Figure 4.13 Exhaust skin temperature before resonator
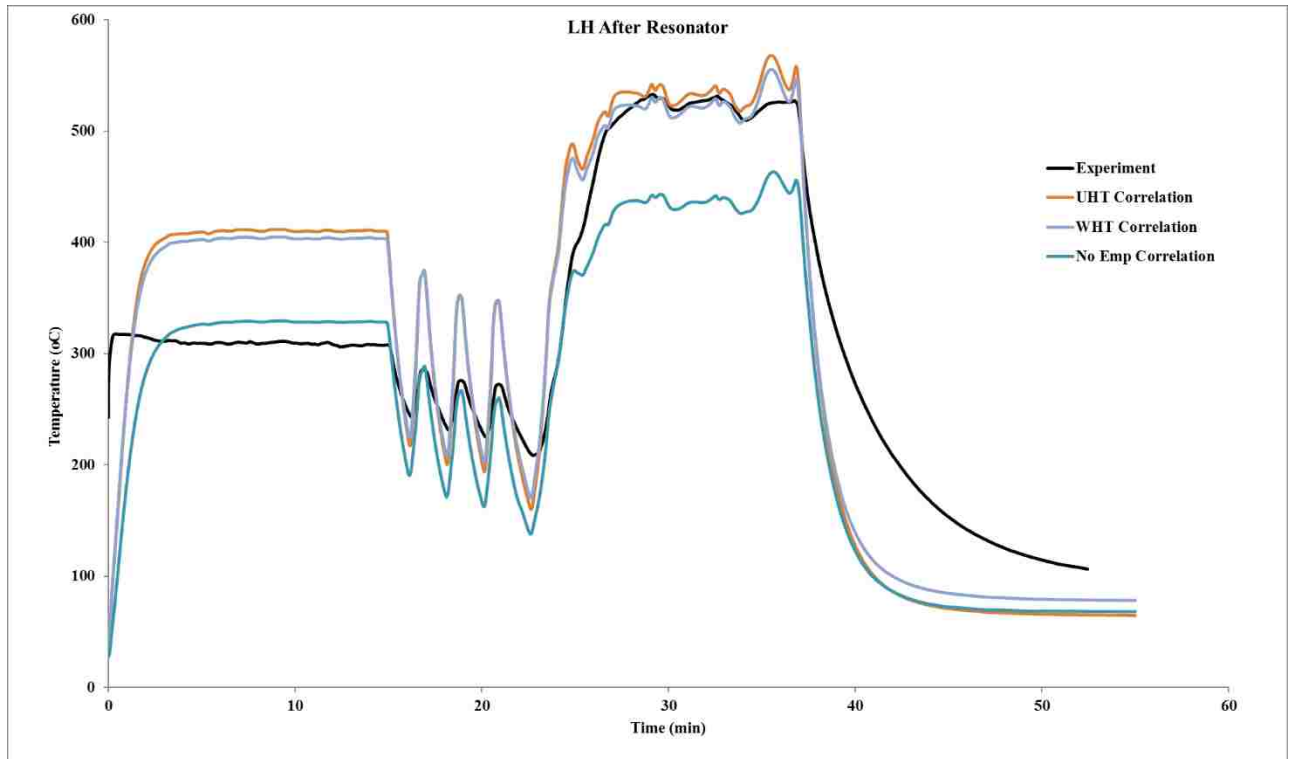
Figure 4.14 Exhaust skin temperature after resonator

Figures 4.14 and 4.15 presents the skin temperatures at locations after the resonator and before the resonator respectively. In the approach segment, both UHT and WHT correlations highly over predicts the skin temperature. The case without empirical correlation now starts to over predict the skin temperature. However, the difference for this case is less than 20°C. For the grade portion in figure 4.14, both the UHT and WHT correlation accurately predicts the skin temperature.

The differences seen in the peaks of the grade portion could again be due to the lack of thermal mass in the system. The minor differences seen in the peaks could be neglected, as the main objective of the work is to not only predict the skin temperature accurately, but also to develop an efficient procedure with minimized computation time and resources. For grade portion in Figure 4.15 both UHT and WHT correlation start to over predict the skin

75

temperature. Whereas, for the case without the empirical correlation, still under predicts the skin temperature. For the cooldown segment all the three cases not only under predict the skin temperature, but show a similar behaviour to the upstream locations.
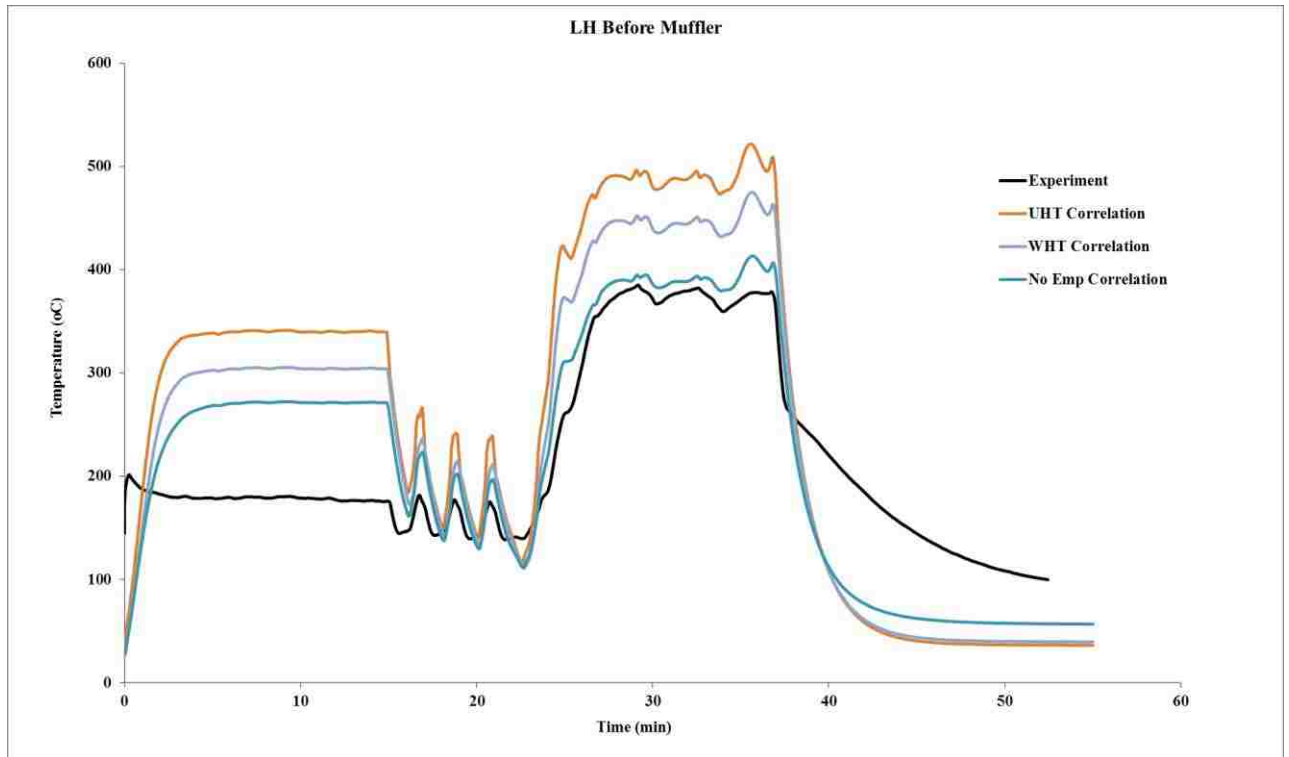
Figure 4.15 Exhaust skin temperature before muffler

4.4 Conclusion:

A 1D model containing the engine and exhaust system used for the study was modelled using GT-Power. Three different cases were simulated for WOT conditions to validate the model with the test data. The preliminary results indicate good agreement for both UHT and WHT correlations. The reason for the similarity in both the correlations being the use of WHT correlation data in the development of UHT correlation. The 1D model was then simulated for a transient drive cycle. The results from the transient simulation reveal significant overprediction of skin temperatures in the approach segment of the drive cycle.

76

Further, some initial assumptions were used for the external heat transfer such as the heat transfer coefficient. These assumptions were based on previous steady state tests. However, the lack of sufficient boundary conditions for the external heat transfer could be one of the reason for underprediction in the cooldown regions. Further the sudden overpredition of the skin temperature in the approach segment between the CAT and the resonator has to be investigated. This could be due to multiple reasons. First is the use of heat rejection rates for the CAT based on the steady state WOT simulations.

The available data for the heat rejection rates were from the start of the grade segment in the transient drive cycle. The software interpolates the data for the start and the end points based on the available data. However this has to be examined. The other reasons could be due to factors such as CAF values used, added thermal mass, and external heat transfer boundary conditions for convection and radiation. The exact reason cannot be concluded without the use of a CFD simulation to obtain the required boundary conditions for external heat transfer. A full scale vehicle level model delivering the necessary boundary conditions would be meaningful for further analysis. In order to proceed with this, a 3D vehicle level model is simulated using STAR-CCM+. The model is then integrated with 1D model for further study. Subsequent studies pertaining to this are described in Chapter 5.

Chapter 5

Prediction of Skin Temperature Using 1D Model and Vehicle Level 3D Model

5.1 Introduction:

As mentioned in the previous sections, in order to investigate the heat transfer characteristics in detail, the current work involves 3D simulation of a full scale vehicle level model along with the test section. The first set of simulations for the 3D model was carried out using the preliminary exhaust skin temperature data from the 1D simulation as a boundary condition. A numerical investigation using steady RANS equations with Realizable $k\text{-}\varepsilon$ with two layer approach was conducted to determine the external flow and heat transfer characteristics for the full vehicle. A heat exchanger model for radiator and moving reference frame (MRF) were used to model the front end flow and heat transfer. Three modes of heat transfer; forced convection, free convection and radiation were accounted to model the heat transfer. A K-Means Clustering algorithm was used to identify the best operating points to represent the drive cycle accurately. The operating points obtained using the algorithm was then used for steady state simulations.

Using the results from the simulation, a new process or methodology has been identified to predict the exhaust skin temperature. Optimum values for the available empirical correlations have also been suggested. Further the effect of radiation on the heat transfer characteristics is also justified.

5.2 Vehicle Level 3D Steady State Simulation Setup:

Figure 5.1 shows a schematic of the actual drive cell test section with dimensions corresponding to the vehicle tests. Insets show vehicle distance from the inlet of the drive cell. Initial CAD model of the vehicle with the test section was provided by FCA, Canada. The computational domain of the model is shown in Figure 5.2. The entire domain was split into six different regions consisting of condenser, radiator, radiator fan, transmission oil cooler, power steering oil cooler and an airstream. The airstream region along with the radiator fan is modelled as fluid region while the condenser, TOC and radiator are modelled as porous regions. The region airstream consists of the complete test section and the vehicle. Air with an ideal gas formulation is used as the fluid medium. For meshing, hexahedral cells were used for airstream, condenser, TOC and radiator, while polyhedral cells were used for the fan region. Individual mesh size values were specified for the six regions. Three prism layer cells were employed for resolving the wall effect. The prism layers were packed in a 0.01mm width with the stretching factor of 1.5. Figure 5.3 (a) and (b), shows the mesh of the vehicle model. A velocity inlet and pressure outlet boundary condition was specified for the inlet and outlet of the domain. All the other boundaries within the airstream such as the vehicle was set as no-slip wall. For the porous region, inertial and viscous resistance were specified as an axisymmetric tensor. For the fan, a Moving Reference Frame (MRF) was used to account for the rotation of the radiator fan.

A K-means clustering algorithm was used to partition the entire transient drive cycle into a set of cluster points to be used for steady state simulations. Figure 5.4 shows the K-means clustering methodology, to obtain the steady state wind speed points that would give a best representation of the transient drive cycle. From the K-Cluster simulations it was seen that

the change in total sum of distance point-to-centroid was negligible after nine clusters. Hence nine cluster points were considered sufficient for the steady state simulations using the above mentioned algorithm. Six additional speed points were chosen to divide the wind speed to an interval of 5mph. Since 0mph for a vehicle stand-still condition is less possible to simulate, wind speed of 1.5mph was chosen as the lowest wind speed. The wind speed points obtained from the clustering algorithm along with additional wind speed points are presented in Table 5.1. These windspeeds are then used in the velocity inlet condition for steady state simulations.

Cluster#	Selected Wind Speed Points (mph)	Additional Speed Points (mph)
1	46.2	30, 37.7
2	24.89	-
3	57.29	-
4	47.29	19.29
5	55	-
6	49	-
7	35.7	-
8	5	1.5, 9.6, 17
9	52.2	-

Table 5.1 Wind speed points for 3D simulation based on K-Mean Clustering algorithm

For the thermal boundary condition, the skin temperatures from the initial 1D simulations were used. Each of the steady state simulations were run for 5000 iterations to attain convergence.

5.3 Results and Discussion:

5.3.1 Skin Temperature Prediction using 1D-3D Models (Part-I)

Figure 5.5 shows the HTC values over the exhaust system at 55mph. The HTC values are averaged over each of the component surfaces and exported to be used in the 1D simulations. Figure 5.6 shows the HTC values from all the simulations representing the transient drive cycle for the exhaust downpipe and intermediate pipe. A preliminary investigation into the distribution of HTC over the exhaust system shows that the HTC values for the upstream of the resonator are lower than those seen downstream. Figures 5.7 and 5.8 shows the contours of velocity magnitude at two locations on the Z and Y-plane respectively. Examining the figure, it can be seen that the velocities are higher in the downstream region compared to the upstream. Further the presence of skid plate underbody starting from the air dam up to the resonator on the left side contributes to lower convection rates seen in the downpipe portion. The HTC values obtained from the steady state simulations are then used in the 1D simulation as a boundary condition for external heat transfer.

Figures 5.9 and 5.10 show the gas temperatures at the inlet to the manifold and tailpipe respectively. The temperatures at the manifold inlet remains the same as seen in the previous chapter with the used of the 3D vehicle level model. Clearly the cases with and without the correlation all predict the gas temperatures close to the test data. However, the

cases with the correlations seems to underpredict the gas temperatures at the tailpipe, for the core part of the test. For the approach segment WHT correlation predicts the gas temperature more accurately. On the other hand, the UHT correlation underpredicts the temperatures by around 30ºC. Comparing the Figure 5.10 with Figure 4.8 for the cooldown segment, it can be seen that the use of transient HTC values gives a good trend in temperature similar to the test data.

The manifold skin temperature for the left of the exhaust is shown in Figure 5.11. From the comparison the UHT correlation accurately predicts the skin temperatures for the approach and the cooldown segment. For the initial portion of the grade segment, the higher and the lower peaks are underpredicted and overpredicted respectively. This might be mainly due to the fact that the thermal mass (flange) hasn't been considered in the 1D model. The quick rise and drop in the peaks at a faster rate compared to the test data signifies the loss of higher thermal energy accumulation.

Figure 5.12 and 5.13 show the skin temperature before and after the resonator. Both the UHT and WHT correlations overpredicts the skin temperatures for the approach segments. The difference in the temperature is between 50-70ºC to test data. At the start of the grade segment, the lower peaks for both the correlations agree well with the test data. However the higher peaks are overpredicted from the test data for both the correlations. In the second part of grade segment, both the UHT and WHT correlation gives and accurate prediction of the skin temperatures. The difference seen for the approach could primarily be due to the heat rejection rates from the CAT.

As per our initial assumptions, the heat rejection rates for the CAT was primarily based on engine speeds used in the steady state simulations. The data for the heat rejection rates from the steady state engine speed were between the start and the end of the grade for the approach and the cooldown. The software was set for the interpolation of heat rejection rates from the start and end points of the initial data. However from the results it can be seen that the software uses the heat rejection rate from the point corresponding to the start of the grade as the first point for the driving cycle. This confirms the sudden high temperatures seen in the approach to the downstream of the CAT. The data from the second part of the core segment matches due to the fact that the engine speeds seen in this part of the segment are similar to the WOT conditions. A similar trend can be seen in Figure 5.14. However, the only difference seen is the case without empirical correlation, which matches to the test data in the second part of the grade segment. In all other locations along the exhaust system, the case without any empirical correlation performs poorly interms of predicting the skin temperatures.

5.3.2 Skin Temperature Prediction using 1D-3D models (Part-II)

The initial 3D simulations performed in the previous set of simulations, does not include thermal conditions such as, heat rejection from the radiator, condenser and TOC. However, in the real world scenario, this assumption becomes invalid. Further, the surface average of the HTC values for the downpipe and the intermediate pipe are less accurate. In order to counter these setbacks, a second round of 1D-3D simulations were performed. For the 3D simulations in this case, the exhaust system is broken up into several subvolumes to match with the 1D model. The discretization was performed mainly for the downpipe and the intermediate pipe to match with the subvolumes in 1D. This is shown in Figure 5.15. The

radiator was set as a heat exchanger to emulate the real world conditions. For the heat exchanger model, a target exit temperature and heat exchanger temperature were specified to calculate the heat rejection rate from the radiator.

In order to capture the variable air flow rate from the radiator fan shown in Figure 5.16, the fan speeds corresponding to the set of points from the K-Cluster were used in the MRF model. Using the above mentioned set up the geometry was remeshed and simulated using the same wind speed points from the cluster. Figures 5.17 and 5.18 shows a comparison of temperature contours at 55mph on Z-planes for the initial and the current case with respect to heat rejection from the radiator. It can be clearly seen from the figures that the influence of the heat rejection rates on the thermal environment underbody as well as around the exhaust system is significant. This could mean that the HTC values are more accurate compared to the previous results. Further in order to make sure the HTC values are grid independent, a specified $y+$ heat transfer coefficient field function was used. The specified y+ HTC values were calculated based on a $y+$ value of 100. The results were then used as a boundary condition for the 1D simulations.

For the 1D simulations, the high skin temperatures seen in the approach segment for the previous set of simulations, were primarily due to the heat rejection rates for the CAT. Hence for the second set of 1D simulations, the heat rejection rates from the CAT were removed. Instead, the gas temperatures were augmented to account for this change. The 1D simulations were then rerun with the CAF value of 3, 1.6, 1.6 for the manifold, downpipe, intermediate pipe respectively. As it can be seen from the previous results, the UHT correlation gives a good prediction for most part of the drive cycle at all the locations.

Hence, for the subsequent simulations only the UHT correlation is used. The results from the simulation is discussed in the following section.

Figure 5.19 and 5.20 present the gas temperature at the manifold and the tailpipe. The results from the manifold portion matches with the test data. However the gas temperatures from the tailpipe still doesn't give an accurate match with the test data. For the approach segment, the temperature difference seen is about 20°C. The peaks in the initial part of the grade segment is unpredicted. In the second part of the grade segment, until the cooldown, the difference in temperature seen is 20-30°C.

Figures 5.21 to 5.24 gives the skin temperature of the manifold to the location before muffler. Until the location after the resonator, the UHT correlation gives accurate prediction of skin temperatures. However for the location before the muffler, there is a slight overprediction in the approach and the second segment of the grade. This difference is about 30°C. For the cooldown portion in Figure 5.26, the correlation underpredicts the temperature by a maximum of 12°C. The difference seen is primarily due to the effect of thermal mass. Here in too, the presence of flange joining the intermediate pipe and the muffler accounts for this difference. With respect to the difference seen in the gas temperature at the tailpipe (Fig 5.22), is partially due to the effect of thermal mass in terms of chrome exhaust tip and partially due to the effect of external emissivity in radiant heat transfer.

5.4 Parametric Study Involving the Effect of External Emissivity:

In order to investigate the effect of external emissivity, a parametric study was conducted by varying external emissivites of the components from 0.2 representing a well-polished

or shiny exhaust to 0.8 representing a highly oxidized or a painted exhaust. The boundary conditions representing the emissivity values were used for the 1D model from the above discussed results. The analysis pertaining to the study are presented in the following section.

Figure 5.25 and 5.26 shows the gas temperatures at the manifold and tailpipe. For the manifold gas temperature, the effect of emissivity is negligible. However, some differences are seen for the gas temperatures at the tailpipe. It can be seen from figure 5.28 that an emissivity value of 0.2 to 0.4 gives an accurate prediction for gas temperatures. Hence the assumption made in the previous section for tailpipe gas temperature seems to be valid. With the presence of chrome tip shiny in nature, the heat rejected from the gas is conserved.

Figure 5.27 to 5.30 shows the skin temperatures for different emissivities from manifold to the location just before the muffler. For the manifold, the difference is limited between the emissivity values of 0.4 to 0.8. This would represent the best case scenario where the manifold seems to have an emissivity with in the above mentioned range. For figure 5.30, the best prediction is seen between an emissivity values of 0.6 to 0.8. The primary reason for this agreement is due to the fact that, upto the location before the resonator, the exhaust is partially covered with the skid plates. The presence of the skid plates could delay the oxidation or wear of the exhaust while shielding it from harsh environmental conditions. This also confirms, lower HTC values seen up to the location before the resonator. For the locations after the resonator up to the tailpipe, an emissivity value of 0.7 to 0.8 seems to representing a scenario where the exhaust has been exposed completely to the environment.

The study was further investigated for the overall contribution of external emissivity and radiation heat transfer to the overall heat transfer characteristics of the exhaust system.

Figure 5.31 (a) and (b), shows the rate of heat transfer for an emissivity value of 0.2 and 0.8 respectively. From the figure it can be seen that the combined energy rate out of the fluid matches with the average convective heat transfer rate to the walls of the exhaust. This implies that the convection is the only mode of internal heat transfer. Looking at Figure 5.31 (a) the average heat transfer rate from the external surface of the exhaust to the ambient, shows that the dominant mode of external heat transfer is convection in both approach and the grade segment. In the cooldown however, due to the lack of sufficient forced convection, both radiation and free convection contributes equally to the heat transfer.

In the figure 5.31 (b), contribution of both radiation and forced convection seem to be more or less equal. In the grade segment however, the dominant mode of heat transfer seems to be from radiation. In the cooldown segment, both the convection and radiation contributes equally to the heat transfer. Figure 5.32 (a) and (b) shows the average convective heat transfer rate and average radiative heat transfer rate for different emissivities. The variation of the convective heat transfer rate seems to be minimum with the variation of emissivity. The average radiative heat transfer rate however seems to increase by over four times for an emissivity value of 0.2-0.8.

Figure 5.33 (a) and (b) shows the variation of external specified $y+$ heat transfer coefficient for two different emissivity values over the downpipe and intermediate pipe. It can be seen that the effect of emissivity on HTC is negligible. Figure 5.34 (a) and (b) shows the heat

shield temperatures at a wind speed of 49 mph for emissivity values of $\varepsilon = 0.2$ and $\varepsilon = 0.8$. The heat shield temperature for the higher emissivity is close to 200ºC higher than the temperature for lower emissivity. This confirms the influence of emissivity at speeds where forced convection is expected to be the more dominant form of heat transfer. Similarly it can be seen from the Figure 5.35 (a) and (b) showing the heat shield temperature at a wind speed 1.5 mph. In this scenario the expectation would be for either the natural convection or radiation to be more dominant for of heat transfer. However, both convection (natural and forced) and radiation contribute equally. One of the key reasons for the difference seen is that, though the vehicle is in a stand still condition after high load run, the fan from the radiator seems to provide some convection for the initial part of the exhaust system. Further components such as airflow management devices along with the skid plate might guide the air underbody over the exhaust system.

5.5 Conclusion:

A novel approach and a numerical methodology utilizing the effectiveness of both 1D and 3D vehicle level models were used to predict the skin temperature of the exhaust system. The initial study showed the effectiveness of using the vehicle level 3D model to for studying the external heat transfer characteristics of an exhaust system. The 3D model included free convection and radiation models. The HTC values obtained from the steady state simulations were used as a boundary condition for external heat transfer in the 1D model. This way both the codes were integrated transferring the required data between the codes. Three loops of data transfer between the code was found to be optimal for the coupling. This was confirmed by comparing the change in the heat transfer coefficient values at every loop. Since the change between the second and third loop was found to be

less than 5%, the results from the third loop were used as final results. Initial loop simulation showed very good agreement with the test data in the cooldown segment of the drive cycle. The UHT correlation gives an accurate prediction of skin temperature in all the simulations. The set backs from the initial simulations of 1D-3D models were resolved by eliminating the heat rejection rates for the CAT. An improper heat rejection rate for the CAT results in severe overprediction of the skin temperature after the CAT. Further, CAF values of 3, 1.6, and 1.6 were found to be the optimum values for manifold, downpipe and intermediate pipe respectively. Further, the contribution of external emissivity in the radiation heat transfer and overall heat transfer characteristics has been demonstrated.
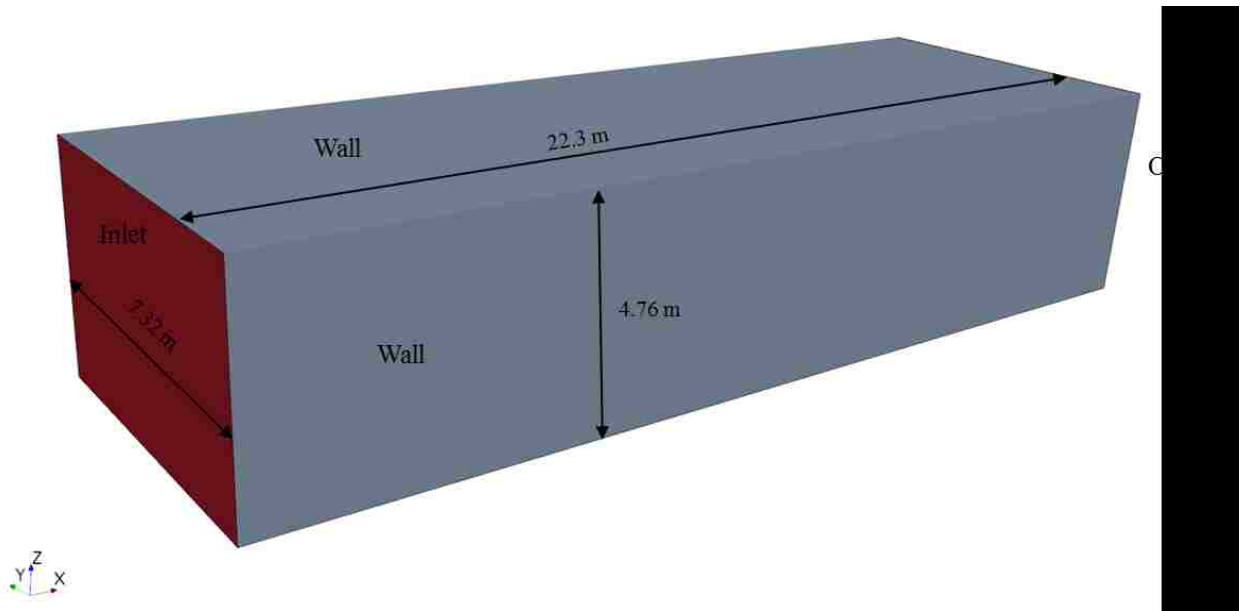
Figure 5.1 Drive cell test layout
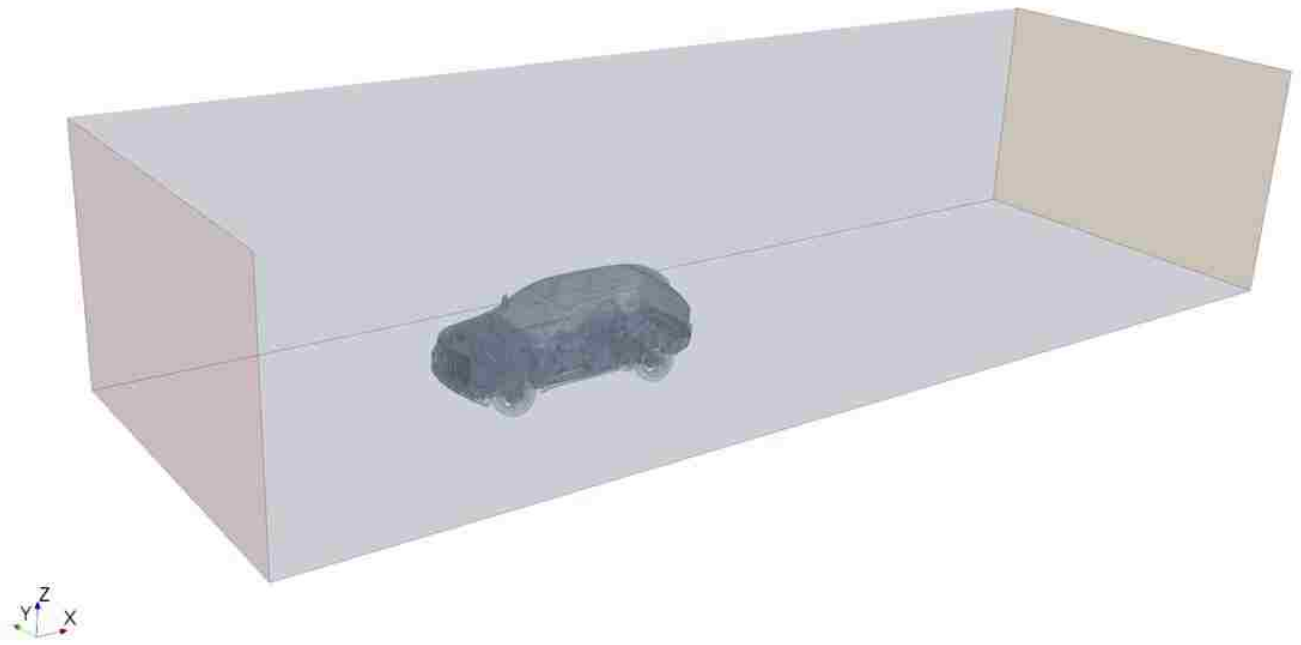
Figure 5.2 Computational domain with the vehicle
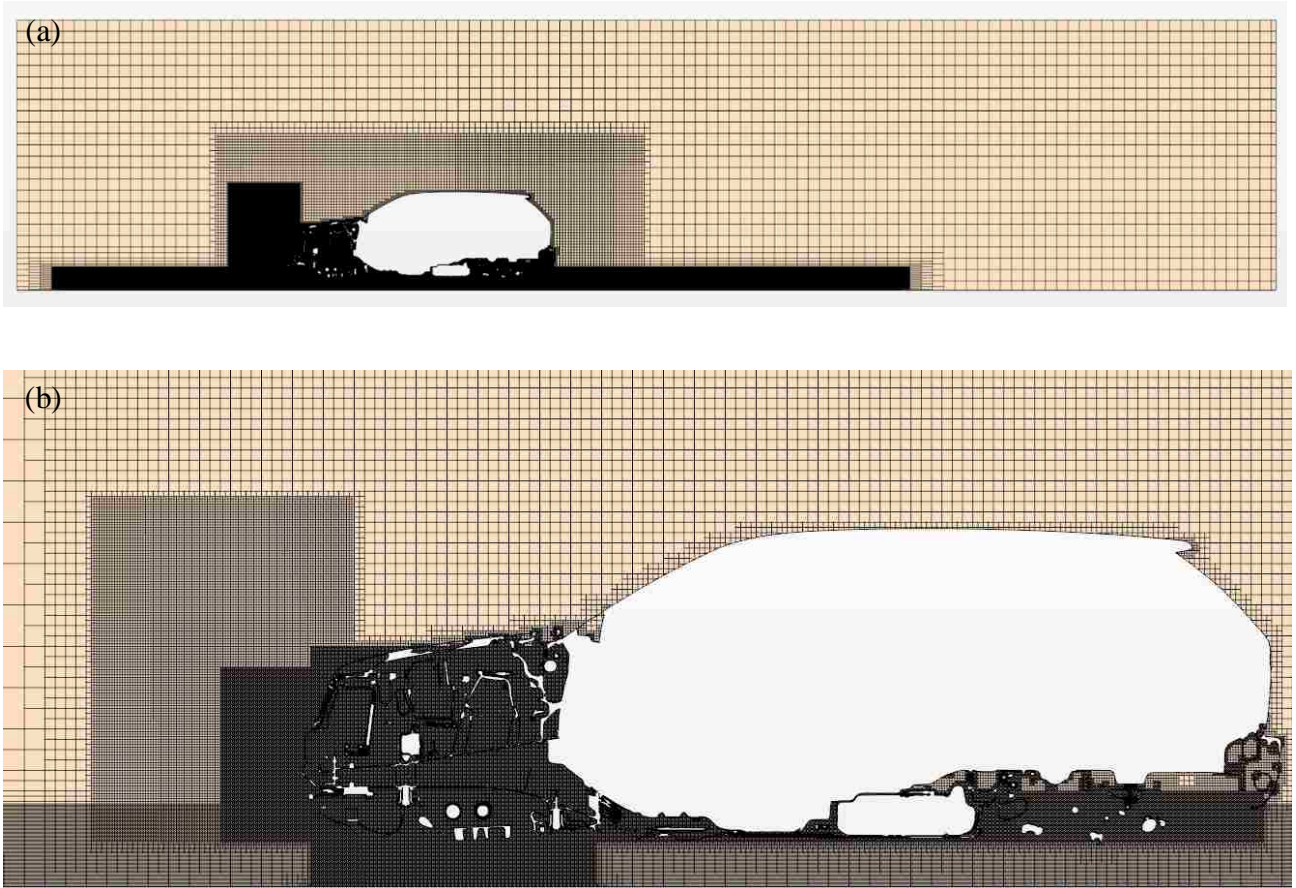
Figure 5.3 (a) Computational mesh for the entire domain (b) close up view of mesh near

the vehicle
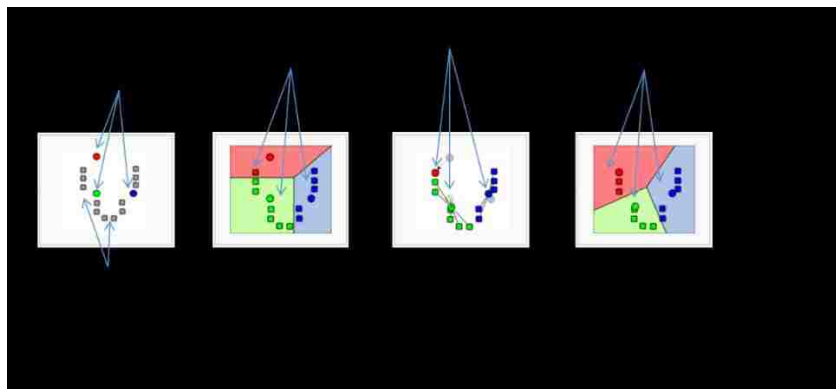
5.4 K-Cluster methodology for steady state speed points (https://en.wikipedia.org/wiki/K-

means_clustering)

(a)
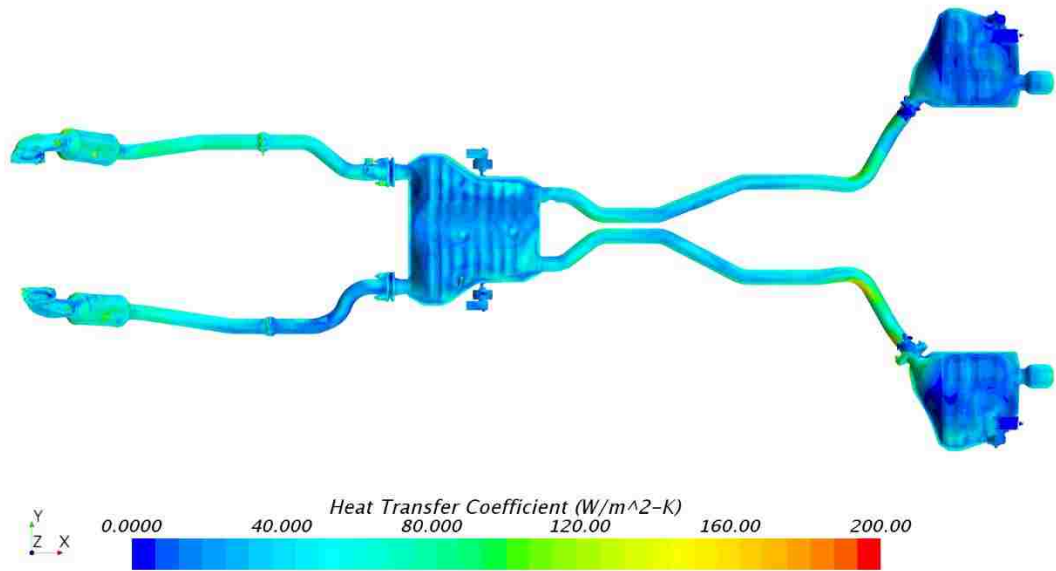
(b)
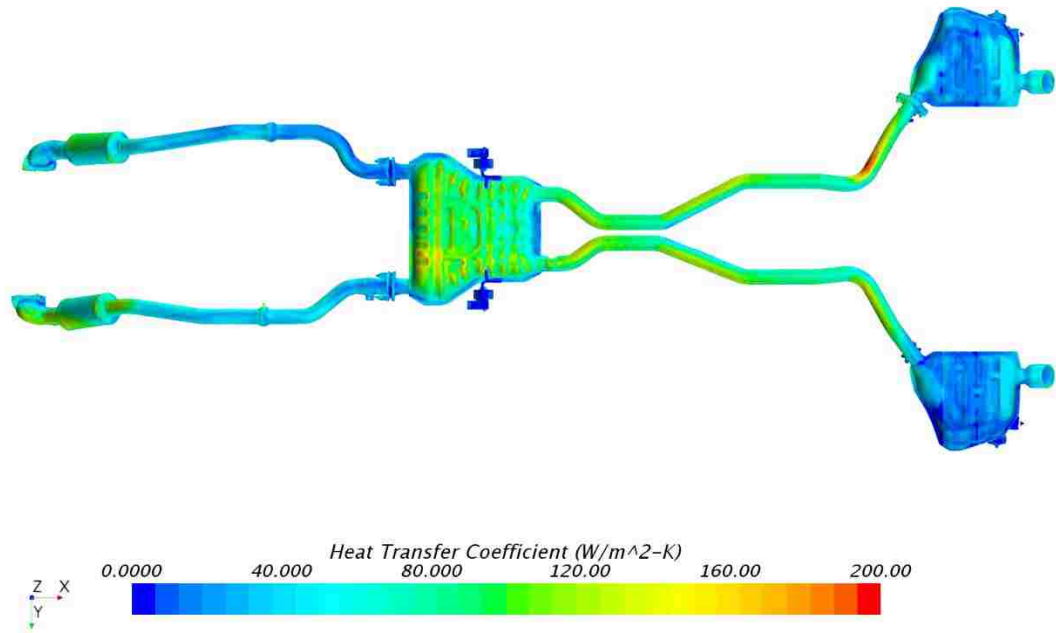
5.5 HTC values at 55mph on the (a) top and (b) underside of the exhaust system
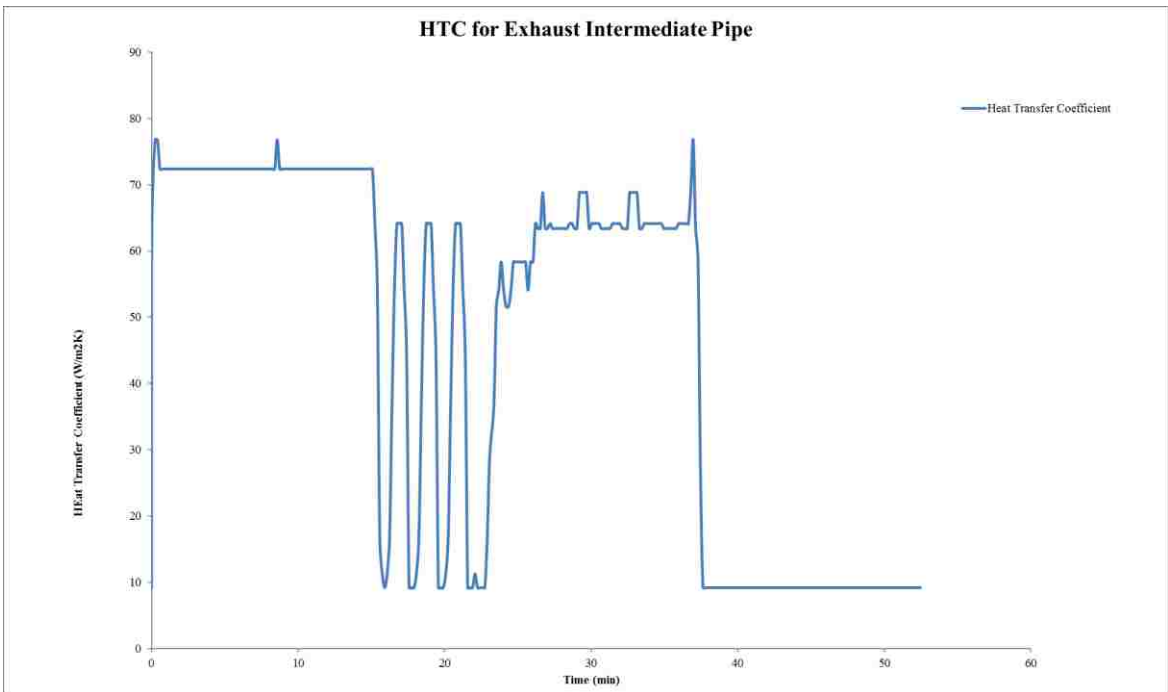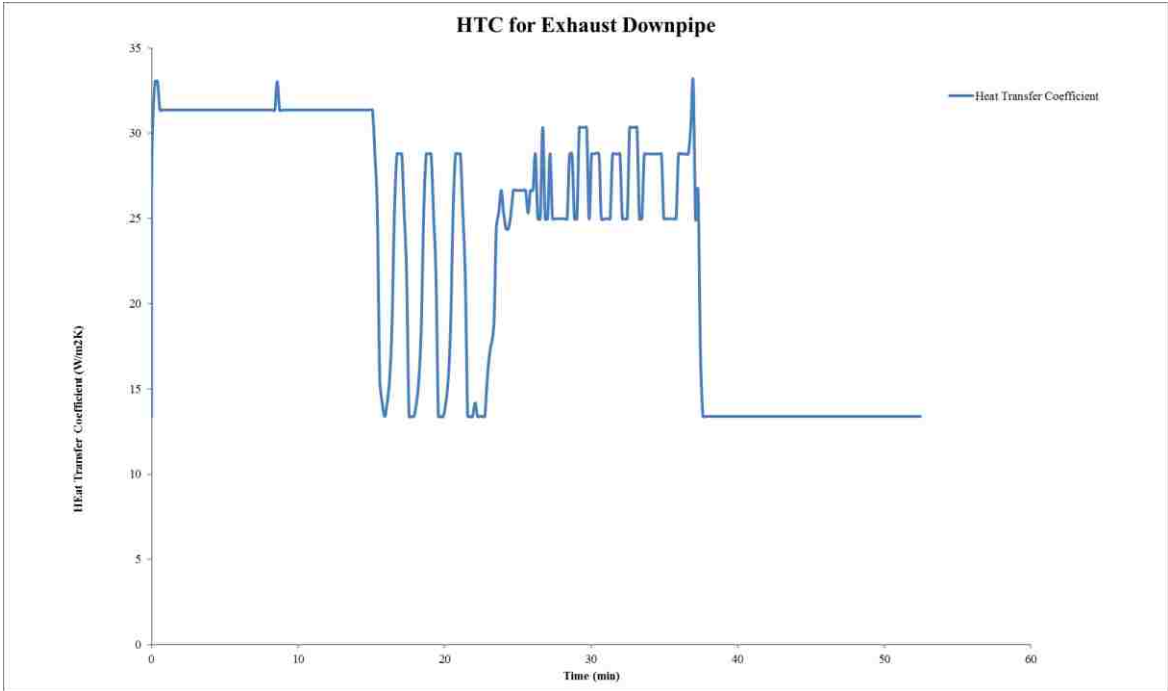
5.6 HTC values from steady state simulations representing transient condition for (a) downpipe and (b) intermediate pipe
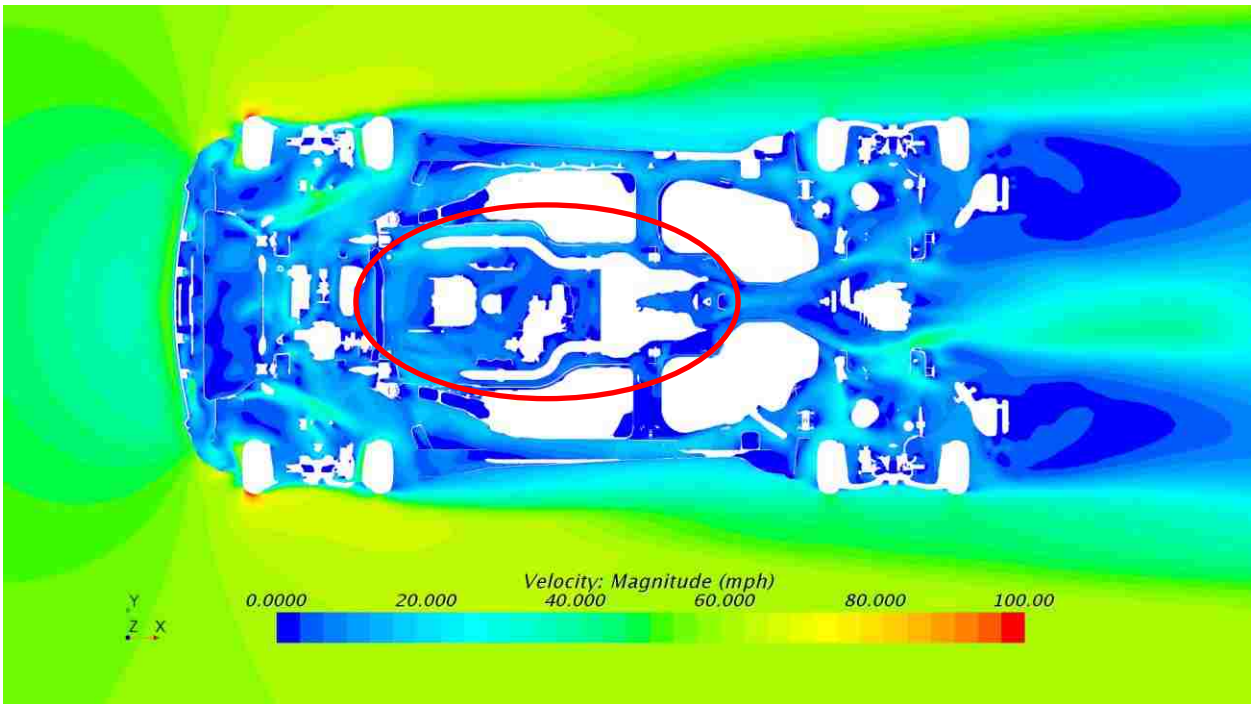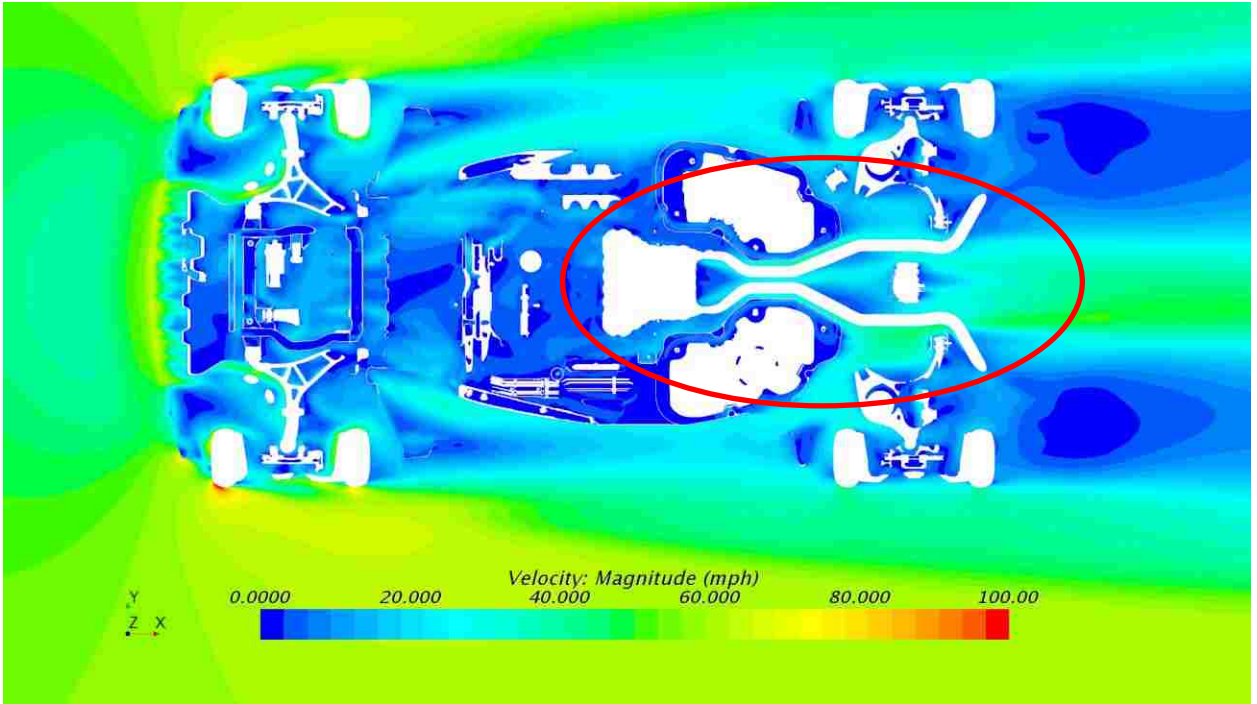
5.7 Contours of velocity magnitude at two locations on Z-plane highlighting the exhaust
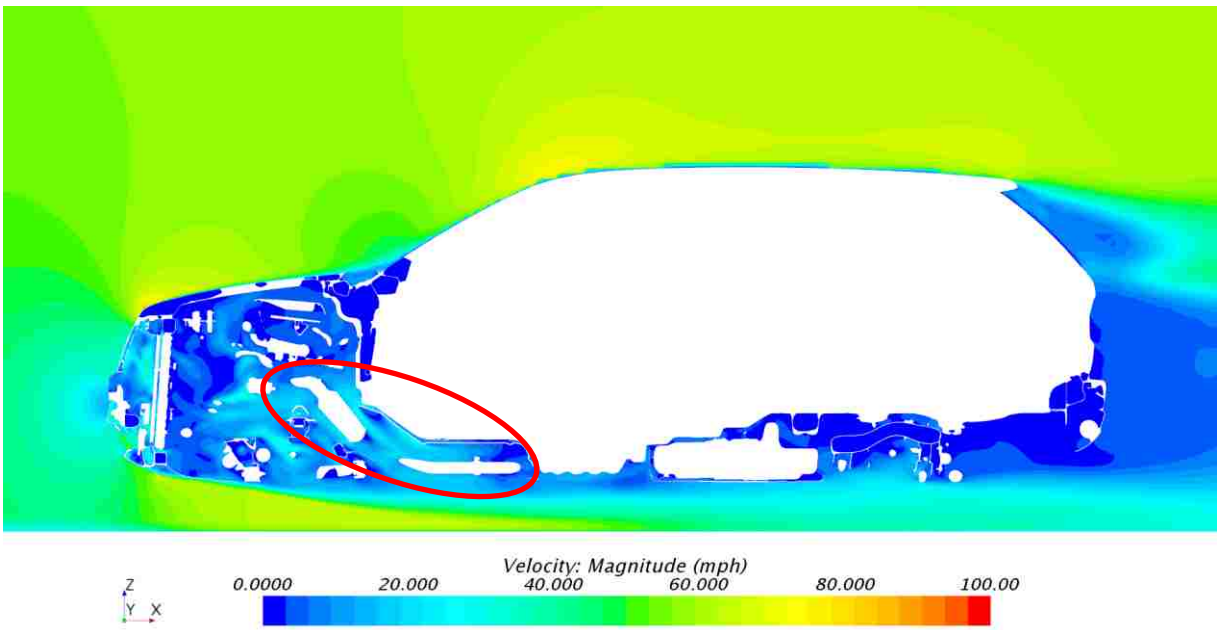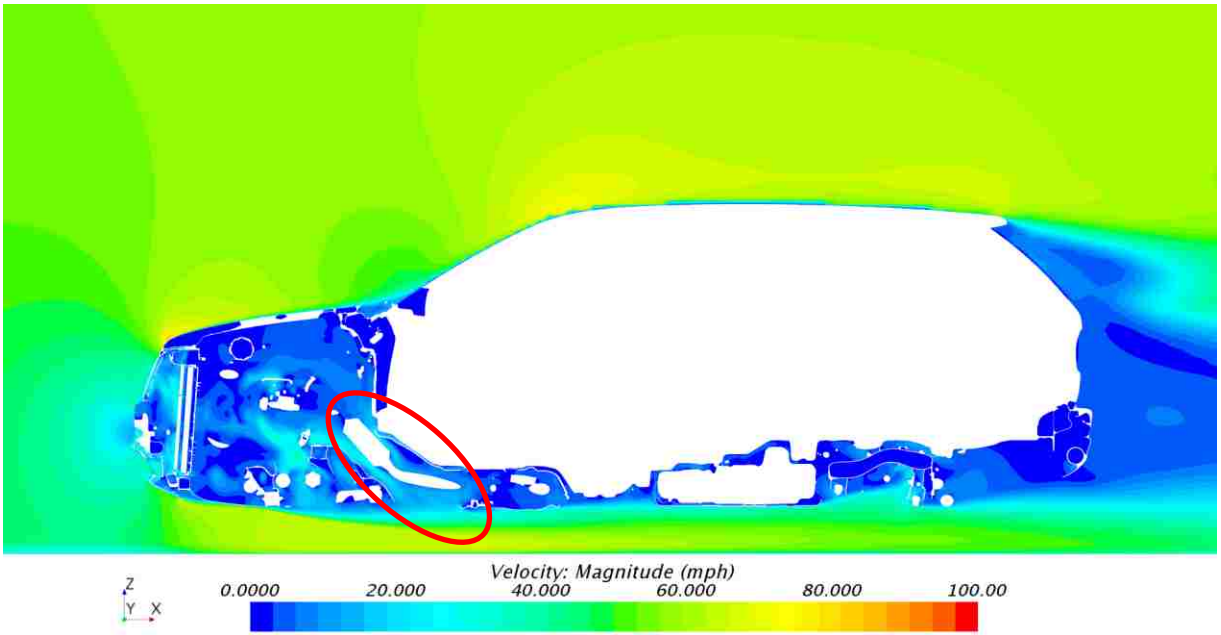
system

5.8 Contours of velocity magnitude at two locations on Y-plane highlighting the exhaust

system
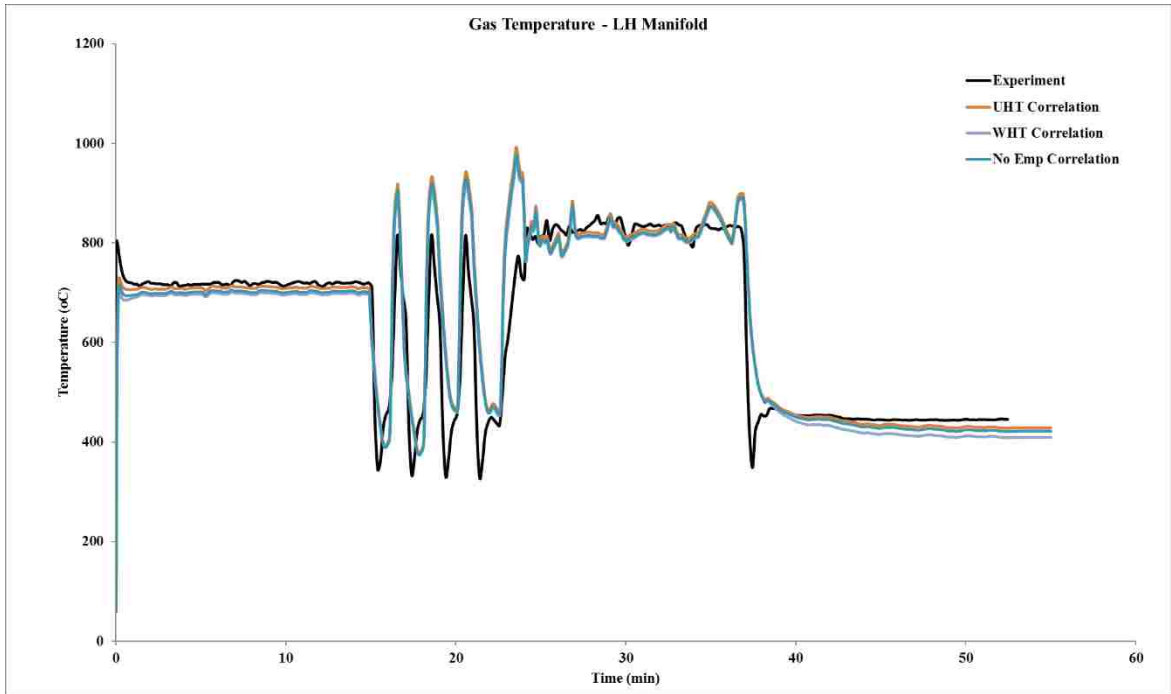
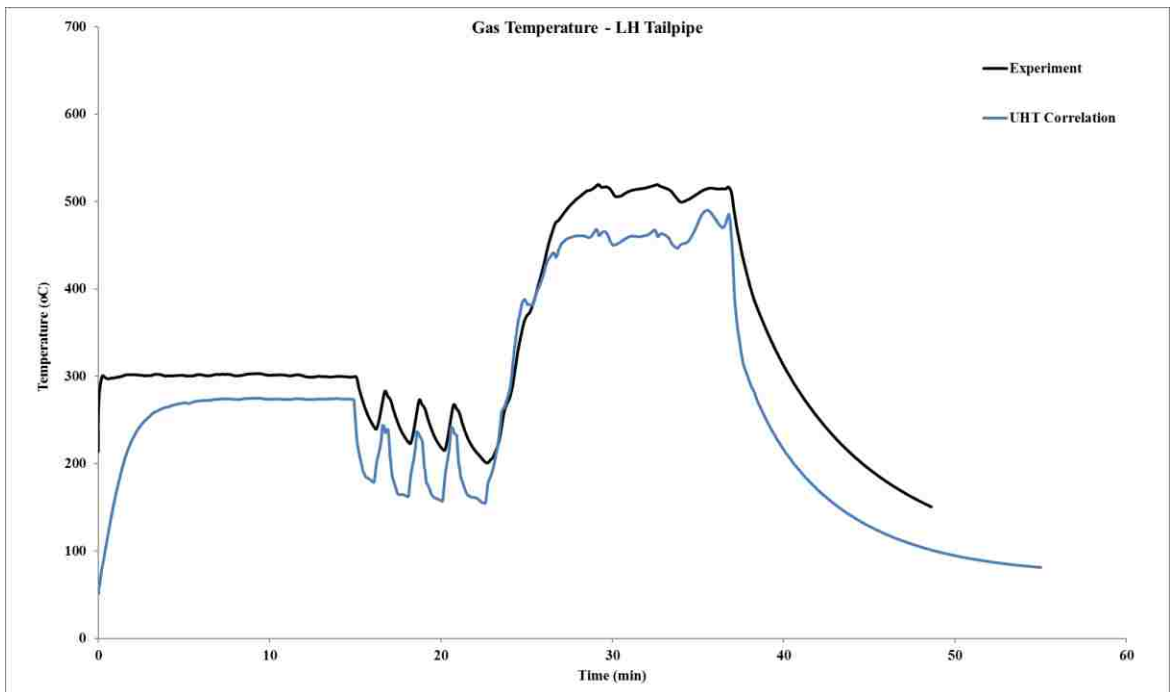Figure – 5.9 Left manifold inlet gas temperature
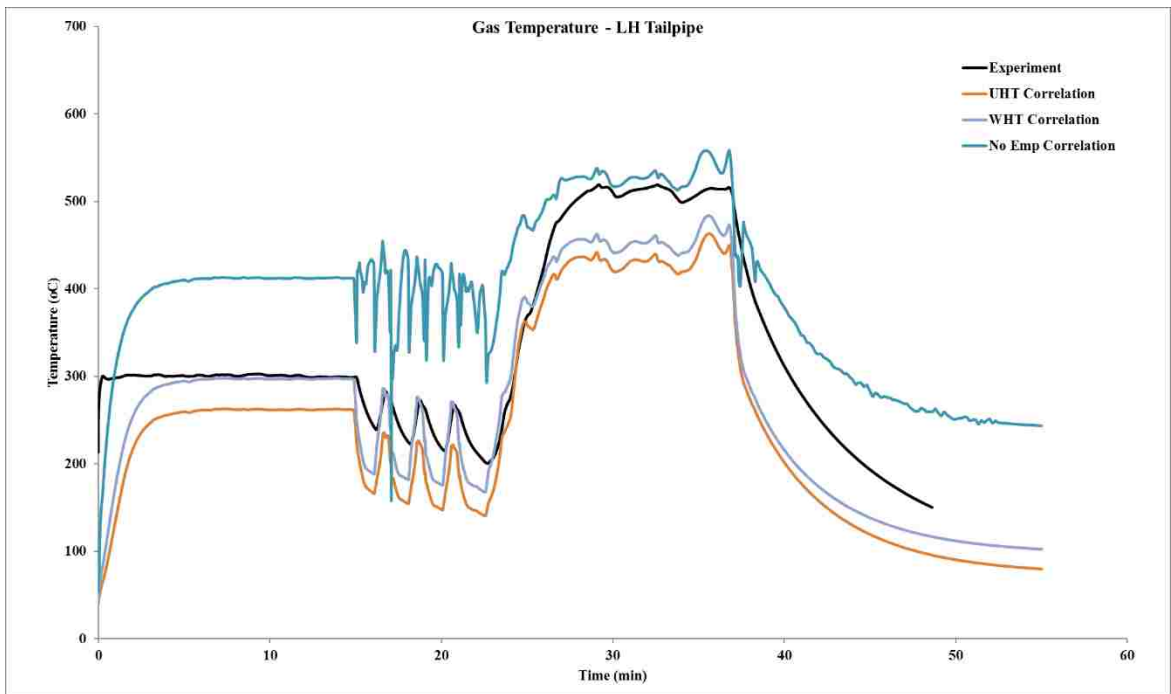
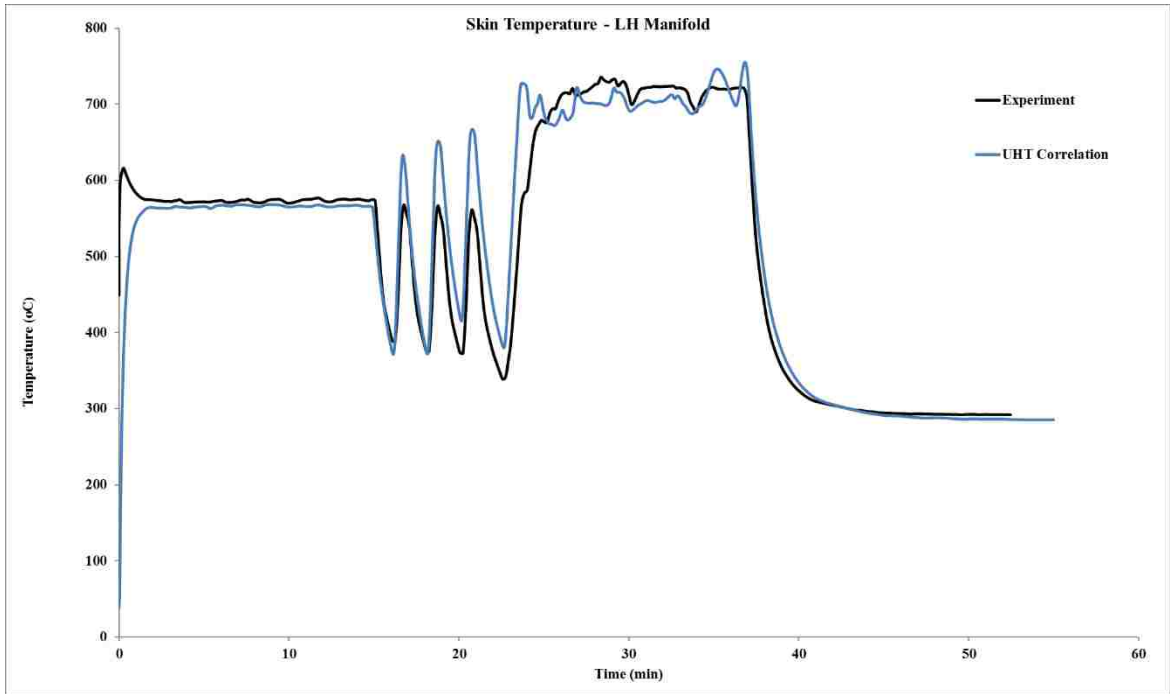Figure 5.10 Left tailpipe gas temperature

96
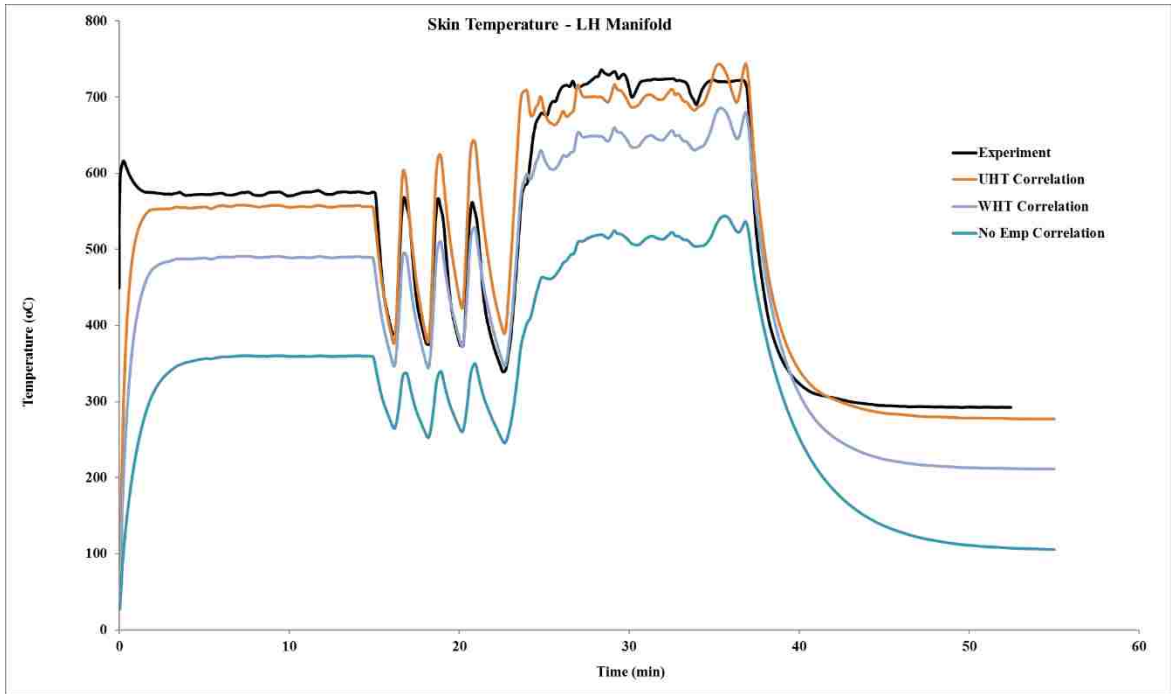
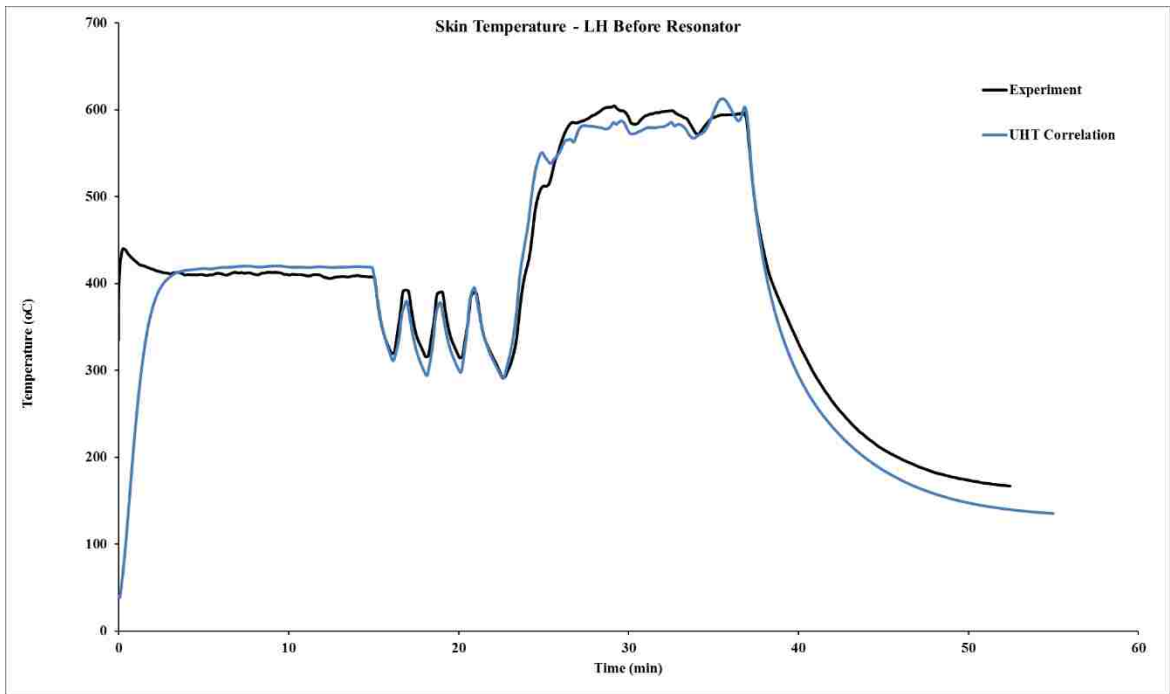Figure 5.11 Left manifold skin temperature
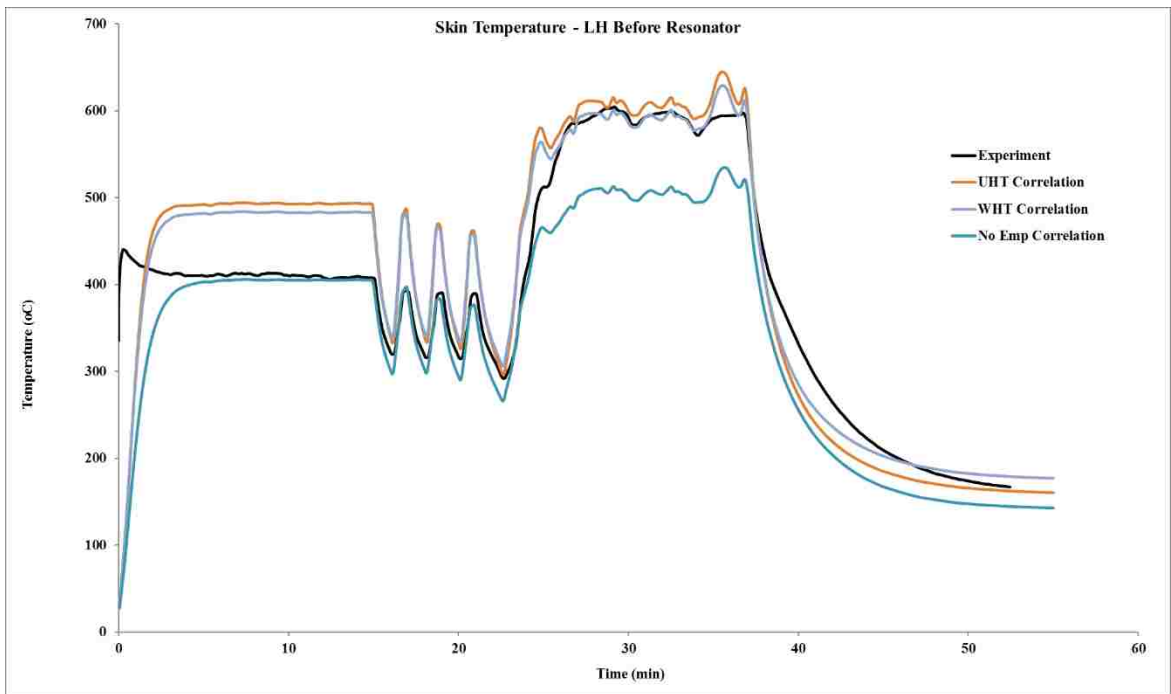
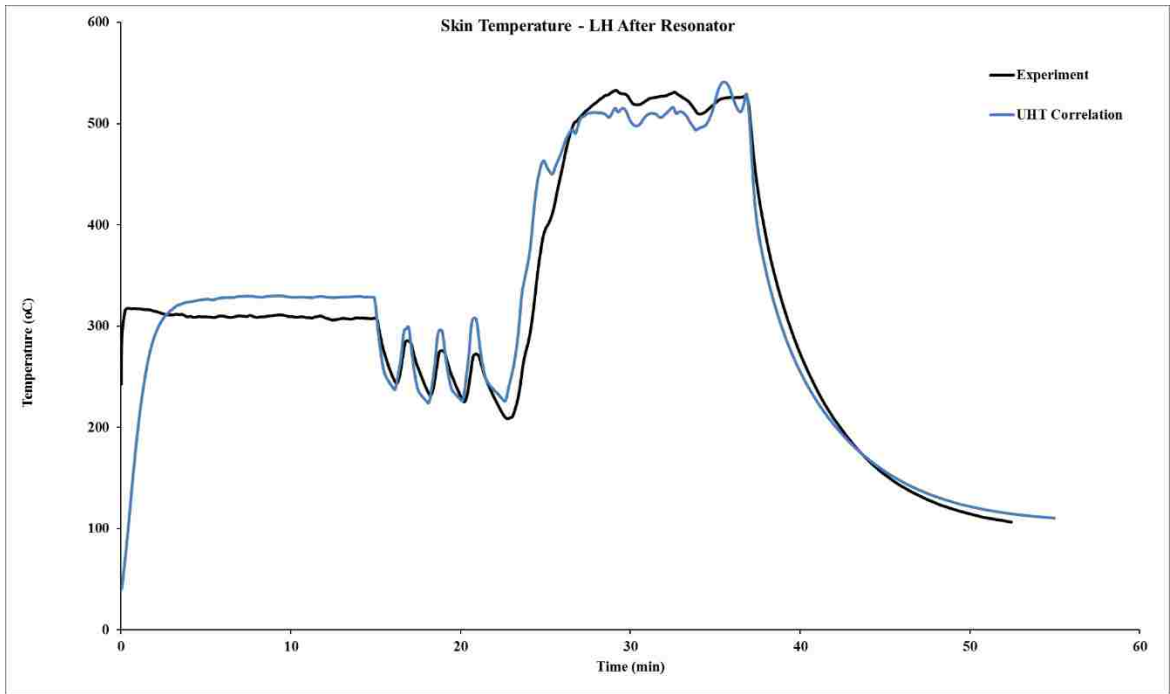

Figure 5.12 Skin temperature before resonator on the left
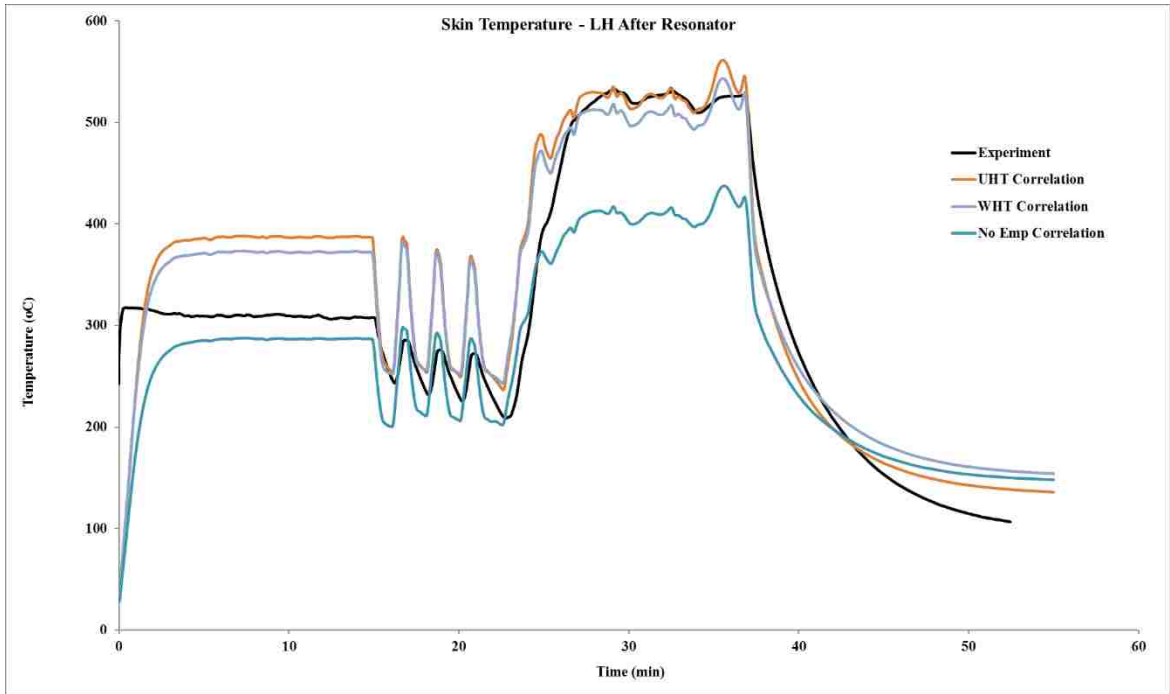
Figure 5.13 Skin temperature after resonator on the left side
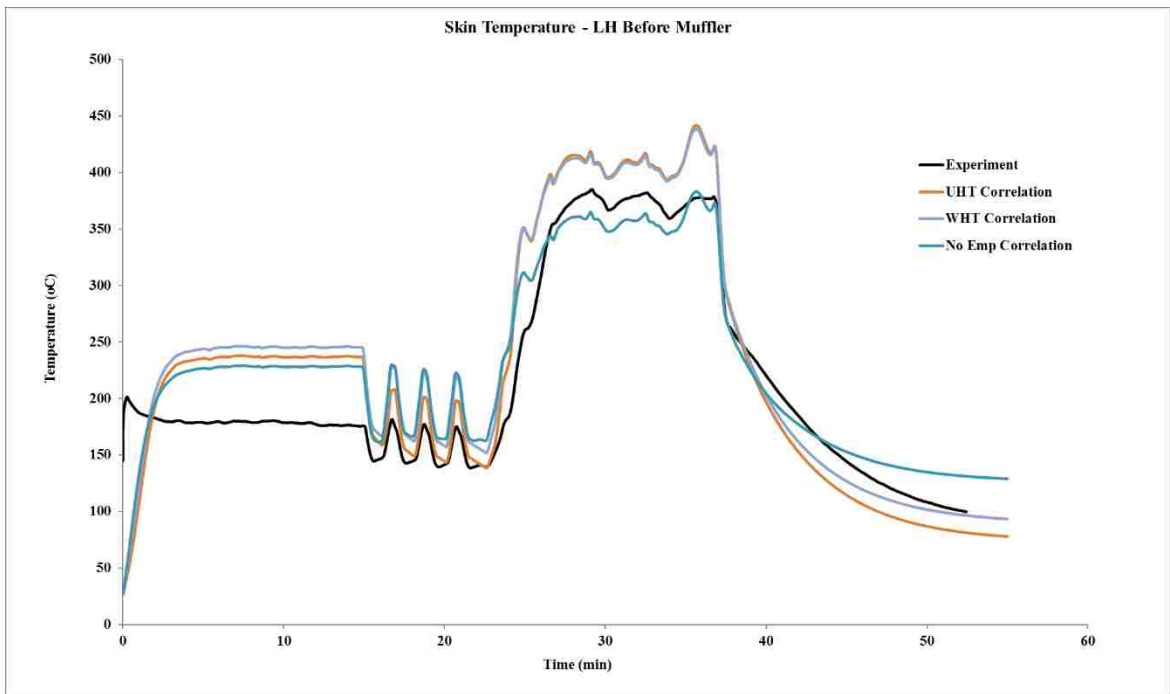
Figure 5.14 Skin temperature before left muffler

98
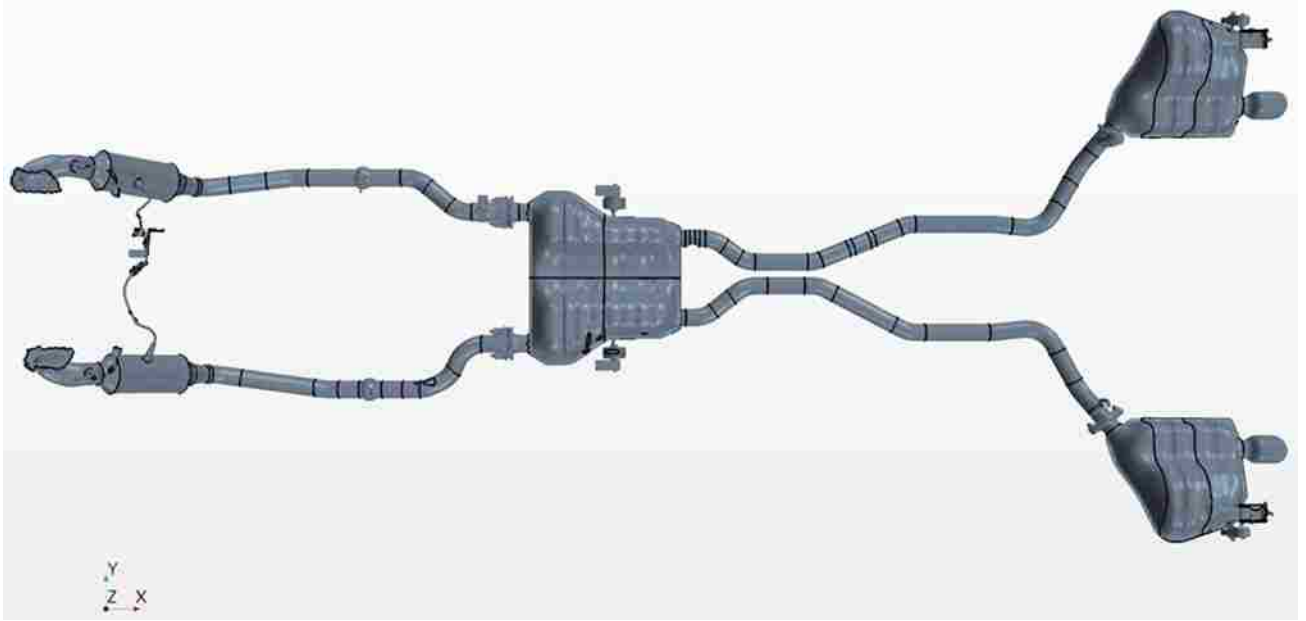
Figure 5.15 Re-split sections of the exhaust system similar to 1D model
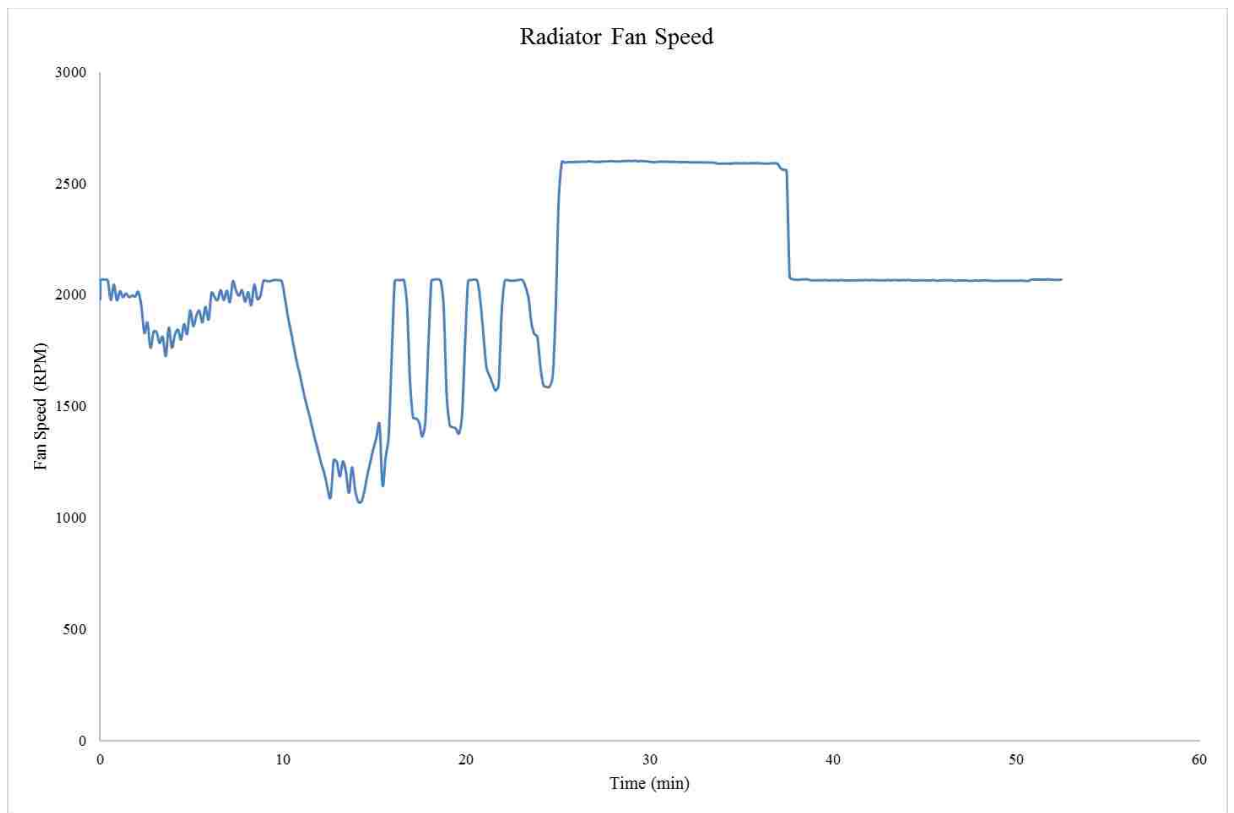
Figure 5.16 Radiator fan speed for the drive cycle
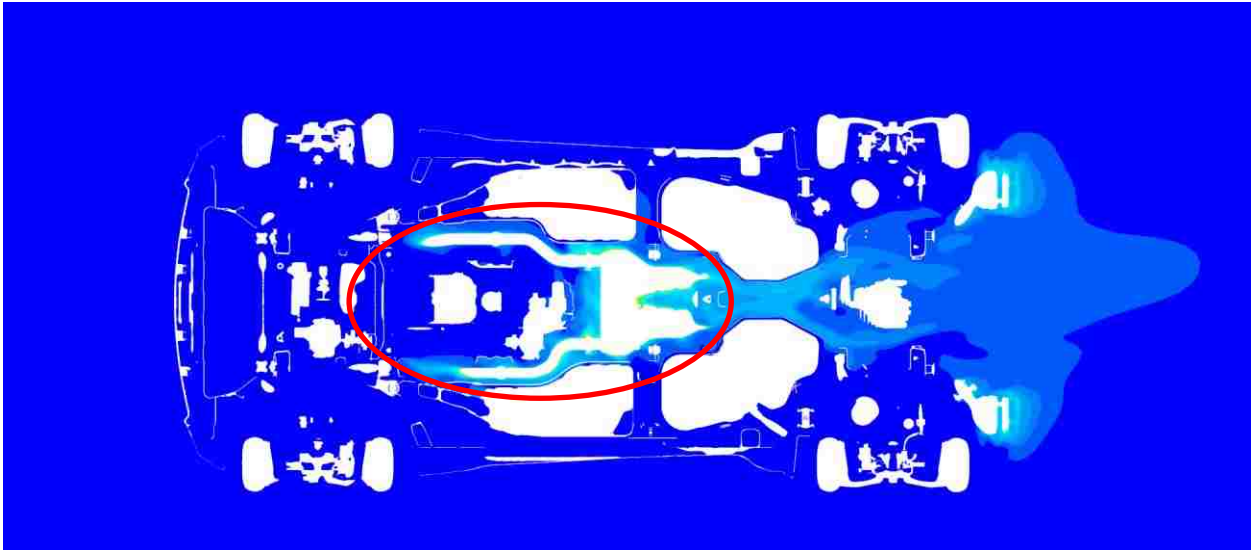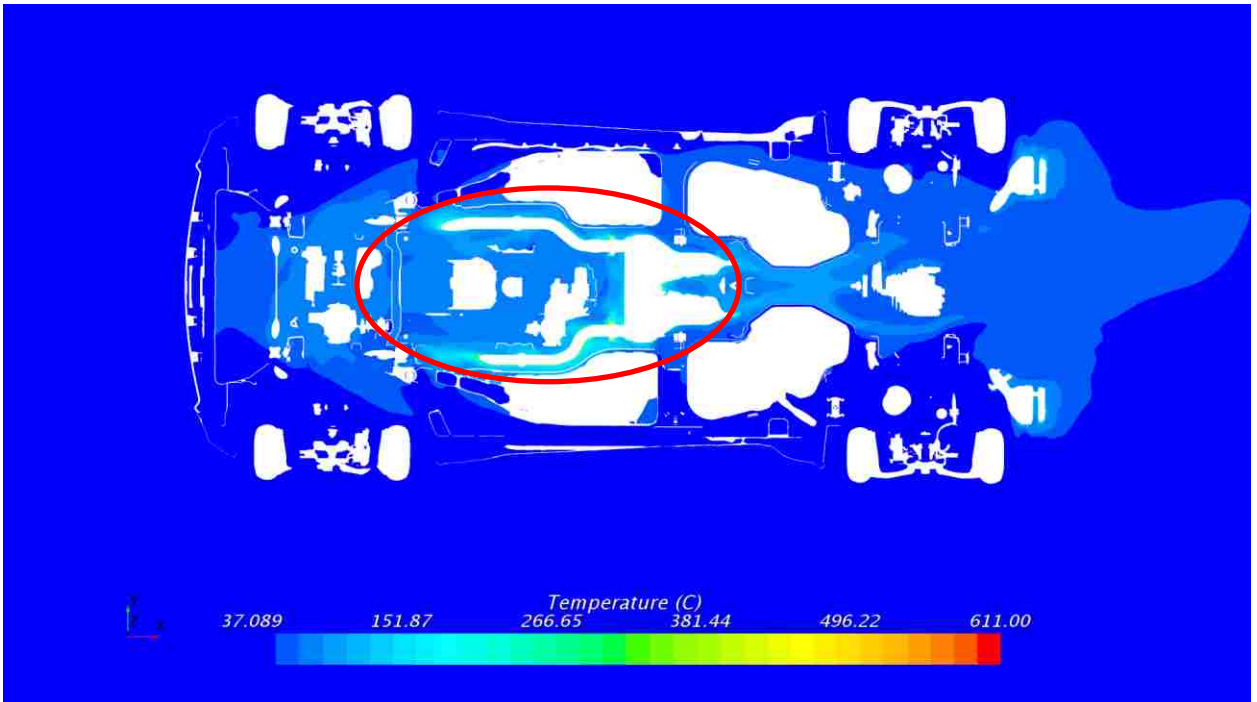
5.17 Contours of temperature at 55mph on Z-plane highlighting the exhaust system for

(a) without heat rejection from radiator (b) with heat rejection from radiator
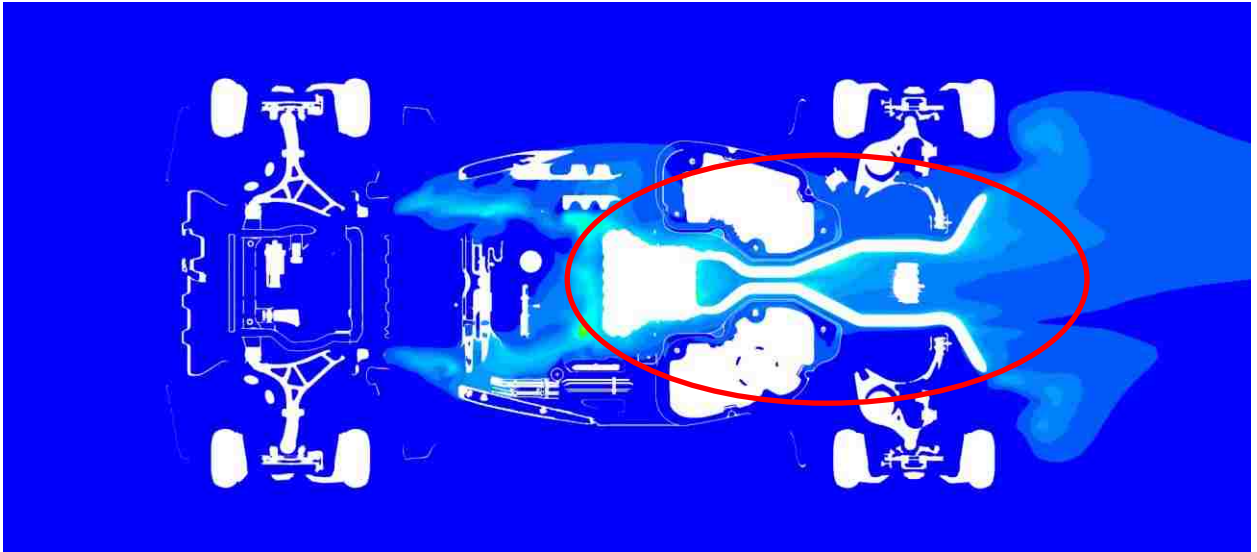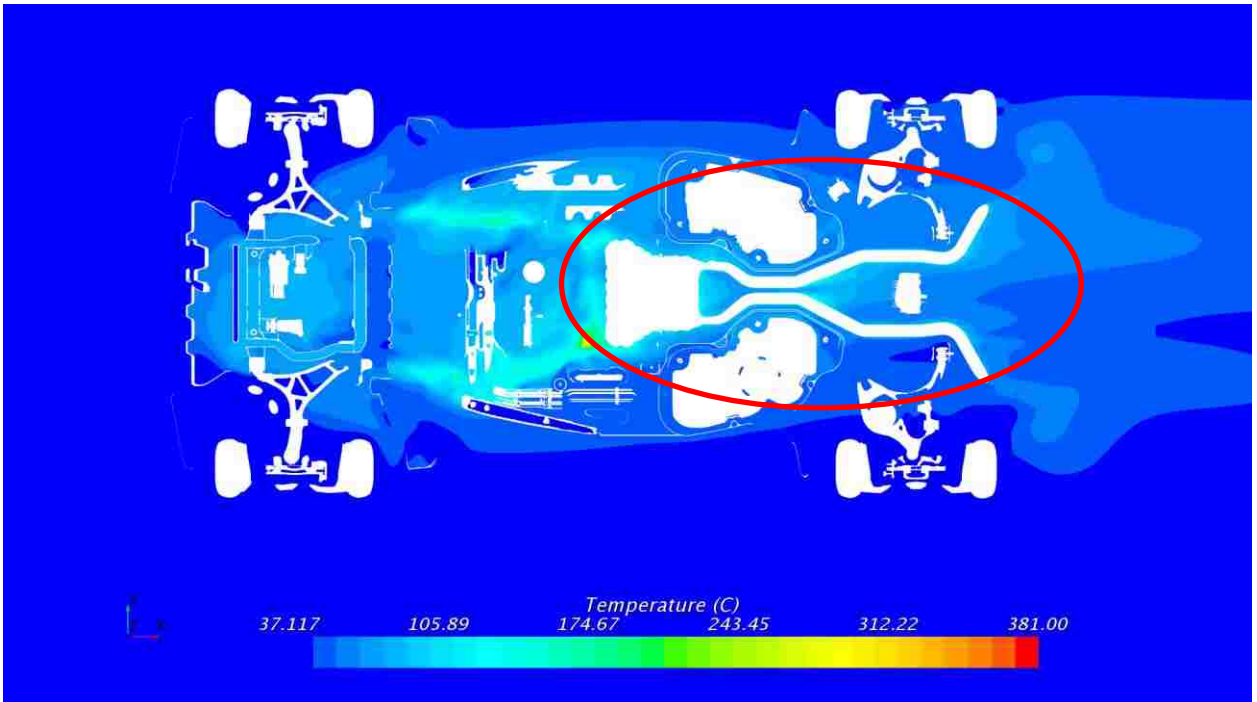
5.18 Contours of temperature at 55mph on Z-plane highlighting the exhaust system for

(a) without heat rejection from radiator (b) with heat rejection from radiator
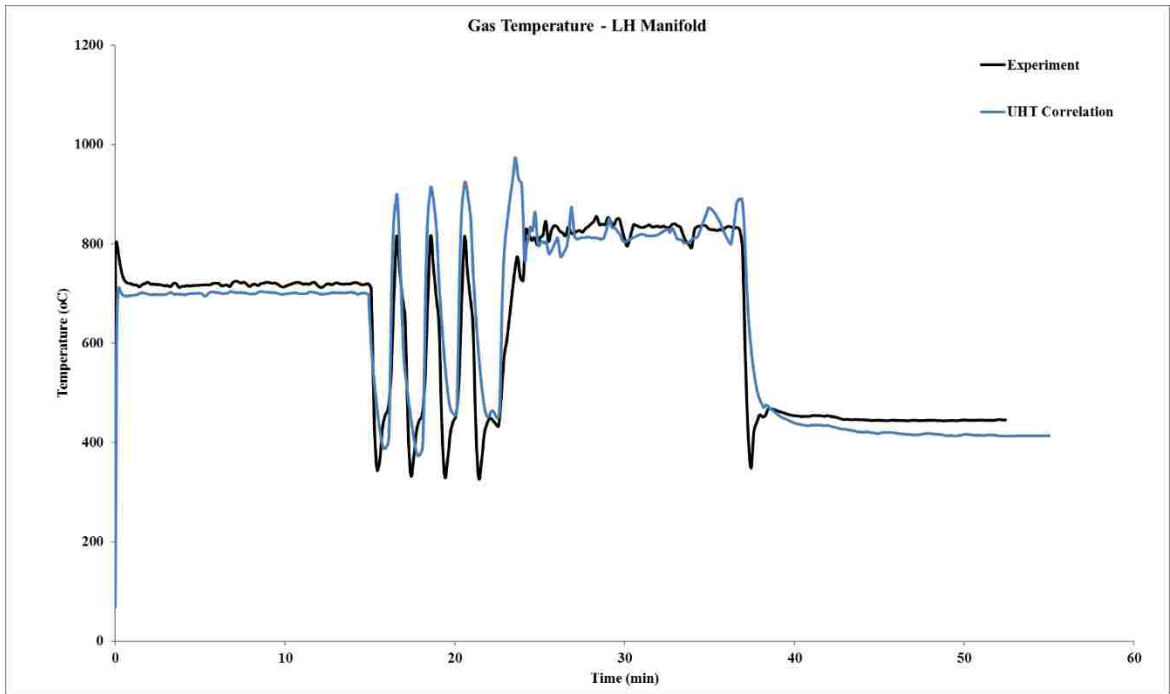
Figure – 5.19 Left manifold inlet gas temperature

Figure – 5.20 Left tailpipe gas temperature

Figure 5.21 Left manifold skin temperature

Figure 5.22 Skin temperature before resonator on the left

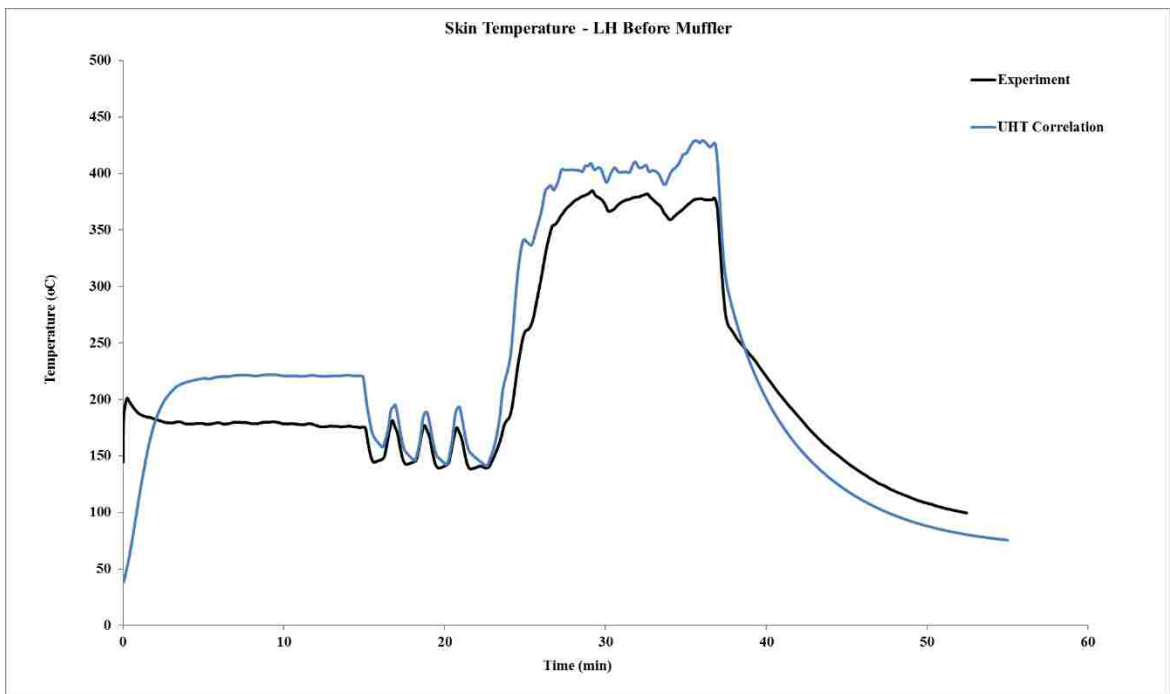Figure 5.23 Skin temperature after resonator on the left

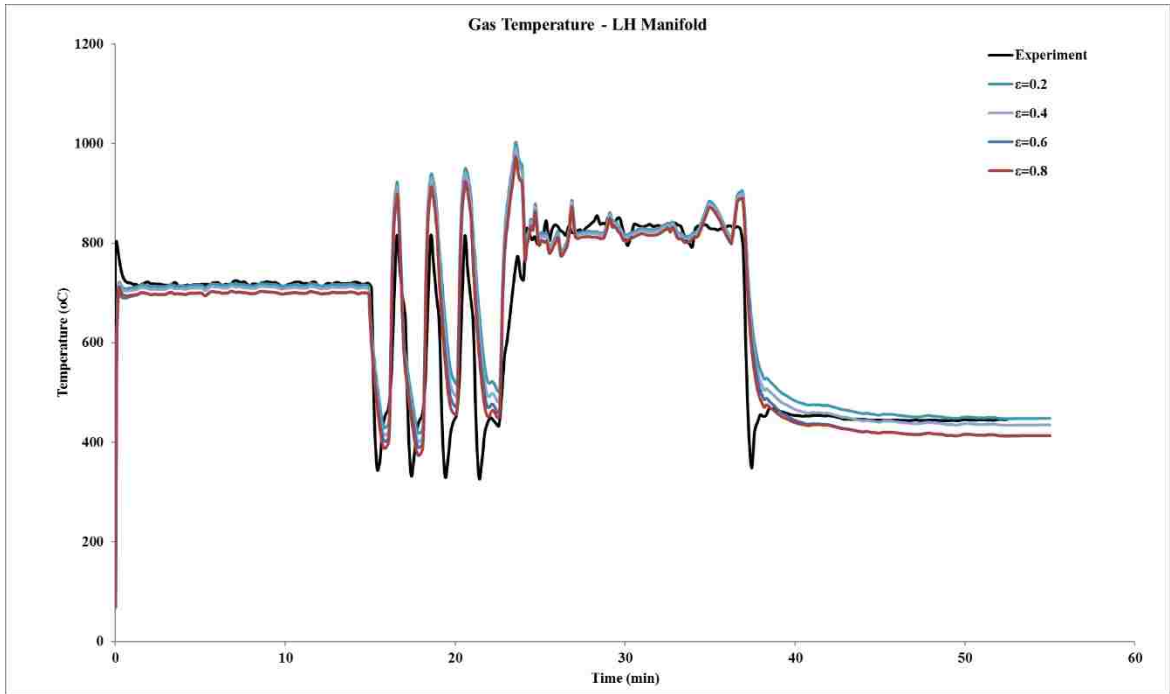Figure 5.24 Skin temperature before muffler on the left

104

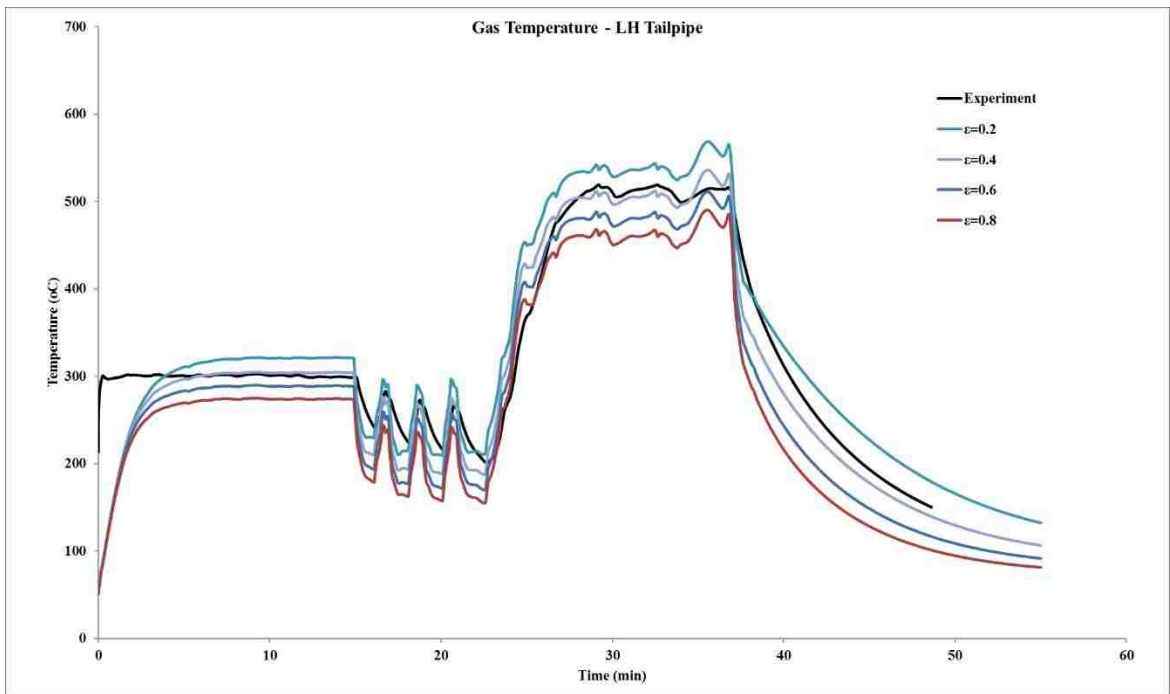Figure 5.25 Left manifold inlet gas temperature

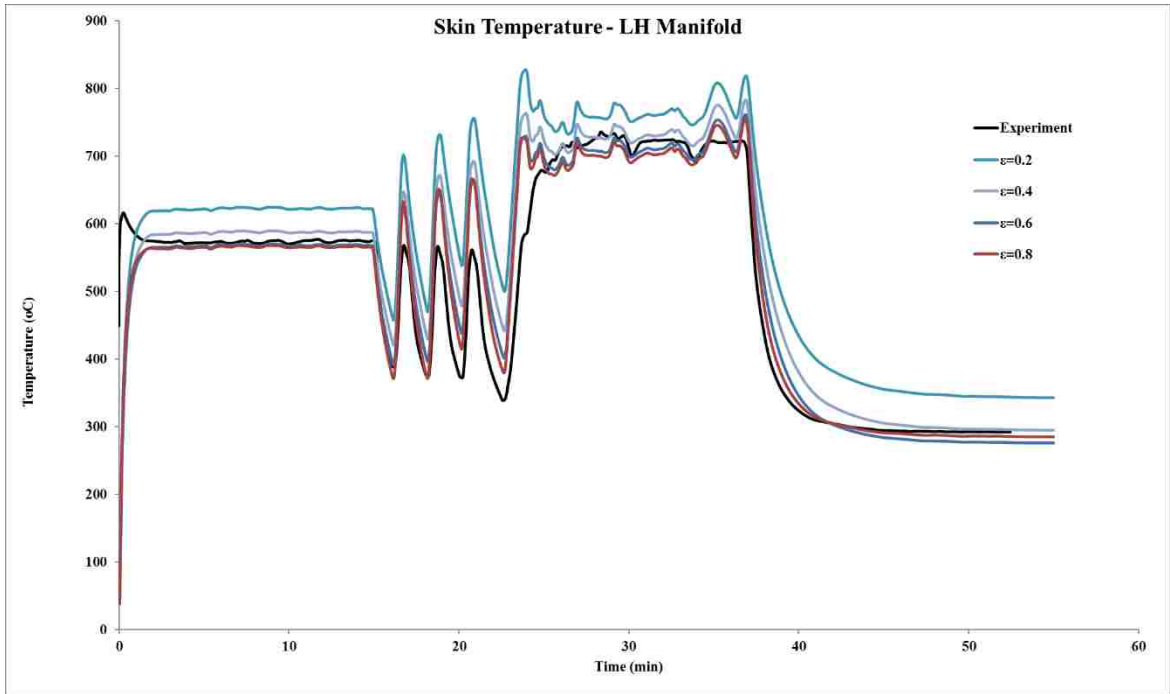Figure 5.26 Left tailpipe gas temperature

105

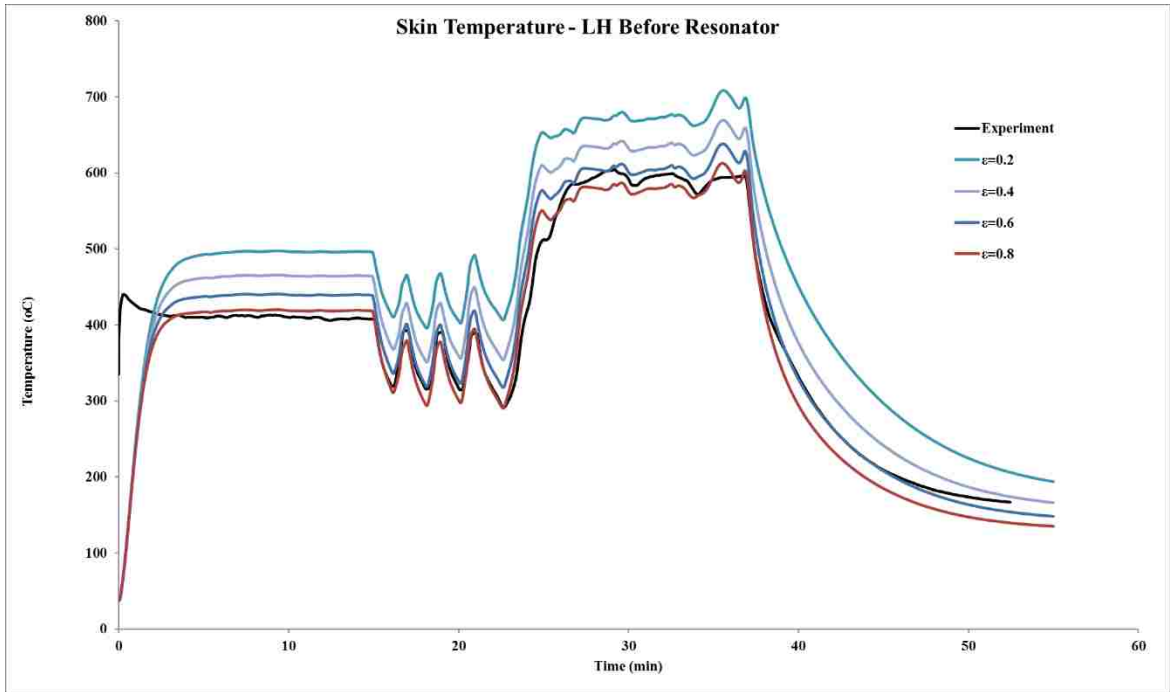Figure 5.27 Left manifold skin temperature

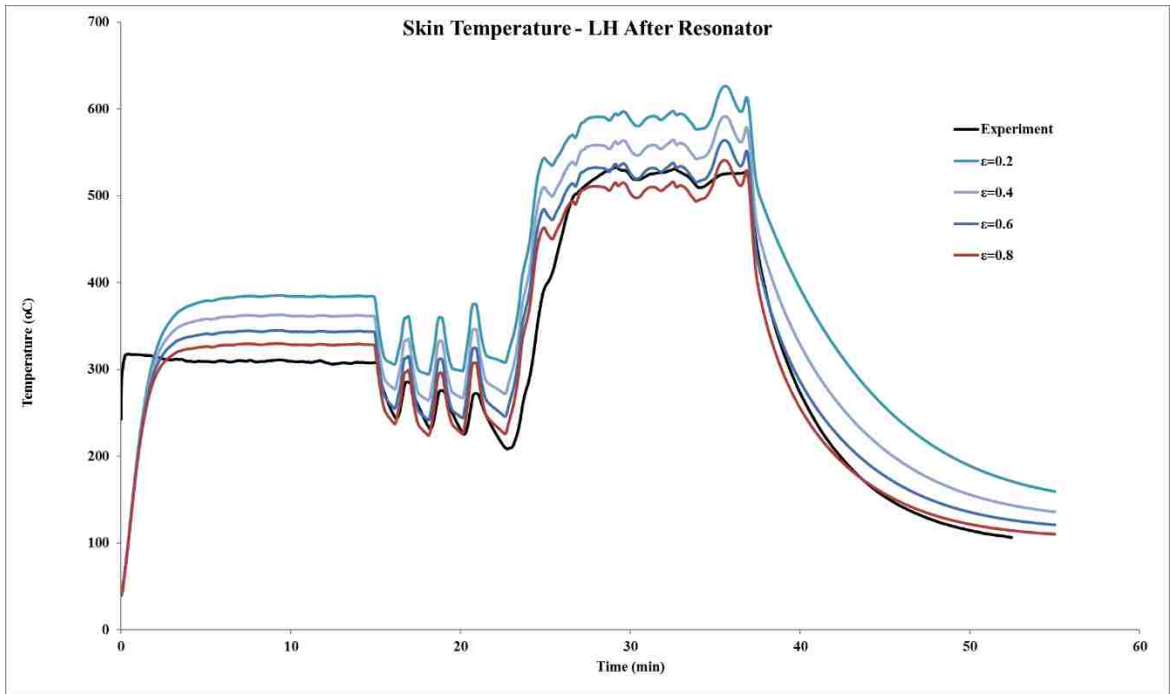Figure 5.28 Skin temperature before resonator on the left
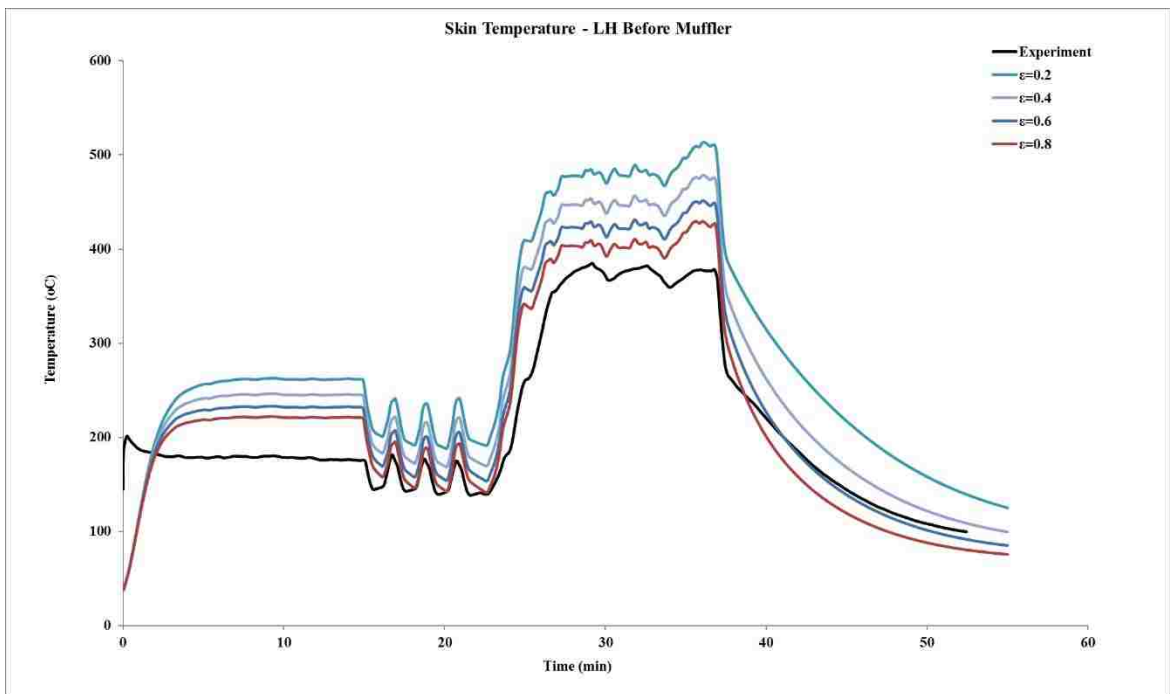
106

Figure 5.29 Skin temperature after resonator on the left

Figure 5.30 Skin temperature before muffler on the left
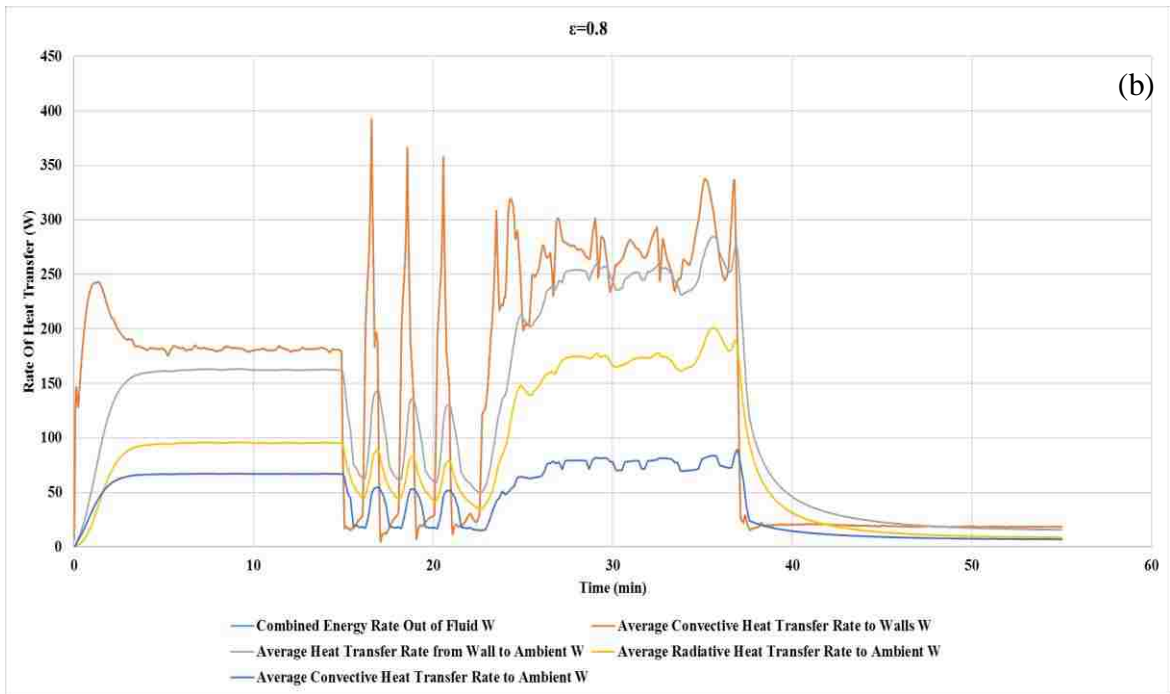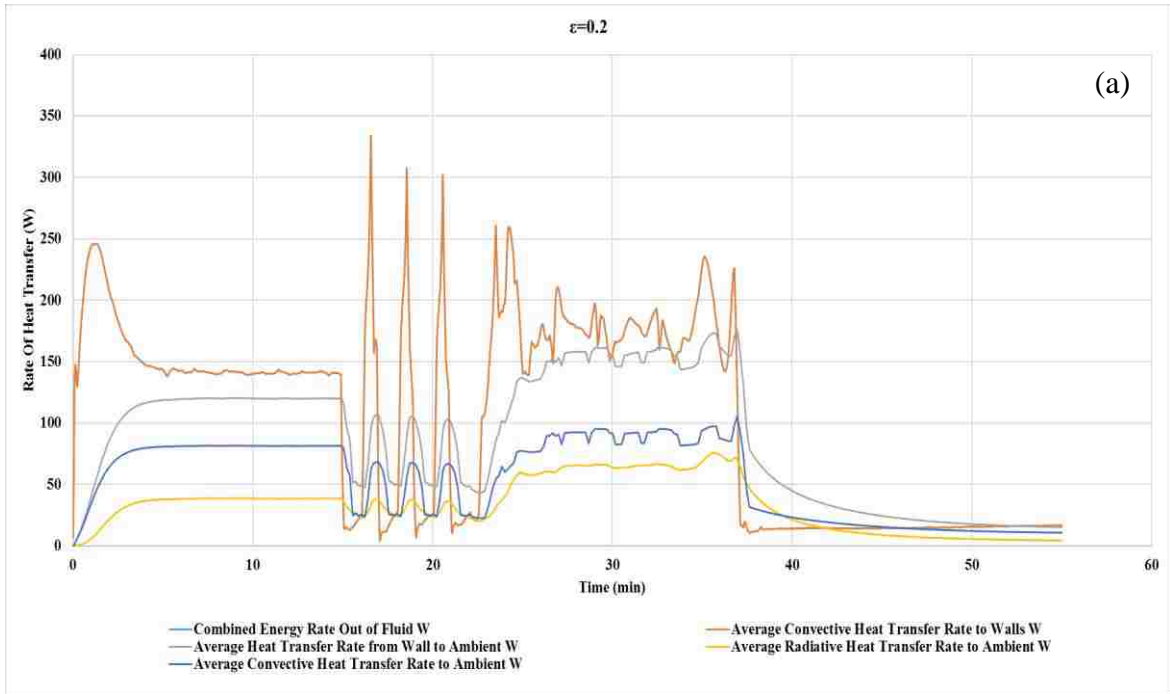
Figure 5.31 Rate of heat transfer for emissivities of (a) ε = 0.2 (b) ε = 0.8
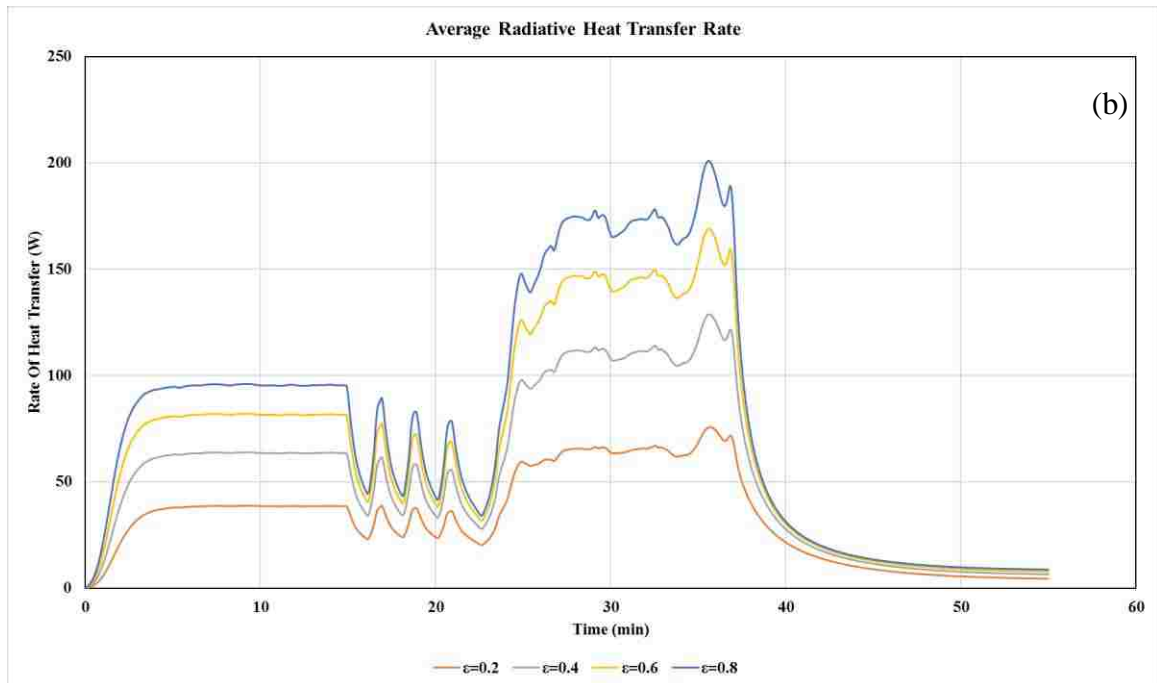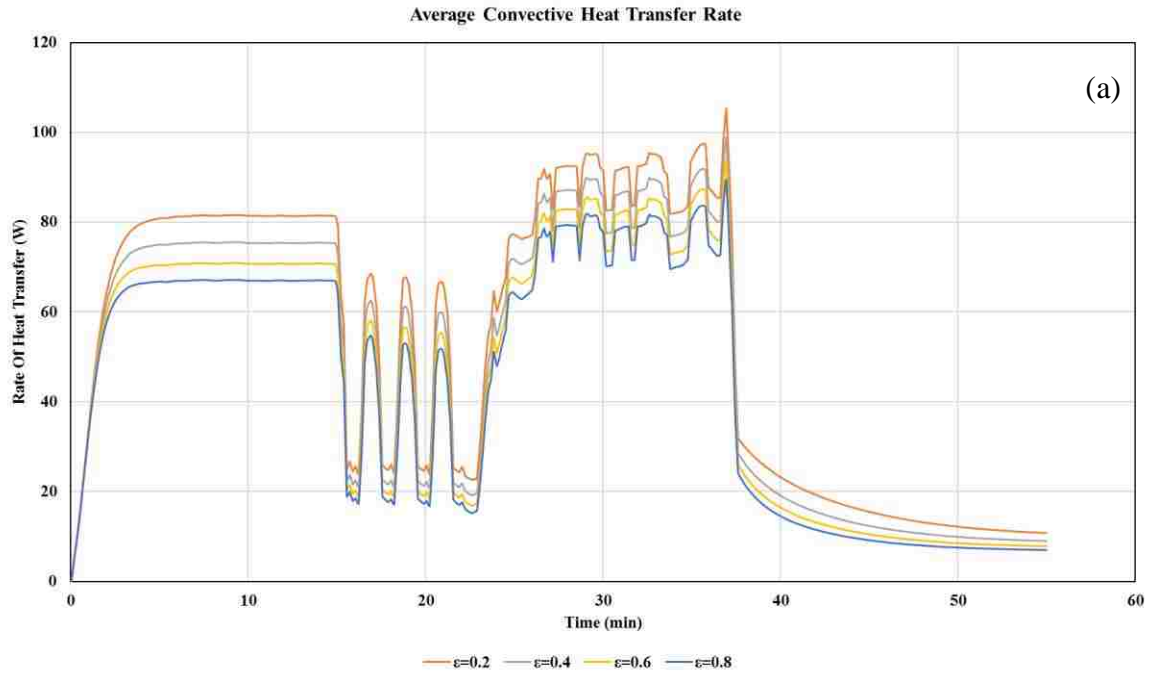
Figure 5.32 (a) Average convective heat transfer rate and (b) average radiative heat transfer rate for different emissivities
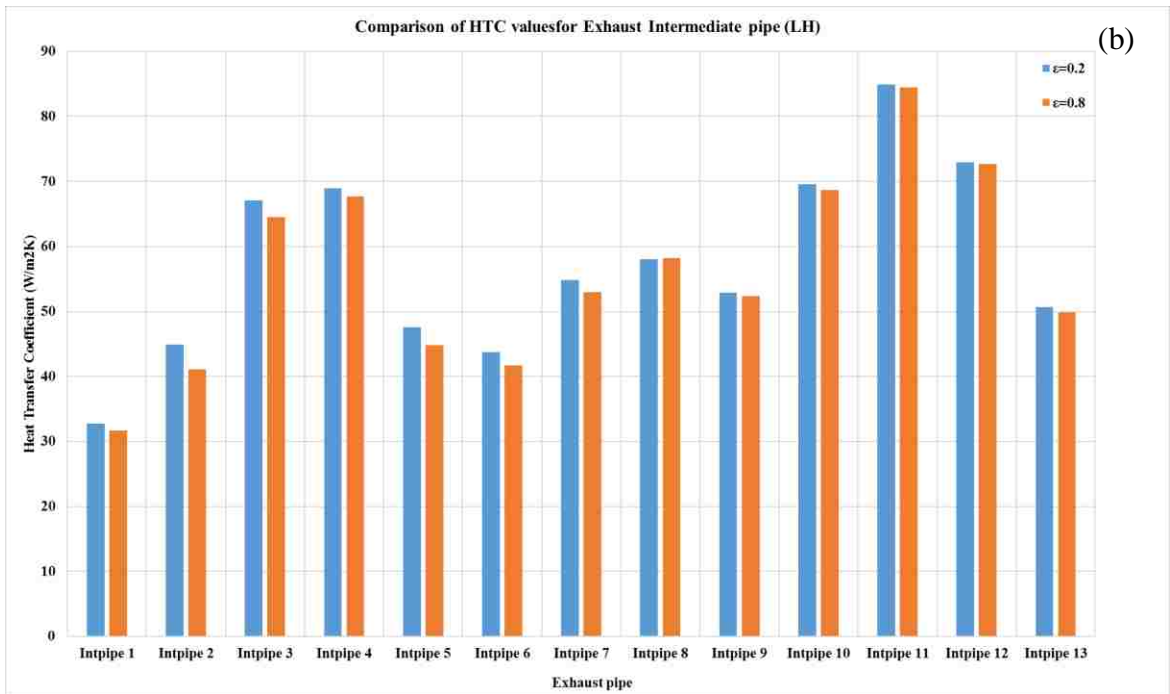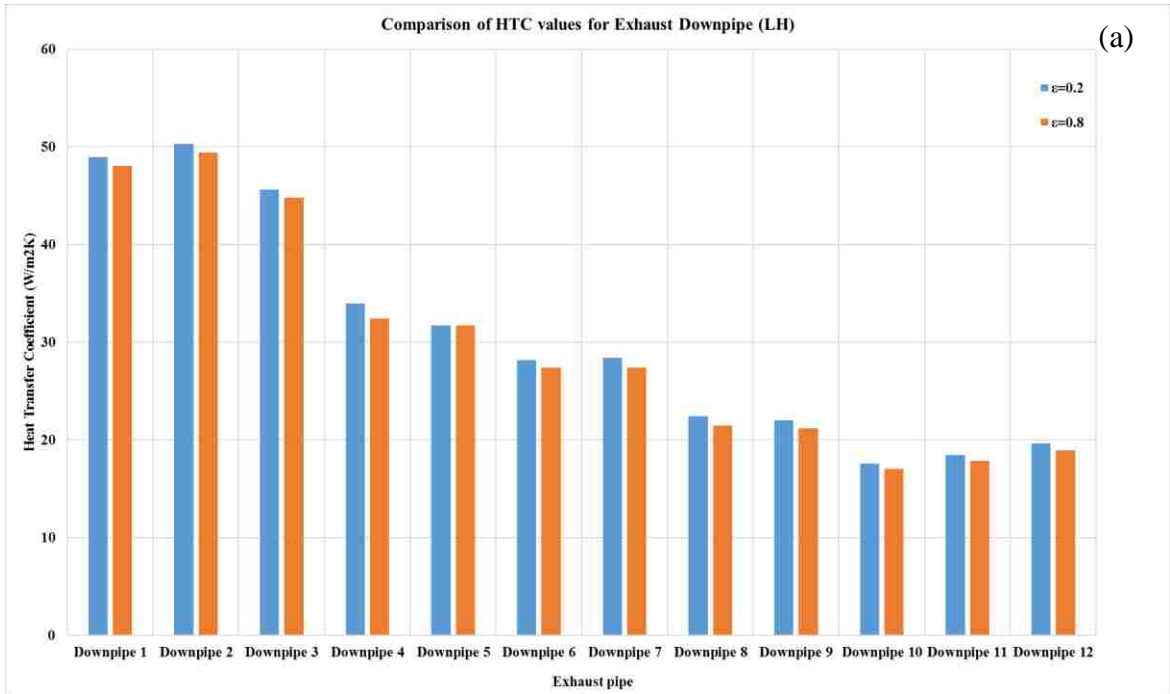
Figure 5.33 Variation of external specified y+ heat transfer coefficient for two different emissivity values over (a) Downpipe and (b) intermediate pipe

(a)

(b)
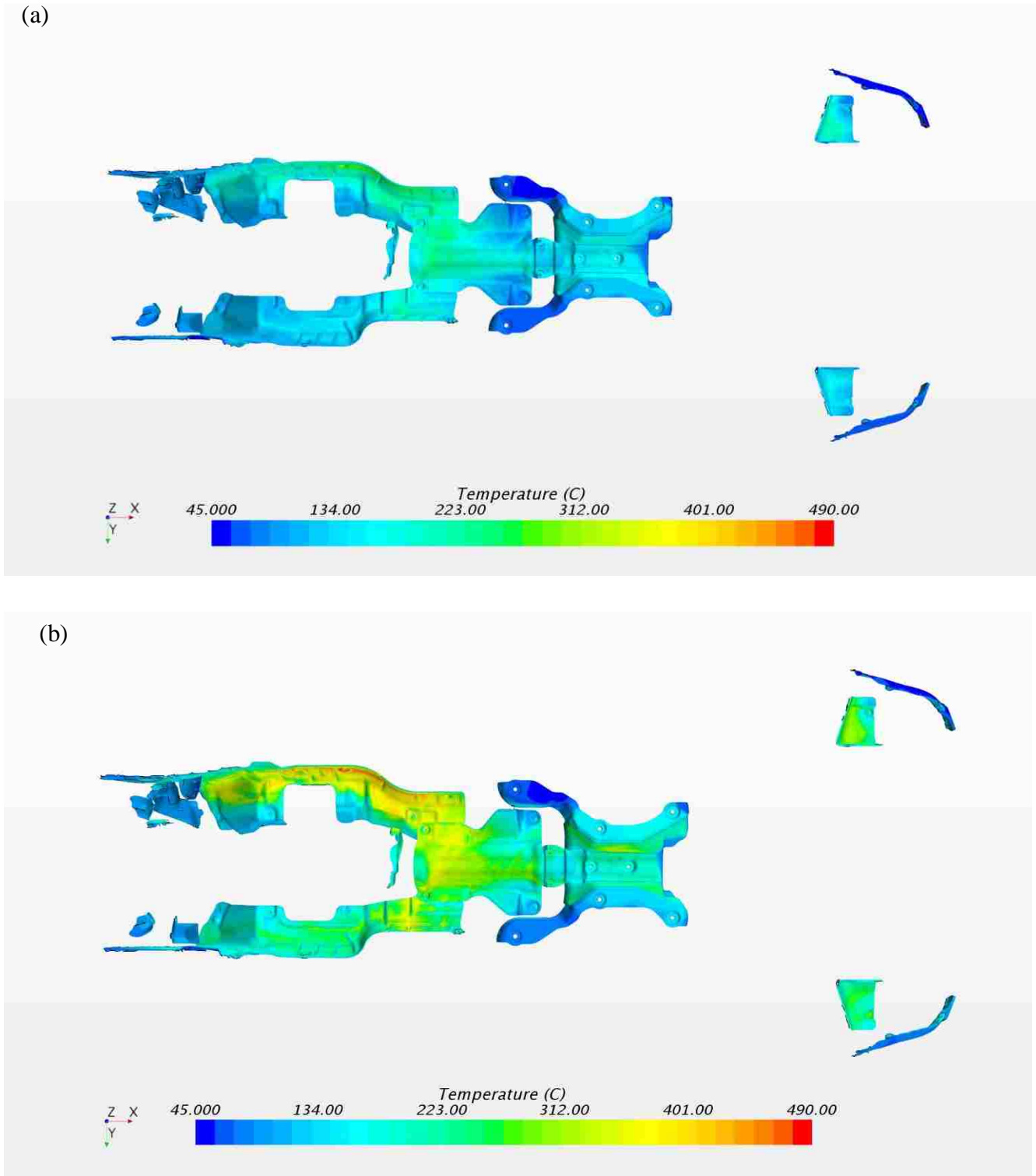
Figure 5.34 Heat shield temperatures at a wind speed of 49 mph for emissivity values (a) ε = 0.2 (b) ε = 0.8

(a)

(b)

Figure 5.35 Heat shield temperatures at a wind speed of 1.5 mph for emissivity values (a) $\varepsilon = 0.2$ (b) $\varepsilon = 0.8$

CHAPTER 6

Conclusions and Recommendations

6.1 Conclusion:

The study was focussed on prediction of exhaust skin temperature using 1D model and vehicle level 3D model. The 1D simulations were conducted using GT-SUITE, while the 3D vehicle level simulations were conducted using SIEMENS's STAR-CCM+. An efficient process and numerical methodology has been identified from this research. The study consisted of three sta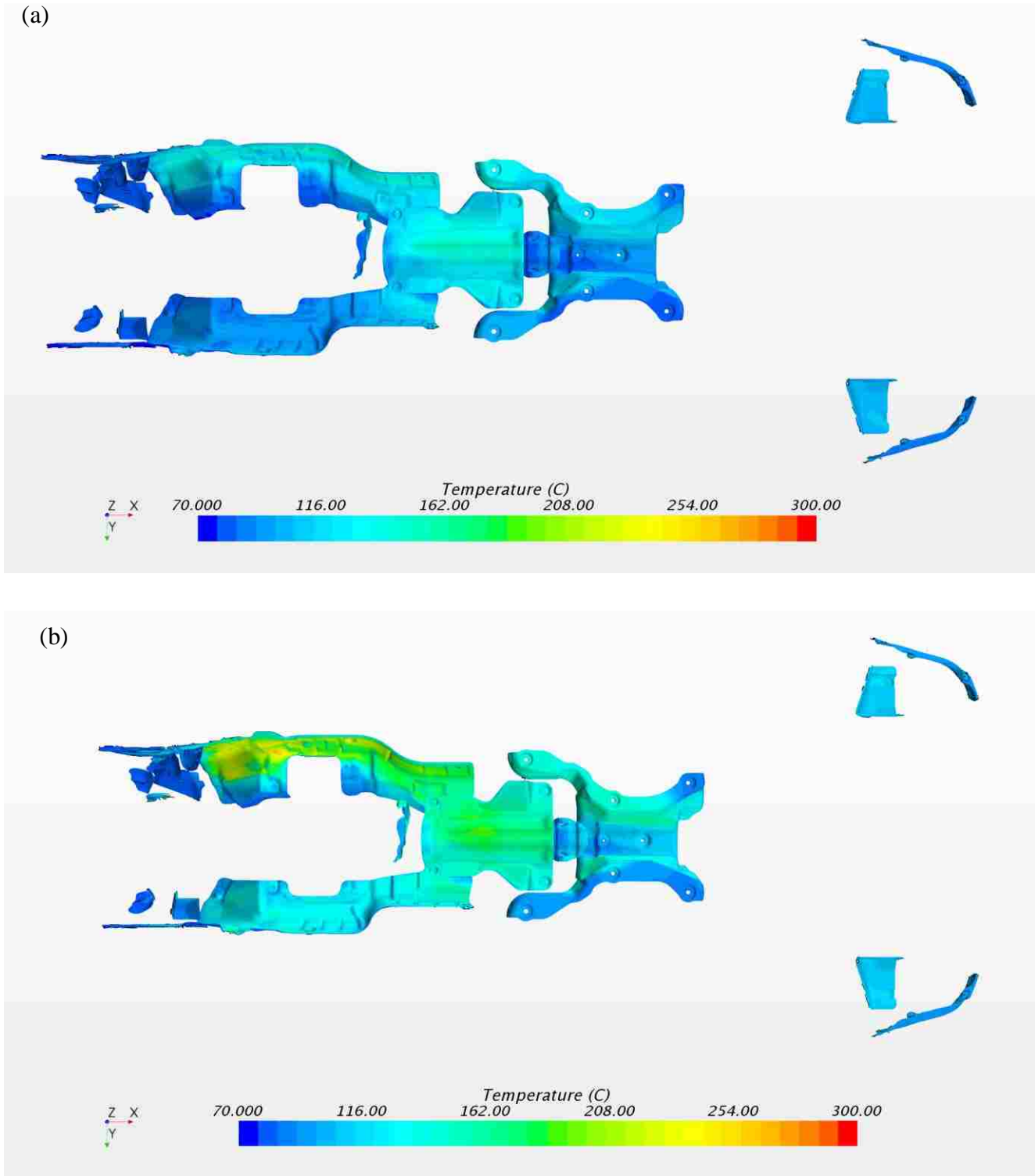ges: (1) 1D simulation for internal flow using steady state WOT and transient conditions, (2) 3D vehicle level steady state simulations representing specific points of a transient drive cycle and (3) Integration of results from 3D simulations into 1D model for prediction of exhaust skin temperature. Specific remarks were presented at the end of each chapter based on the results of the simulations explained in that chapter. The summary of major conclusions are presented as follows:

- For the first stage, the 1D model for internal fluid flow and heat transfer in the exhaust system consisted of a 3.5L V6 engine coupled with exhaust system to be studied. Coupling the engine provided a real-time closed loop control for combustion and exhaust requirements. The model was initially validated using steady state WOT conditions. Two different empirical correlations from literature: a universal heat transfer (UHT) correlation (Depcik and Assanis, 2002) and Wendland's (1993) correlation (WHT) were used to estimate the gas side internal heat transfer coefficients. The results showed good agreement for the test data. In all the simulations the case using the default correlations in GT-Power

113

overpredicted the gas temperatures. By default, GT-Power uses Colburn analogy to estimate the heat transfer coefficient. The correlation was less accurate compared to the user defined correlations.

- Modifying the 1D model in order to simulate transient drive cycles required additional data pertaining the exact drive test conditions. The initial simulation using the available empirical correlations provided a good agreement for the manifold gas and skin temperature. However, in the approach segment after the CAT the temperatures are highly overpredicted due to the heat rejection rates from the CAT. The initial assumption made for the use of heat rejection rates for the CAT based on RPM ranges from the WOT data seems invalid.

- The use of constant heat transfer coefficient values and lack of external heat transfer effects for the transient drive cycle could contribute to significant underprediction of skin temperatures in the cooldown segment of the drive cycle.

- The initial time for the transient drive cycle was 8 days due to the use of complex engine model. The simulation of combustion and other parameters for exhaust reading over every crank angle degree accounts for expensive CPU time. For this reason, the engine and the exhaust was decoupled after an initial run. All the exhaust gas parameters were exported to be used for further simulations. This approach of decoupling the engine and exhaust is seen to accelerate the computational solution and reduce the cost interms of CPU time from 8 days to 3.5 hours. Further, using the data from the coupled engine and exhaust for the decoupled exhaust model doesn't seem to reduce the accuracy of the computational solution.

- In order to eliminate the deficiencies with respect to external heat transfer, the use of a 3D vehicle level model is still necessary. The 3D model provides heat transfer coefficients required for the boundary condition in the 1D model to account for external convection.

- A K-means clustering algorithm was used to obtain a set of cluster points based on engine speed and torque. The set of cluster points represent a transient drive cycle. These cluster points were then used to obtain the wind speeds for steady state simulations in the 3D.

- Significant variation in heat transfer coefficients are seen in the downstream of the CAT primarily due to high velocities seen after the resonator. The presence of skid plate accounts for lower HTC values seen on the left side of the exhaust system.

- UHT correlation gives a more accurate prediction of skin temperature compared to the other two cases. This is primarily due to the formulation used in fixing the exponent for Reynolds number, based on microscales of turbulence. Thus in the regions where pulsation effects are dominant such as the manifold and regions before the resonator and muffler where the effects of turbulence are dominant, the UHT correlation gives an accurate prediction of skin temperature.

- External emissivity plays a significant role in overall external heat transfer thereby affecting the gas temperatures as well. Comparison of two different cases in 3D as well as the parametric study shows the importance of assigning a proper boundary condition for external heat transfer. The contribution of radiation heat transfer heat transfer varies from 25% to over 50% for emissivities of 0.2 to 0.8. Further, the variation of emissivity doesn't affect the overall convective heat transfer rate.

- The overall methodology integrating 1D and 3D models give a good prediction of exhaust skin temperature with efficient use of computational resources.

- Further, the same methodology of integrating both 1D and 3D numerical models could be used for any heat transfer related problems apart from the automotive industry

6.2 Recommendations for Future Work:

Through this research several issues pertaining to the exhaust skin temperature prediction have come to light. Some recommendations for the future work are:

- The current integration of the 1D and 3D models require the transfer of data between the codes manually, through the user. Automating the code to interact over homogenous or heterogeneous systems could accelerate the simulation time for the computational model more than the current time limit for the overall process.

- The use of different turbulence models for the vehicle level simulations could provide more insight into the relationship between external fluid flow and heat transfer.

- A detailed study pertaining to radiation heat transfer and the dynamic behaviour of external emissivity have to be investigated.

REFERENCES

Alkidas, A. C., Battiston, P. A., & Kapparos, D. J. (2004). Thermal Studies in the Exhaust System of a Diesel-Powered Light-Duty Vehicle. *SAE Technical Paper 2004-01-0050.* https://doi.org/10.4271/2004-01-0050

Apolloni, M. (2006). Derivation of a 1-D Thermal Model of Vehicle Underhood Temperatures on the Basis of Test Data Using an Evolutionary Algorithm, Master's Thesis. https://doi.org/10.3929/ethz-a-005189116

Arpaci, V.S., Dec, J.E. & Keller, J.O. (1993). Heat Transfer in Pulse Combustor Tailpipes. *Combustion Science and Technology*, **94**:131-146.

Bannister, C. D., Brace, C. J., Lock, G. D., Taylor, J., Brooks, T., & Fraser, N. (2009). Experimental Characterisation of Heat Transfer in Exhaust Pipe Sections. *SAE International Journal of Materials and Manufacturing*, **1**(1):136–144.

Chen, D. K. S. (1993). A Numerical Model for Thermal Problems in Exhaust Systems. *SAE Technical Paper 931070.* https://doi.org/10.4271/931070

Condie, K. G., & McEligot, D. M. (1995). Convective Heat Transfer for Pulsating Flow in the Takedown Pipe of a V-6 Engine. *SAE Technical Paper 950618.* https://doi.org/10.4271/950618

Depcik, C., & Assanis, D. N. (2002). A Universal Heat Transfer Correlation for Intake and Exhaust Flows in an Spark-Ignition Internal Combustion Engine. *SAE Technical Paper 2002-01-0372*. https://doi.org/10.4271/2002-01-0372

El-Sharkawy, A., Arora, D., Hekal, A. E.-R., Sami, A., & Hendy, M. (2016). Transient Modeling of Vehicle Under-hood and Underbody Component Temperatures. *SAE International Journal of Materials and Manufacturing*, **9**(2):330-337. https://doi.org/10.4271/2016-01-0281

Eriksson, L. (2002). Mean Value Models for Exhaust System Temperatures. *SAE Technical Paper 2002-01-0374*. https://doi.org/10.4271/2002-01-0374

GT-Power Flow Theory Manual, Gamma Technologies, 2014.

Fortunato, F., Caprio, M., Oliva, P., D'Aniello, G., Pantaleone, P., Andreozzi, A., & Manca, O. (2007). Numerical and Experimental Investigation of the Thermal Behavior of a Complete Exhaust System. *SAE Technical Paper 2007-01-1094*. https://doi.org/10.4271/2007-01-1094

Fulton, B., Van Nieuwstadt, M., Petrovic, S., & Roettger, D. (2014). Exhaust Manifold Temperature Observer Model. *SAE Technical Paper 2014-01-1155*. https://doi.org/10.4271/2014-01-1155

Grose, D. J., & Austin, K. (2001). Coupling of One Dimensional and Three Dimensional Simulation Models. *SAE Technical Paper 2001-01-1770*. https://doi.org/10.4271/2001-01-1770

Haehndel, K., Frank, T., Christel, F. M., Spengler, C., Suck, G., & Abanteriba, S. (2013). The Development of Exhaust Surface Temperature Models for 3D CFD Vehicle Thermal Management Simulations Part 1 - General Exhaust Configurations. *SAE International*

Journal of Passenger Cars - Mechanical Systems, **6**(2):847–858. https://doi.org/10.4271/2013-01-0879

Haehndel, K., Jefferies, A., Schlipf, M., Frank, T., Christel, F., & Abanteriba, S. (2014). The Development of Exhaust Surface Temperature Models for 3D CFD Vehicle Thermal Management Simulations Part 2 - Exhaust Acoustic Silencer Configurations. *SAE Technical Paper 2014-01-0646*. https://doi.org/10.4271/2014-01-0646

Jajcevic, D., Fitl, M., Schmidt, S., Glinsner, K., & Almbauer, R. (2010). Exhaust System Simulation of a 2-Cylinder 2-Stroke Engine Including Heat Transfer Effects. *SAE Technical Paper 2010-32-0035*. https://doi.org/10.4271/2010-32-0035

Kerai, H., & Verem, A. (2016). Physically Based Models for Predicting Exhaust Temperatures in SI Engines (Student thesis). Retrieved from http://urn.kb.se/resolve?urn=urn:nbn:se:liu:diva-129029

Konstantinidis, P. A., Koltsakis, G. C., & Stamatelos, A. M. (1997). Transient heat transfer modelling in automotive exhaust systems. *Proceedings of the Institution of Mechanical Engineers, Part C: Journal of Mechanical Engineering Science*, **211**(1):1–15. https://doi.org/10.1243/0954406971521610

Liu, Z., Hoffmanner, A. L., Skowron, J. F., & Miller, M. J. (1995). Exhaust Transient Temperature Response. *SAE Technical Paper 950617*. https://doi.org/10.4271/950617

Malchow, G. L., Sorenson, S. C., & Buckius, R. O. (1979). Heat Transfer in the Straight Section of an Exhaust Port of a Spark Ignition Engine. *SAE Technical Paper 790309*. https://doi.org/10.4271/790309

Martinez Laurent, J. C. (2011). Transient Thermal Simulation Process over a Diesel Exhaust System during Regeneration. *SAE Technical Paper 2011-01-0658.* https://doi.org/10.4271/2011-01-0658

Peters, A. R., & Crum, W. B. (1976). Vehicle Underbody Temperature and Heat Rejection Correlation-Wind Tunnel Versus Track. *SAE Technical Paper 76036.* https://doi.org/10.4271/760363

Ranganathan, R. P., Turner, D. W., & Franchett, M. E. (2005). Exhaust Manifold Gas Temperature Predictions using System Level Data Driven Modelling, *SAE Technical Paper 2005-01-0698.* https://doi.org/10.4271/2005-01-0698

Shayler, P. J., Hayden, D. J., & Ma, T. (1999). Exhaust System Heat Transfer and Catalytic Converter Performance. *SAE Technical Paper 1999-01-0453.* https://doi.org/10.4271/1999-01-0453

Sieder, E. N., & Tate, G. E. (1936). Heat Transfer and Pressure Drop of Liquids in Tubes. *Industrial & Engineering Chemistry*, **28**(12):1429–1435. https://doi.org/10.1021/ie50324a027

Srinivasan, K., Woronowycz, G., Zabat, M., & Tripp, J. (2005). An Efficient Procedure for Vehicle Thermal Protection Development. *SAE Technical Paper 2005-01-1904.* https://doi.org/10.4271/2005-01-1904

STAR-CCM+ Manual, 2016.

Wendland, D. W. (1993). Automobile Exhaust-System Steady-State Heat Transfer. *SAE Technical Paper 931085*. https://doi.org/10.4271/931085

Wu, Y. H., Srinivasan, K., Patterson, S., & Bot, E. (2013). Transient Thermal Analysis for the Automotive Underhood and Underbody Components, *ASME 2013 Heat Transfer Summer Conference*, V004T14A028. https://doi.org/10.1115/HT2013-17716

Xiao, G., Yang, Z., Wang, D., & Zhang, W. (2008). Investigation of Radiation and Conjugate Heat Transfers for Vehicle Underbody. *SAE Technical Paper 2008-01-1819.* https://doi.org/10.4271/2008-01-1819

Ye, Z. M., & Mohamadian, H. (2014). Simple Engine Exhaust Temperature Modeling and System Identification Based on Markov Chain Monte Carlo. *Applied Mechanics and Materials*, *598*, 224–228. https://doi.org/10.4028/www.scientific.net/AMM.598.224

Zhang, X., Meda, L., & Keck, M. (2005). Numerical Study on Skin Temperature and Heat Loss of Vehicle Exhaust System. *SAE Technical Paper 2005-01-1622.* https://doi.org/10.4271/2005-01-1622

Zhang, Y., Phaneuf, K., Hanson, R., & Showalter, N. (1992). Computer Modeling on Exhaust System Heat Transfer. *SAE Technical Paper 920262.* https://doi.org/10.4271/920262

VITA AUCTORIS

NAME: Sudharsan Annur Balasubramanian

PLACE OF BIRTH: Coimbatore, Tamil Nadu, India

YEAR OF BIRTH: 1988

EDUCATION: Anna University, Chennai, India

                                B.E. in Mechanical Engineering, 2009

                                University of Windsor, Windsor, Ontario

                                M.Eng. Mechanical Engineering (Automotive option), 2012

                                University of Windsor, Windsor, Ontario

                                Ph.D. in Mechanical Engineering, 2018